INSIGHTS INTO THE EFFECTS OF KCC2 MODULATION ON EPILEPTIFORM ACTIVITY

By

Francis Joseph Prael III

Dissertation

Submitted to the Faculty of the

Graduate School of Vanderbilt University

in partial fulfillment of the requirements

for the degree of

DOCTOR OF PHILOSOPHY

in

Pharmacology

June 30th, 2021

Nashville, Tennessee

Approved:

C. David Weaver, PhD (Advisor)

Jerod S. Denton, PhD (Committee Chair)

Eric Delpire, PhD

Andre H. Lagrange, MD, PhD

Gary A. Sulikowski, PhD

DEDICATION

This work is dedicated to my family, especially my parents, Francis J. Prael Jr. and Gilda

Fule-Prael, for their constant love and support

ACKNOWLEDGEMENTS

I would not have been able to complete this work without the support of many, many wonderful people – more so than I could reasonably list here. I would like to take this opportunity to try and offer some of these people my sincere thanks.

I'd like to start off by thanking my thesis advisor, Dave Weaver. I was told at the beginning of my PhD that by the end of it I'd hate my thesis advisor. Whoever told me that couldn't have been more wrong. Not only do I not actively hate Dave, but I still hold him in extremely high esteem – even after slogging through a challenging PhD over all these years. Dave has been an extraordinary mentor throughout my PhD: from helping me at the bench when I was starting out, to somehow still enthusiastically checking in on experiments as I wrapped up my thesis work, Dave's thoughtful comments, suggestions, and insights into science have had a tremendous impact in shaping me into the scientist I am today. Over the course of this PhD I've matured into a capable scientist, and I deeply appreciate how Dave's mentorship has been an integral part of that process.

I have also benefited from other sources of excellent mentorship during my PhD. I'd like to thank my thesis committee, consisting of Jerod Denton, Eric Delpire, Andre Lagrange, and Gary Sulikowski for their constant support. Jerod has been an excellent chair, advocate for me throughout my PhD, and electrophysiology domain expert. Eric's domain expertise in cation-chloride cotransporter biology has been invaluable throughout my PhD, together with all of the technical help and experimental data he produced in collaboration with our laboratory. Andre's expertise in epilepsy and electrophysiology have also been very important in shaping the direction of my project. Lastly, Gary's chemistry expertise and mentorship through the Chemistry-Biology Interface program have been highly beneficial for my thesis project and graduate education in

general. I'd also like to thank Chan Lek Tan and Baris Bingol for their excellent mentorship at Genentech during my internship there. Their enthusiasm and talent for research in industry helped solidify my interest in industry as a career.

Scientifically, I have benefited tremendously from collaborators and the excellent core facilities at Vanderbilt. This work would have been impossible without the High-Throughput Screening Core Facility, where I ran the majority of my experiments. Thank you to Paige Vinson, Erin Gribben, Josh Bauer, Debbie Mi, David Baughman, and David Westover for your technical expertise and help with administrative/technical issues in the core facility throughout my PhD. In particular, I'd like to thank Corbin Whitwell for all of the compound management help throughout my PhD, especially all of the last-minute compound requests she helped me with during the iterative screening process. Another major portion of this thesis was the chemistry; thank you to the Chemical Synthesis Core, especially Kwangho Kim for your help with the re-synthesis of our lead compounds and medicinal chemistry help during the project, together with Brendan Dutter for your help with analytical chemistry/purification. I would also like to thank Nathalie Pacico, Ana Mingorance, Garrett Kaas, Kirill Zavalin, and Roman Lazarenko for their help in culturing primary neurons/glia so I could set up the Ca^{2+} oscillation assay in the laboratory.

I also want to thank the other past and present members of the Weaver Laboratory. You all made the Weaver laboratory an extraordinary place to earn my PhD. Krystian Kozek, thank you (dziękuję ci bardzo) for being a dear friend; I always appreciate talking with you about science, politics and a host of other things –whether we are arguing or not– and look forward to seeing you and Lindsay in the Northeast after graduate school. Sunny Du, thank you for all your mentorship throughout my PhD, for teaching me a bit of Mandarin, and for always elevating lab morale through being kind and supportive. Brittany Spitznagel, thank you for also raising lab morale with a beer or two during the lows of science, and being there to celebrate its highs, along with being

an excellent colleague in the laboratory. Kris Abney and Susan Ramos-Hunter, thank you for being good friends and always keeping lab interesting. I would also like to thank the two students I mentored, Viola Donahue & Almond Sugumalwang, for being excellent mentees and showing me the joys of mentorship.

Additionally, I would like to thank the Department of Pharmacology, the VICB, and the BRET office for their support, both in terms of my education and financially. Thank you to Sean Davies and Christine Konradi for being excellent, supportive, and helpful DGSs during graduate school. Thank you to Karen Gieg, Kandi Granberry, and Tia Patton for all of your help with the many, many administrative underpinnings of the PhD. I would like to especially thank Karen Gieg for raising morale through her Coffee with Karen meetings, which kept me fed and caffeinated and also helped bring the Pharmacology Department together. Thank you to the BRET office, especially Ashley Brady, for all the support throughout the PhD. I benefited tremendously from the ASPIRE program, improving everything from my coding ability to career skills to scientific communication ability with its help, and I deeply appreciate everyone who helped create and share those resources. Financially, thank you to the BRET office and the Chemistry-Biology Interface training grant for funding my initial years of graduate school, VICTR for funding some of my research, and the Department of Pharmacology for financial assistance towards the end of my PhD.

Lastly, my friends and family have been an unwavering source of support throughout my life, and graduate school has been no exception. I've made some extraordinary friends in graduate school, and I'm thankful that the scientific community can feel a bit small at times, so I can constantly cross paths with these wonderful people going forward. Whether it's at a potluck, a board game night, or an early morning at the Villager, I feel privileged to have met so many wonderful people throughout my time at Vanderbilt. I'd also like to thank good friends from college

TABLE OF CONTENTS

LIST OF FIGURES

LIST OF TABLES

LIST OF ABBREVIATIONS

$[Cl^-]_i$	intracellular chloride
4-AP	4-aminopyridine
AaKCC	Aedes aegypti KCC
APC	amino acid-polyamine-cotransporter
AUC	area under the curve
BDNF	Brain-derived neurotrophic factor
Ca^{2+}	calcium
CBZ	carbamazepine
CFP	cyan fluorescent protein
Cl^-	chloride
CNS	central nervous system
cryo-EM	cryogenic-electron microscopy
CTD	C-terminal domain
DIDS	4,4'-Diisothiocyanostilbene-2,2'-disulfonic Acid
DIOA	[(dihydroindenyl)oxy]alkanoic acid
DmKCC	Drosophila melanogaster KCC
DMSO	Dimethylsulfoxide
EC50	Half maximal effective concentration
ECD	Extracellular domain
Egr4	early growth response 4
EIMFS	epilepsy of infancy with migrating focal seizures
Emax	Maximal efficacy
FLT3	fms-like tyrosine kinase 3
GABA	γ-aminobutyric acid
GABA-R	GABA receptor
GRCC	GABA-receptor-chloride-channel
GSK3β	glycogen synthase kinase 3β
HTS	High-throughput screening
IC50	half maximal inhibitory concentration
ID50	half maximal insecticidal dose
K^+	potassium
KCC2	potassium-chloride cotransporter 2
KEECs	KCC2 expression–enhancing compounds
KO	knockout
LC50	half maximal lethal concentration
LOF	loss of function
Mg^{2+}	magnesium
Na^+	sodium
NEM	N-ethylmaleimide
Neto-2	neuropilin and tolloid like-2
NKCC1	sodium-potassium-chloride cotransporter 1

NRSF	neuron-restrictive silencer factor
NTD	N-terminal domain
PB	phenobarbital
PKC	protein kinase C
PLCγ1	phospholipase Cγ1
PMA	phorbol 12-myristate 13-acetate
PPI	protein-protein interaction
Rab11b	Ras-associated binding protein 11b
Rb^+	rubidium
REST	repressor element-1 transcription factor
Shc	src homology 2 domain containing transforming protein
Tc	Tanimoto coefficient
TGF-β2	Transforming growth factor β2
Tl^+	thallium
TM	transmembrane
TrkB	Tropomyosin receptor kinase B
UCB	*Union Chimique Belge*
USF	upstream stimulating factor
WNK	With No Lysine
YFP	yellow fluorescent protein

CHAPTER 1

INTRODUCTION

Overview and significance

This work investigates the contribution of neuronal potassium (K^+)-chloride (Cl^-) cotransport to physiology and disease. The study of neuronal K^+-Cl^- cotransport is worthwhile because of its central importance to the development and proper functioning of the nervous system, together with its relevance as a potential avenue of treatment for a host of neurological disorders – including epilepsy. This work is broken down into four major sections: **Chapter 1** introduces and gives context for our study of neuronal K^+-Cl^- cotransport, **Chapter 2** focuses on the epileptogenic effects of KCC2 inhibition in the insect nervous system, **Chapter 3** focuses on the antiepileptic effects of KCC2 potentiation in mammalian systems, and **Chapter 4** explores the conclusions and future directions of this work.

The principal findings of **Chapter 2** are that (a) K^+-Cl^- cotransport mediated by the insect cotransporter KCC is coupled to inhibitory Cl^- channels in the *Drosophila melanogaster* nervous system, and (b) that KCC inhibition is a novel insecticidal mechanism useful for the control of an insect vector of human disease, *Aedes aegypti*. The finding that (a) K^+-Cl^- cotransport and inhibitory Cl^- channel activity are coupled in the *Drosophila* nervous system is significant because of *Drosophila*'s use as a model organism; *Drosophila* is regularly used to model aspects of human neurotransmission, and, given the importance of KCC and Cl^- channel coupling in the mammalian nervous system, our work reinforces the use of this model system for the study of inhibitory neurotransmission going forward. The finding that (b) KCC inhibition is insecticidal is significant

because mounting insecticide resistance necessitates the discovery of new insecticidal mechanisms. Insecticides are widely used to control agricultural pests and vectors of human disease. However, insecticidal resistance is eroding our ability to combat these deleterious interactions with insects. Our discovery of a new insecticidal mechanism therefore contributes to our continued ability to prevent agricultural pests and vectors of human disease from adversely affecting human wellbeing.

The principal findings of **Chapter 3** are that (a) we have discovered a new class of small molecule KCC2 potentiator and (b) this new KCC2 potentiator class prevents seizure-like activity. Our discovery of (a) a new class of KCC2 potentiator is significant because of the therapeutic potential KCC2 potentiation has to a host of neurological disorders with unmet medical need, and because KCC2 pharmacology is underdeveloped. Our discovery therefore helps develop KCC2 pharmacology further, and supplies the field with a new class of KCC2 potentiator useful for investigating KCC2 biology as it pertains to human health and disease. Our finding that (b) small molecule KCC2 potentiation attenuates seizure-like activity is important because of its direct contribution to discovering new antiepileptic mechanisms. Given that epilepsy is a widespread and debilitating disease with significant unmet medical need, the discovery of new antiepileptic mechanisms helps lay the foundation for the development of future antiepileptic treatments, which stand to benefit millions of epilepsy patients burdened with refractory epilepsy.

To provide context for this research, findings, and interpretations, this introduction will review neuronal K^+-Cl^+ cotransport biology, disease relevance as it pertains to epilepsy, and its chemical biology. Owing to the limited research on insect KCC and the parallels that our work and others have drawn between the human neuronal K^+-Cl^- cotransporter, KCC2, and insect KCC, this introduction will focus on the chemistry and biology of human KCC2.
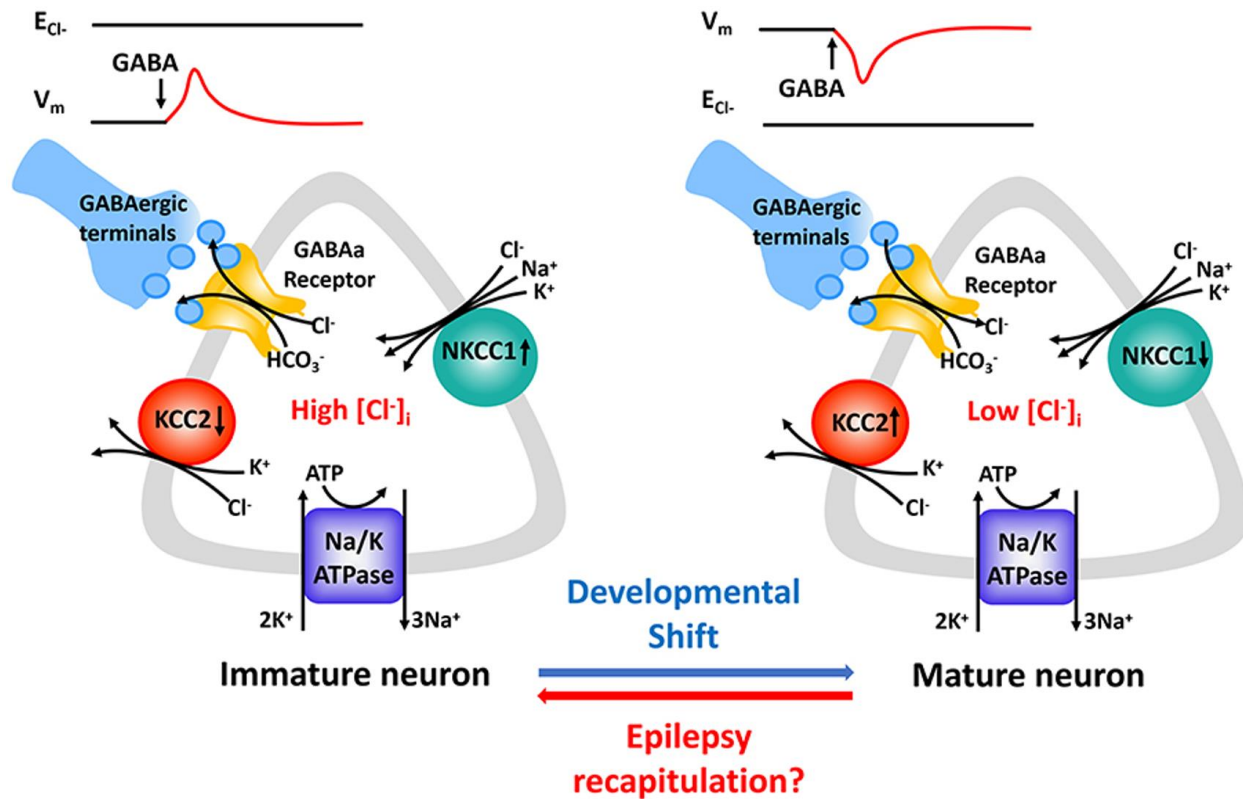
Figure 1.1. Influence of KCC2 function on fast inhibitory neurotransmission**. *Left*: in developing neurons and in epileptic tissue, KCC2 function is low relative to NKCC1 function. This generates a high $[Cl^-]_i$ and prevents ligand-gated Cl^- channels, like $GABA_A$ receptors, from hyperpolarizing cells in response to inhibitory signaling. Under conditions where the imbalance between KCC2 and NKCC1 activity is great, ligand-gated Cl^- channel gating leads to Cl^- efflux and neuronal depolarization. *Right*: in mature neurons, KCC2 activity is high relative to NKCC1 function. Under these conditions, there is low $[Cl^-]_i$ and ligand-gated Cl^- channel gating allows for Cl^- to flow down its concentration gradient and into the cell. This influx of negative charge hyperpolarizes cells and attenuates electrical signaling in neurons. Adapted from Ru Liu et al. (2020) *Frontiers in Neurology*.

KCC2 function and inhibitory neurotransmission

Electrical signals mediated by neurons are responsible for fast communication of information within the nervous system. These electrical signals are propagated through the movement of ions across the neuronal plasma membrane as transient depolarizations known as action potentials. Two major classes of neurotransmission control this ionic movement, and therefore control rapid information transfer across the nervous system: excitatory neurotransmission and inhibitory neurotransmission. Excitatory neurotransmission increases the amount of electrical signaling by depolarizing neurons to cause firing of action potentials, while inhibitory neurotransmission decreases the amount of electrical signaling by hyperpolarizing the cells to diminish the frequency of action potential firing (1).

The ability for inhibitory neurotransmission to attenuate electrical signaling is critically important to proper information transfer in the brain. Evidence of inhibitory neurotransmission's importance is evidenced by a host of neurological disorders that have been linked to imbalances between excitation and inhibition, including: autism spectrum disorders, schizophrenia, and epilepsy (2). Moreover, many therapeutics for these disorders are thought to function through either inhibition of excess excitatory signaling (3) or promoting inhibitory signaling (4). Inhibitory signaling itself is mediated by inhibitory neurotransmitters, such as GABA and glycine, and consists of many components which work in concert to hyperpolarize neurons to diminish electrical activity in a tightly regulated fashion.

Fast inhibitory neurotransmission is a major arm of inhibitory signaling. As implied by its name, fast inhibitory neurotransmission consists of components of inhibitory neurotransmission that work on rapid timescales. These components are typified by ligand-gated anion channels, such as $GABA_A$ and glycine receptors, that are permeable to Cl^- (1). Upon gating by inhibitory neurotransmitters, these anion channels facilitate the passive flow of Cl^- across the plasma membrane of the cell. In contrast to immature neurons, mature neurons typically maintain a low intracellular Cl^- concentration ($[Cl^-]_i$) relative to the outside of the cell; under these conditions, the

4

electrochemical gradient of Cl⁻ will favor flow of Cl⁻ into the cell, and the influx of negative charge will hyperpolarize the cell and therefore attenuate electrical signaling (1). The maintenance of low $[Cl^-]_i$ is therefore essential for ligand-gated anion channel function, neuronal hyperpolarization mediated by fast inhibitory neurotransmission, and therefore proper electrical signaling within the nervous system (Figure 1.1).

KCC2 is critically important for inhibitory neurotransmission because it is essential for maintenance of low $[Cl^-]_i$ and therefore the Cl⁻ gradients required for fast inhibitory neurotransmission (5, 6) (Figure 1.1). KCC2's ability to efflux Cl⁻ against its concentration gradient generates the low $[Cl^-]_i$ that $GABA_A$ and glycine receptors use for their function, as seen by disrupted $GABA_A$ and glycine receptor signaling in the presence of KCC2 knockdown (5–7) or knockout (8, 9). Moreover, a wealth of pharmacological and genetic evidence demonstrates that KCC2 loss-of-function (LOF) in model systems generates seizure-like activity (*see below*), downstream of diminished fast inhibitory neurotransmission. KCC2's importance for inhibitory transmission is further underscored by KCC2 LOF observed in neurological disorders with imbalances in excitation and inhibition, including: chronic pain (10, 11), autism (12, 13), Rett syndrome (14), schizophrenia (13), spinal cord injury (15, 16), and epilepsy (2, 17–20).

Epilepsy is a widespread neurological disorder with unmet medical need

Epilepsy is a debilitating neurological disorder characterized by recurrent seizures. Epilepsy is debilitating because people afflicted with this disorder experience decreased quality of life and stigma associated with the illness (21), together with significant risk for cognitive impairment (22), and increased risk of mortality (23). Additionally, epilepsy is extremely widespread: epilepsy is one of the most common neurological disorders, afflicting an estimated 2 million individuals in the United States alone (24).

There is a large unmet medical need in epilepsy. Despite the advent of antiepileptic drugs, roughly 20% - 40% of epilepsy patients are unable to manage their condition with current

treatments (25). This leaves hundreds of thousands of patients in the United States, and millions across the globe, which currently do not have their epilepsy managed with available antiepileptic drugs. The discovery of new antiepileptic mechanisms is therefore crucially important for millions of people afflicted with epilepsy.

Potentiation of KCC2 is a promising approach to the treatment of epilepsy (2, 17–20). One hypothesis for the origin of epileptic seizures is an imbalance between excitatory and inhibitory signaling, which features excessive excitatory signaling and diminished inhibitory signaling (17). Under conditions of excessive excitatory signaling, KCC2 potentiation could be antiepileptic by decreasing $[Cl^-]_i$ and thereby facilitating fast inhibitory neurotransmission and reducing excessive excitatory signaling thought to drive epileptic seizures. The established antiepileptic efficacy of GABAergic-directed antiepileptic drugs, such as phenobarbital, diazepam, tiagabine, and vigabatrin (4) supports the idea that increased inhibitory signaling is antiepileptic. Additionally, there is a wealth of empirical evidence linking clinical and preclinical deficits in KCC2 function to exacerbated seizures, and preclinical evidence linking KCC2 potentiation with seizure attenuation, which will be reviewed below. These empirical findings further underscore the therapeutic potential of KCC2 potentiation in human epilepsy.

Clinical data linking deficits in KCC2 activity to human epilepsy

Beyond KCC2's conceptual link to electrical regulation and seizures via its Cl^- transport function, a wealth of empirical data links deficits in KCC2 activity to epilepsy in humans. There are two main lines of evidence linking KCC2 LOF to epilepsy: resected tissue from epileptic patients that exhibit KCC2 LOF and LOF mutations in KCC2 discovered in epileptic patients.

Resected tissue from epileptic patients with intractable epilepsy exhibit hallmarks of KCC2 LOF across multiple studies. KCC2 LOF has been detected in: (a) patients with congenital disorders with severe seizure phenotypes, including focal cortical dysplasia type I and type II (26–30) and hemimegaloencephaly (28); (b) patients with tumor-associated seizures, such as glioma

(28, 31, 32) and hypothalamic hamartoma (33); and (c) in patients with intractable temporal lobe epilepsy (34–36). Across these studies, KCC2 LOF has been inferred through: a decrease in overall KCC2 expression, an alteration of subcellular KCC2 staining, and through electrophysiological abnormalities consistent with KCC2 LOF. Decreases in KCC2 expression were detected through lowered mRNA levels (27, 35) and KCC2 immunoreactivity (26, 32) relative to unaffected controls; these decreases in expression where then inferred to result in decreased KCC2 function. Alterations in subcellular KCC2 staining seen in patient samples, relative to unaffected controls, featured increased cytosolic staining and decreased KCC2 staining along the plasma membrane (26, 28, 30); these changes in subcellular distribution were then inferred to result in decreases KCC2 surface expression and therefore decreased Cl^- efflux from cells. Moreover, in many of these histopathology studies, neurons with lowered KCC2 expression or altered subcellular staining of KCC2 were dysmorphic, further implying a link between decreased neuronal health and lower/altered levels of KCC2 expression, although a causal relationship cannot be inferred from these data (26, 28, 33). Lastly, a study in patients with intractable temporal lobe epilepsy demonstrated that resected tissue from epileptic patients, in addition to displaying decreased KCC2 expression, also featured electrophysiological dysfunction consistent with KCC2 LOF (35).

In recent years, over a dozen mutations in KCC2 have been linked to human epilepsy, further underscoring the critical role KCC2 function has in this debilitating illness. The first two studies describing KCC2 LOF mutations found in epileptic patients were published simultaneously in 2014 (37, 38). These studies used a targeted sequencing approach to discover a number of LOF mutations in epilepsy that tracked within families afflicted with febrile seizures (37) and idiopathic generalized epilepsy (38). A number of mutations came out of these studies, all of which exhibited decreased Cl^- efflux (37, 38), while some also exhibited altered dendritic spine morphology, additionally highlighting the potential of deficits in KCC2's scaffolding function to contribute to disease pathology (37). However, owing to the targeted sequencing approach in

these studies, a monogenic link between KCC2 mutations and epilepsy could not be established. The first evidence of a causal, monogenic mutation in KCC2 was reported in 2015 (39). This group completed whole exome sequencing in patients with epilepsy of infancy with migrating focal seizures (EIMFS), and discovered a number of mutations which decreased KCC2 function *in vitro* that were associated with epilepsy (39). Two subsequent studies using whole exome sequencing further expanded the number of mutations in KCC2 causally associated with EIMFS, and further investigated how these mutations can lead to KCC2 dysfunction *in vitro* (40, 41). Mutations in KCC2 were distributed throughout the transporter, with most mutations being clustered in the extracellular domain or C-terminal domain. All described mutations created deficits in KCC2 ion transport activity, whether detected indirectly through gramicidin-perforated patch experiments (40) or through flux experiments (38). However, not all mutations had the same effect on KCC2 trafficking *in vitro*. Most mutations had deficits in trafficking which were inferred to result in their lowered ion transport ability, with some mutations causing an altered glycosylation pattern which may be responsible for the altered transporter trafficking (38, 39). However, some mutations did not have any appreciable alteration in KCC2 trafficking to the cell surface (40); these mutations are thought to be associated with defects in intrinsic KCC2 ion transport activity. Together, these genetic data are important for linking KCC2 dysfunction to human epilepsy and for understanding the ways in which deficits in KCC2 activity manifest in a biological setting.

Preclinical data associating deficits in KCC2 activity with exacerbated seizure activity

It is important from a translational perspective that systems used to model epilepsy reflect the human condition; in the case of deficits in KCC2, there is an abundance of evidence showing that deficits in KCC2 activity correlate with exacerbation of seizure-like activity in model systems, consistent with data seen in the clinic. These findings strongly support the translational relevance of these model systems. Studies linking decreased KCC2 activity with exacerbated seizures can

be categorized by their ability to: monitor endogenous KCC2 levels, genetically knockout (KO) KCC2, genetically knockdown KCC2, or pharmacologically inhibit KCC2.

Studies monitoring endogenous KCC2 levels track the levels of KCC2 activity or expression in different models of epilepsy. These studies have discovered that prolonged epileptiform activity, either through convulsant- (6) or electrical stimulation-mediated seizures (36), typically downregulates KCC2 expression. In contrast, acute epileptiform activity can increase KCC2 activity by increased KCC2 surface expression without affecting overall KCC2 levels, potentially as an intrinsic antiepileptic mechanism (42). These studies, along with the clinical data in humans, support KCC2 downregulation as a part of pathology associated with seizures.

Studies genetically knocking out KCC2 have demonstrated that KCC2 LOF is sufficient to cause spontaneous seizure activity. Full KCC2 KO is lethal shortly after birth, due to respiratory failure (8). However, KCC2 KO in hippocampal neurons alone is sufficient to generate spontaneous seizure-like activity in brain slices and *in vivo* (9). Furthermore, local KO of KCC2 in the hippocampus also produces hippocampal sclerosis in rodents (9), a pathology seen in some patients afflicted with epilepsy (27).

Studies genetically knocking down KCC2 confirm that partial KCC2 LOF is sufficient to exacerbate seizure-like activity. Experiments knocking down KCC2 using RNAi demonstrated that KCC2 knockdown produces spontaneous seizures in neuronal cultures and in awake and behaving rodents (6). Selective KO of the major KCC2 isoform, KCC2b, produces a knockdown of total KCC2 expression, leaving 15% - 20% of the transporter remaining; these mice have generalized seizures and die shortly after birth (5). Moreover, multiple studies have reported that heterozygous KCC2 KO mice have increased susceptibility to convulsant-induced seizures (5, 43). Another method to produce partial KCC2 LOF is through the use of phospho-mutants of KCC2. The T906/T1007 phosphorylation sites are phosphorylated downstream of WNK signaling and lead to inhibition of KCC2 activity. In mice harboring T906E/T1007E phosphomimetic

mutations, the mutant mice develop touch-evoked status epilepticus (44). In contrast, the S940 site phosphorylated by PKC is linked to increased KCC2 surface expression and activity. In mice harboring an S940A mutation, which prevents this PKC-mediated phosphorylation, mice have exacerbated epileptiform activity and increased lethality in response to convulsant-induced status epilepticus (45).

Lastly, studies pharmacologically inhibiting KCC2 further underscore the link between decreased KCC2 activity and seizures. Furthermore, owing to the rapid onset of the activity of these compounds, these studies emphasize the contribution of rapid changes in Cl^- homeostasis to seizure-like activity, as opposed to KCC2's contribution to dendritic spine development, which acts on a much longer timescale. Pharmacological KCC2 inhibition consistently and rapidly exacerbates seizure-like activity in cultured neurons, brain slices, and *in vivo*. KCC2 inhibition in neurons generates spontaneous seizure-like activity (7). KCC2 inhibition exacerbates seizure-like activity in brain slices where 0-Magnesium (Mg^{2+}) and 4-aminopyridine are used to induce epileptiform activity across multiple studies (7, 46–48). Importantly, KCC2 inhibition in awake and behaving animals also leads to spontaneous and acute seizure-like activity on behavioral and electrophysiological levels (7, 48).

Preclinical data supporting KCC2 potentiation as a viable antiepileptic mechanism

Importantly, from a therapeutic perspective, KCC2 potentiation has been linked to attenuation of seizure activity. This attenuation of seizure activity has been observed in similar model systems to the ones linking deficits in KCC2 activity to seizure exacerbation, namely, neuronal cultures, brain slices, and in awake and behaving animals. These studies can be binned into three categories: studies that genetically increase KCC2 activity, pharmacologically increase total KCC2 expression, and pharmacologically increase KCC2 surface expression.

Studies which genetically increase KCC2 activity use either overexpressed KCC2 (6, 49) or use KCC2 phospho-mutants to increase KCC2 activity (50); these studies consistently show

that increased KCC2 activity attenuates chemoconvulsant- or optogenetically-induced seizure-like activity. Chen et al. showed that cultured neurons overexpressing KCC2 are resistant to chemoconvulsant-mediated epileptiform activity (6). Additionally, overexpression of KCC2 attenuated optogenetically-induced seizures in awake and behaving animals, further supporting increases in KCC2 function being antiepileptic across model systems (49). Furthermore, animals overexpressing KCC2 showed no overt phenotypes, consistent with KCC2 overexpression not being toxic by itself (49). A phospho-mutant mouse, which used mutation of the inhibitory WNK sites to alanines to potentiate KCC2 activity (T906A/T1007A) also exhibited resistance to chemoconvulsant-induced seizures, and had no overt adverse effects in the absence of seizure induction (50). These results further underscore the antiepileptic phenotype and lack of overt side effects associated with KCC2 overexpression.

Studies that pharmacologically increase total KCC2 expression have corroborated the antiepileptic activity recorded in genetic studies which increase KCC2 activity. These studies have been limited to tropomyosin-related kinase B (TrkB) modulators in phenobarbital (PB)-resistant neonatal seizures (51–53). These studies consistently show that TrkB modulation produces increases in KCC2 expression and rescue of PB activity in these resistant seizure models (51–53). However, these studies differ in the pharmacological mode of inhibition used in the studies. Two studies demonstrated that TrkB inhibition increased KCC2 activity (51, 52), while one study demonstrated that a TrkB agonist attenuated seizure-like activity in this PB-resistant, ischemic model system (53). These studies highlight the complexities of TrkB signaling during disease-associated pathology. However, the constant association between increases in total KCC2 expression and an antiepileptic effect supports KCC2 potentiation's antiepileptic potential, regardless of the underlying complexities associated with TrkB signaling in these model systems.

A single study used a chemical probe associated with increased KCC2 surface expression to illustrate that increases in KCC2 activity without total increases in KCC2 expression are sufficient to attenuate seizure-like activity; this study showed that CLP257 reduced seizure-like

discharges in a genetic model of epilepsy (54). While these data are a promising start, given the controversy surrounding CLP257's activity at KCC2 (55), additional data are required to confirm that these data are downstream of KCC2 potentiation and not an off-target activity of CLP257.

In conclusion, a wealth of data links KCC2 potentiation to antiepileptic activity. However, owing to limited KCC2 potentiator pharmacology (*see below*), studies investigating whether or not selective KCC2 potentiation is sufficient to attenuate seizure like activity are currently lacking. The discovery of novel chemical probes potentiating KCC2, and studies using these probes to investigate whether acute KCC2 potentiation is sufficient to attenuate seizure activity are therefore warranted.

KCC2 structure and function

KCC2 (encoded by *SLC12A5*) has diverse functions throughout the nervous system that result from its ability to act as an ion transporter and as a scaffolding protein. In terms of its function as an ion transporter, KCC2 is a neuronally expressed, K^+-Cl^- cotransporter that mediates the symport of K^+ and Cl^- across the plasma membrane (56). In addition to its ion transport function, KCC2 also has multiple transport-independent activities stemming from its ability to scaffold multiple proteins important for neuronal development and signaling (57). To give a molecular context and mechanistic basis for these activities, this section will review KCC2's structural biology, ion transport functions, and ion transport-independent functions.

Tremendous progress in KCC2 structural biology has been made in recent years. After preliminary reports describing the crystal structure of a prokaryotic homolog of KCC2's C-terminal domain (58) and a low-resolution negative stain electron microscopy (EM) structure of KCC2's general architecture (59), in 2020-2021 multiple groups reported <4 Å resolution cryo-EM structures of KCC2, which generated the first molecular models of the transporter's overall structure (60–62) (Figure 1.2). All groups reported the structure of KCC2 as a homodimer (60–62) (Figure 1.2.*A*), in agreement with previous biochemical experiments (63). All reported KCC2

structures are in an inward open (62) or inward-facing occluded state (60, 61). The general structure of each KCC2 monomer consisted of four distinct features: (i) a transmembrane (TM) domain, (ii) an extracellular domain (ECD), (iii) a C-terminal domain (CTD), and an N-terminal domain (NTD) (60–62).

(i) the TM domain, which consists of twelve TM helices, has an overall structure similar to other members of the amino acid-polyamine-cotransporter (APC) superfamily; each monomer exhibited a LeuT-fold –a structural motif shared among members of the APC superfamily– which has the topology of transmembrane helices TM1-TM5 and TM6-TM10 related to one another by a pseudo-twofold symmetrical axis (60) (Figure 1.2.*B*). TM11 and TM12 are involved in weak hydrophobic interactions between monomers within the dimeric KCC2 complex (60). Critically, the TM domain also contains the K^+ and Cl^- binding sites that mediate ion transport, with 1 K^+ and 2 Cl^- binding sites being resolved in each structure (60). Given KCC2's electroneutral cotransport of 1 K^+ and 1 Cl^- per transport cycle (56), it is surprising to find 1 K^+ and 2 Cl^- binding sites within the KCC2 structures. However, it has been speculated that, in line with kinetic data of K^+-Cl^- cotransport in erythrocytes, one of these Cl^- binding sites functions as a Cl^--binding allosteric site which can modulate KCC2-mediated ion transport (64).

(ii) the ECD is formed by a large loop between TM5 and TM6 (60–62) (Figure 1.2.*B* & *C*). This rigid structure sits on top of the extracellular face of the TM domain, and is stabilized by multiple intramolecular disulfide bonds (60). While this structure is not involved in KCC2 dimerization, it is important for overall KCC2 function, as evidenced by mutagenesis studies illustrating that the multiple sites of glycosylation (60) and cysteines involved in disulfide bonding within the ECD are essential for KCC2's ion transport ability (65).

(iii) the CTD is a large, structured, cytosolic domain critical for KCC2 regulation and function. The CTD is in a domain-swap configuration, where the CTD of one monomer of the KCC2 dimer is underneath the opposite KCC2 monomer (60) (Figure 1.2). Dimerization appears to mostly be driven by the CTD, owing to numerous hydrophobic interactions between each CTD

13
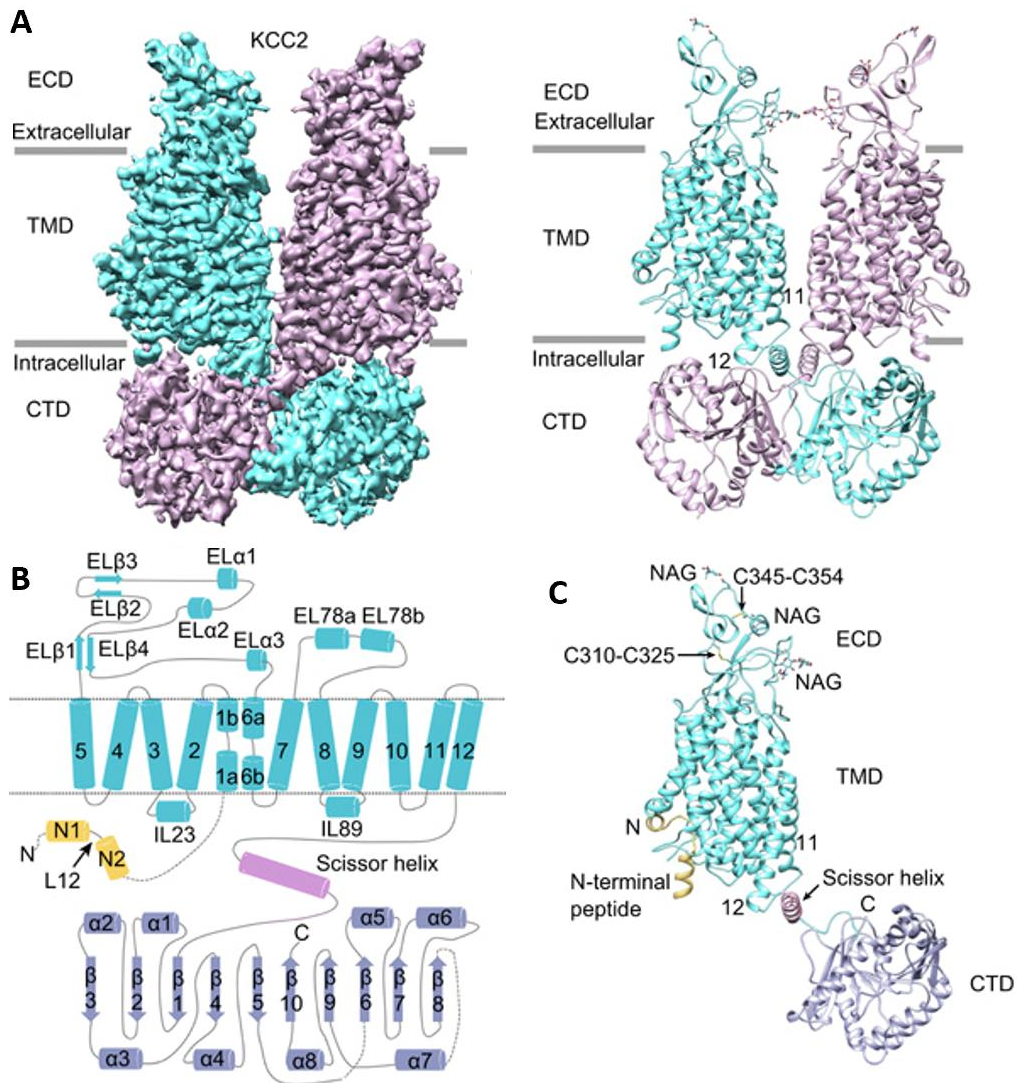
Figure 1.2. KCC2 structural biology**.** (*A*) Cryo-EM structures of the full length KCC2 dimer as a three-dimensional reconstruction (*Left*) and as a cartoon representation (*Right*). Perspective is from within the plane of the membrane. (*B*) Cartoon representation of topological arrangement of a single KCC2 monomer. (*C*) Cartoon structure of a single KCC2 monomer with structurally resolved subdomains labeled. Figure adapted from Yuan Xie et al. (2020) *Science Advances*.

in the dimer, and weak interactions with TM12 and the CTD (60). In addition to being crucial for dimerization, the CTD has numerous sites which are subject to posttranslational modification, including sites for phosphorylation (66, 67) and proteolysis (68). These posttranslational modifications are key regulators of KCC2 activity, owing to their ability to modulate KCC2 ion transport , expression, and trafficking (66–68). Furthermore, the CTD is a key mediator of KCC2's ability to act as a protein scaffold, and is thought to be the protein-protein interaction (PPI) site that mediates KCC2's scaffolding ability (57).

(iv) the NTD is a cytosolic KCC2 domain which is by and large not resolved in reported KCC2 structures (60–62), likely owing to the increased flexibility in this region. The NTD contains reported phosphorylation sites with inhibitory or unknown function (69, 70), and the difference in NTD length is the predominant difference between the two major KCC2 isoforms recorded in mammals: KCC2a and KCC2b (63), which is important for different brain region and subcellular expression patterns of each of these isoforms; for example, in cultured cortical neurons, KCC2b is predominantly expressed near the cell surface, while KCC2a has a predominantly cytosolic distribution (71, 72). The resolved portion of the NTD in reported KCC2 structures consists of a region referred to as the N-terminal inhibitory peptide (Figure 1.2.*C*). The N-terminal inhibitory peptide inserts into a cleft formed by TM1 and TM5 along the membrane surface, and also interacts with the CTD (60). This peptide functionally inhibits KCC2, as mutations within conserved residues of the N-terminal peptide potentiate KCC2 activity (60). Structurally, this inhibition is thought to be brought about by how the N-terminal peptide blocks solvent access to the substrate binding sites in KCC2, and by stabilizing interactions with TM8 – a helix whose dynamic movement is thought to be necessary to complete an ion transport cycle in KCCs (60).

Ion transport by KCC2 is similar to that of other K^+-Cl^- cotransporters within the SLC12 family of transporters, namely KCC1, KCC3, and KCC4. K^+-Cl^- cotransporters by members of this family are distinguished by their ability to electroneutrally transport K^+ and Cl^- at a 1:1 stoichiometry (73). This sodium (Na^+)-independent K^+-Cl^- cotransport ability of these transporters

contrasts with the other members of the SLC12 family of transporters, who either feature Na^+-dependent transport or unknown function (73). These K^+-Cl^- cotransporters couple the transport of K^+ down its electrochemical gradient to facilitate the secondary-active transport of Cl^- against its electrochemical gradient (73). In doing so, these transporters facilitate the development of Cl^- gradients across cellular membranes. Under physiological conditions of high intracellular K^+, these transporters typically mediate the efflux of Cl^- out of cells, and thereby generate Cl^- gradients which feature a low $[Cl^-]_i$ (~5 mM) relative to extracellular Cl^- concentrations (~110 mM) (74). However, under conditions of high extracellular K^+, these transporters can mediate the influx of K^+ and Cl^- (56). The ability for these transporters to switch between influx and efflux under different conditions is regularly used to assay transporter activity in an experimental setting (75). What distinguishes KCC2's ion transport activity from other K^+-Cl^- cotransporters within the SLC12 family is its activity under isotonic conditions (56), and its predominantly neuronal expression (76, 77). Indeed, KCC2's isotonic activity is crucial for its ability to generate a low $[Cl^-]_i$ in mature neurons, which are typically under isotonic conditions. The maintenance of this low $[Cl^-]_i$ in most mature neurons is critically important for inhibitory neurotransmission, as highlighted above.

KCC2 also has ion transport-independent activities that are important for neuronal development and synapse function. KCC2's ion transport-independent functions are thought to arise from PPIs formed within KCC2-containing complexes (57, 78). These activities were initially discovered in neuronal cultures from KCC2 deficient mice, which had abnormal dendritic spine development; these cultures could have their dendritic spine development rescued by transfection of full length KCC2, or an ion transport-deficient KCC2 construct which lacked KCC2's NTD (57). The ability of KCC2 to influence dendritic spine development was shown to be related to KCC2's ability to interact with the cytoskeleton-associated protein 4.1N, and therefore KCC2's ability to form PPIs. This work has been expanded upon to reveal that KCC2's ion transport-independent functions also extend into regulating synaptic activity, for example through KCC2's ability to

influence AMPA receptor localization and therefore efficacy of signaling at glutamatergic synapses (79).

KCC2 regulation

KCC2 is dynamically regulated by multiple mechanisms that fine-tune $[Cl^-]_i$ levels and signaling complexes related to KCC2's scaffolding ability. These regulatory mechanisms can be categorized into four major areas based on their effect on: KCC2 transcription, KCC2 cell-surface expression, KCC2 complex formation, and effect on KCC2's intrinsic ion transport (Figure 1.3).

KCC2 transcription is a key regulatory mechanism of KCC2 because of its ability to control total levels of KCC2 expression. KCC2 transcription is regulated by at least 10 transcription factor binding sites within or proximal to the *SLC12A5* gene (80). Changes in KCC2 transcriptional levels are important during development, where they are critical for the excitatory-to-inhibitory GABA switch (74), and for dynamically regulating KCC2 expression levels in the CNS in response to cellular signaling (81). Important transcription factors influencing the developmental increase in KCC2 expression include early growth response 4 (Egr4), and upstream stimulating factor (USF)1 and 2, and repressor element-1 transcription factor/neuron-restrictive silencer factor (REST/NRSF). Egr4 (80) and USF1 and 2 (82) stimulate the transcription of KCC2 during development, while REST/NRSF interacts with neuro-restrictive silencing elements to repress KCC2 transcription (83). Additionally KCC2 expression in immature neurons is repressed on a post-transcriptional level by the microRNA miRNA-92 (84). Beyond developmental regulation, the brain-derived neurotrophic factor (BDNF)-TrkB pathway regulates KCC2 transcription dynamically in response to BDNF-mediated signaling in a development-specific context. In immature neurons, BDNF-stimulated TrkB signals through Egr4 to promote KCC2 transcription and expression (85). However, in mature neurons, BDNF signaling can either
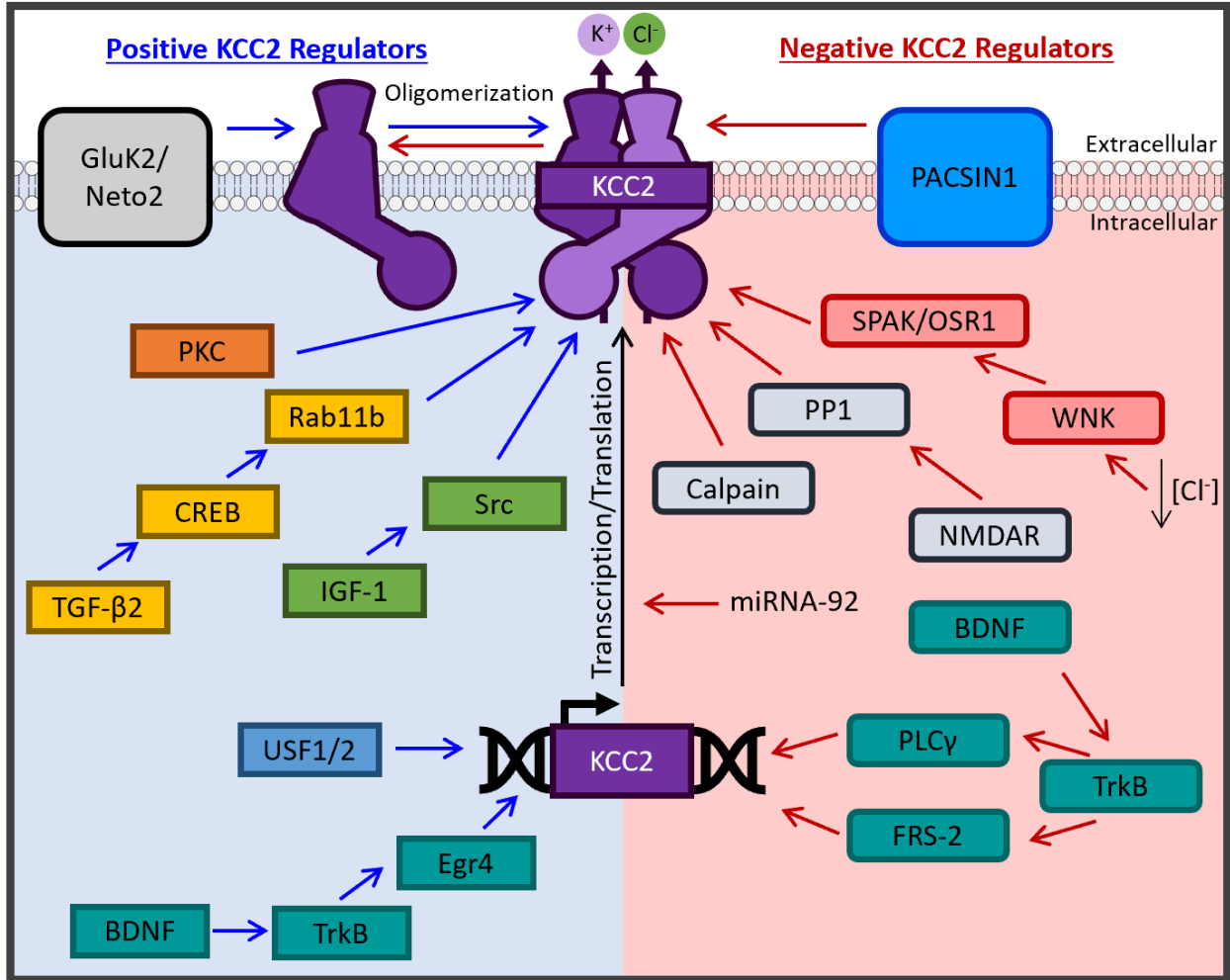
Figure 1.3. Cartoon depicting selected regulators of KCC2 activity. Regulatory interactions that promote KCC2 activity are denoted with blue arrows on the left side of the figure. Regulatory interactions that inhibit KCC2 activity are denoted with red arrows on the right side of the figure. Different proteins within the same regulatory cascade are color coded.

promote KCC2 transcription through a src homology 2 domain containing transforming protein (Shc)-dependent mechanism, or repress KCC2 transcription through a phospholipase Cγ1 (PLCγ1)-dependent mechanism, depending on the cellular context (86).

KCC2 cell-surface expression is a critical regulatory mechanism because KCC2's impact on $[Cl^-]_i$ and on synaptic development are dependent on KCC2's localization at the plasma membrane; therefore, trafficking of KCC2 between intracellular- and surface-pools of transporter dictate levels of KCC2 activity. KCC2 trafficking is modulated by (a) phosphorylation, (b) proteolytic cleavage, and (c) PPIs. (a) KCC2 phosphorylation has site-specific effects on KCC2 activity. Protein kinase C (PKC)-mediated phosphorylation of S940 promotes surface expression of KCC2 (66), and has been shown to be a key determinant of KCC2 levels *in vivo* and in disease states (87). In contrast, phosphorylation downstream of With No lysine (WNK) kinase on T906/T1007 reproducibly reduces KCC2 activity (50, 67); the effect of WNK-mediated phosphorylation on KCC2 surface expression is controversial, with contrasting reports showing decreases in KCC2 surface expression (67), or unchanging levels of KCC2 surface expression (50) in phosphorylation site mutant (phospho-mutant) studies. The effect of tyrosine phosphorylation at Y903 and Y1087 on KCC2 surface expression and function is also controversial, with reports of either enhanced KCC2 activity upon phosphorylation (88), or increased KCC2 internalization and degradation upon phosphorylation of these tyrosine residues (89). N-ethylmaleimide (NEM), a notable nonspecific potentiator of K^+-Cl^- cotransport, has a complex influence on multiple phosphorylation sites to produce a net increase in KCC2 surface expression levels (90). (b) KCC2 proteolytic cleavage is a Ca^{2+}-dependent process that downregulates KCC2 activity and surface expression in response to glutamatergic signaling (68). KCC2 proteolytic cleavage is mediated by calpain, occurs on the CTD of the transporter, and promotes internalization and degradation of the transporter (68). (c) KCC2 PPIs, in addition to their importance for modulating KCC2 function via KCC2 complex composition (*see below*), also influence KCC2 trafficking. Transforming growth factor β2 (TGF-β2) increases KCC2 surface

expression through a mechanism that involves colocalization of Ras-associated binding protein 11b (Rab11b) and KCC2 (91). Additionally, the kainite receptor GluK2 also increases KCC2 surface expression when expressed in KCC2-containing complexes (92, 93).

KCC2 complex formation, by affecting the functional state of KCC2 and the complement of KCC2 interacting proteins, is another key KCC2 regulator. Consistent with structural studies (60), KCC2 forms oligomeric complexes *in vivo* (92, 94). These oligomeric complexes are thought to correlate with KCC2 ion transport activity, where monomeric KCC2 has the lowest ion transport ability, and higher order oligomeric complexes have the most activity (94). In fact, several studies have reported a correlation between decreases in KCC2 oligomerization and reduced KCC2 ion transport (88, 92). Furthermore, KCC2 interacting proteins that increase KCC2 ion transport, e.g. GluK2 (92, 93) and neuropilin and tolloid like-2 (Neto-2) (95), also drive the formation of oligomeric KCC2. In contrast, PACSIN1 inhibits KCC2 function through complex formation (96). Outside of oligomerization, KCC2 complex formation is also important in KCC2's capacity as a scaffolding protein. Through forming complexes with other proteins, such as the actin-associated protein 4.1N, KCC2 has been shown to influence dendritic spine morphology (57) and also influence the function of other critical synaptic proteins, such as AMPA receptors (79).

Lastly, the intrinsic ion transport rate of KCC2 can also be regulated without overt changes to KCC2 surface expression. This phenomenon has been observed by multiple mutagenesis studies. Mutation of key cysteines in the ECD of KCC2 (65) or truncation of the NTD (57) of KCC2 can reduce KCC2 ion transport without affecting overall surface expression of the transporter. Structural studies have also shown how mutations or truncation of the inhibitory N-terminal peptide can also increase KCC2 ion transport without altering overall KCC2 expression, however, these studies do not verify if changes in surface expression underlie these changes in activity (60, 61). Post-translational modifications can also modify the intrinsic transport rate: the S932 and T1008A phosphorylation sites discovered by phosphoproteomics, when phosphorylated or dephosphorylated, respectively, can increase intrinsic KCC2 ion transport as well (70). Overall,

these findings underscore that intrinsic KCC2 ion transport can be directly modulated at the level of the transporter.

Together, these examples show a rich number of mechanisms that can dynamically regulate KCC2 activity in the developing or mature nervous system. These regulators help maintain proper nervous system function, or can contribute to pathology in disease states. Furthermore, these regulators all represent potential mechanisms by which pharmacological modulators of KCC2 could exert their effects on KCC2.

KCC2 inhibitor pharmacology

A number of small molecule inhibitors for KCC2 have been reported in the literature. These compounds have been instrumental in providing understanding of KCC2 function in biological systems and for deepening our understanding of molecular aspects of KCC2 function. The original K^+-Cl^- cotransport inhibitory activity for the first described KCC2 inhibitors were discovered serendipitously as off-target effects. In recent years, directed approaches to KCC2 inhibitory discovery have produced potent and specific KCC2 inhibitors which are used widely throughout the literature. The main classes of KCC2 inhibitor can be broken down into: loop diuretics, stilbene-containing compounds, (aryloxy)alkanoic acids, benzyl prolinates, and ML077-like compounds (Figure 1.4).

Loop diuretics, such as bumetanide (75) and furosemide (56), were some of the first described and widely used KCC2 inhibitors. These compounds were instrumental for the discovery and initial characterization of K^+-Cl^- cotransport in erythrocytes (97), and for functional validation of K^+-Cl^- cotransport after the cloning of KCC2 (56). However, these compounds are not suitable chemical probes for specifically targeting KCC2. Loop diuretics were originally discovered for their diuretic activity, downstream of their potent activity at NKCC1 (98); given the intimate relationship between Cl^- efflux mediated by KCC2 and Cl^- influx mediated by NKCC1,
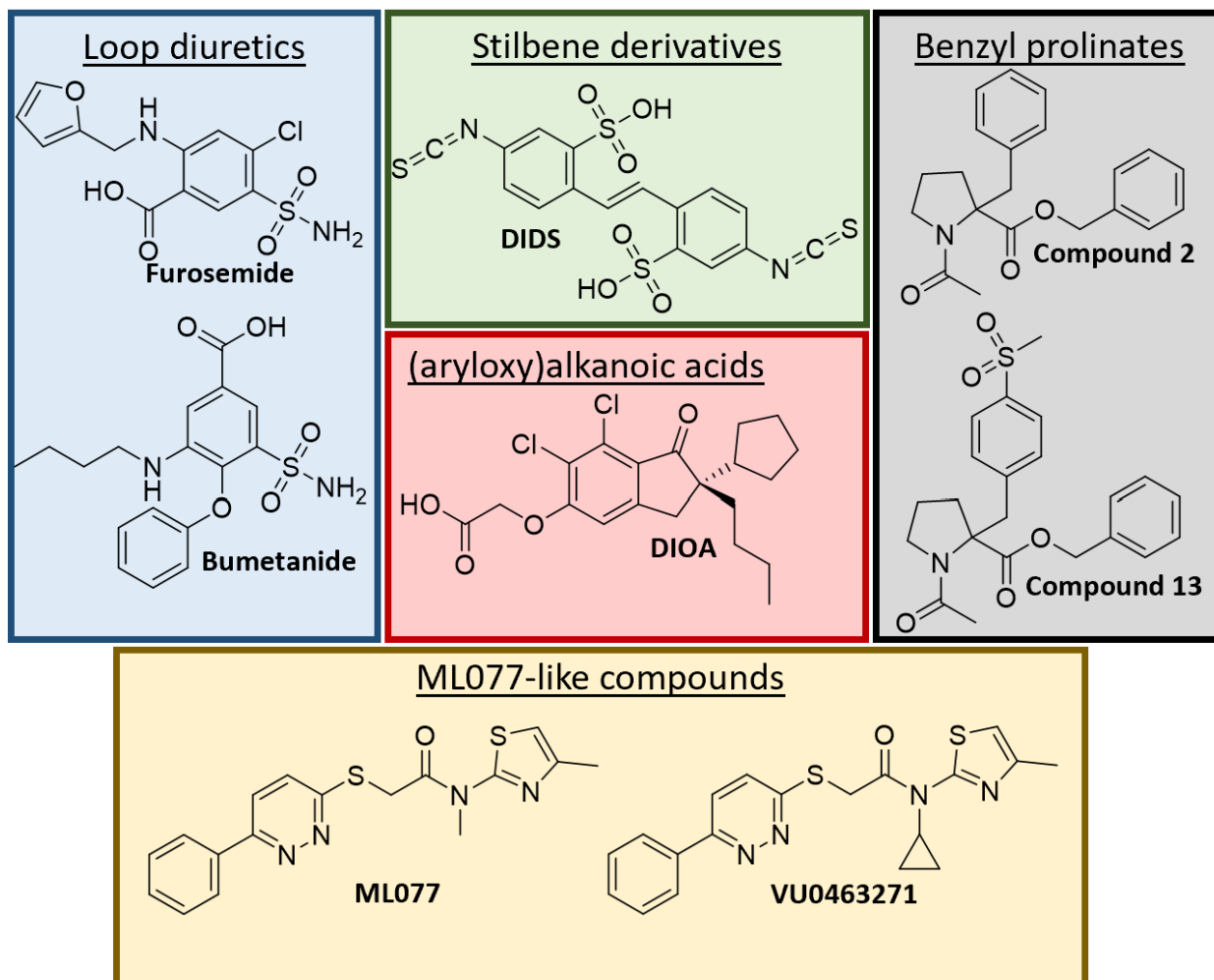
Figure 1.4. Major classes of small molecule KCC2 inhibitor.

this off-target activity is a major liability for selectively investigating the role of KCC2 in different biological systems. Furthermore, loop diuretics have low potency at KCC2 (e.g. bumetanide, IC_{50} = 0.5 mM) (75) and poor blood-brain barrier permeability (99), which further precludes their use as a selective tool compound to investigate KCC2 biology. Owing to their off-target effects at NKCC1 and low potency, these compounds are rarely used to inhibit KCC2 in recent studies.

Stilbene-containing compounds, such as 4,4'-Diisothiocyanostilbene-2,2'-disulfonic Acid (DIDS) (100), are another class of early KCC2 inhibitor. These compounds were used in studies of K^+-Cl^- cotransport in duck and sheep red blood cells and were important for investigating kinetics of K^+-Cl^- cotransport (100). However, these compounds have species specificity and are inactive on human KCC2 (101), in addition to having off-target effects on Cl^- channels, anion exchangers, and other targets (102). Owing to this chemical class's inactivity at human KCC2 and off-target effects on a number of other proteins important for electrical regulation in the nervous system, stilbene derivatives are also rarely used in recent reports to investigate KCC2 biology.

(aryloxy)alkanoic acids, such as [(dihydroindenyl)oxy]alkanoic acid (DIOA) (103), were the first KCC-selective inhibitors of K^+-Cl^- cotransport. These compounds were originally discovered as non-diuretic agents that could be used as a treatment for traumatic brain injury (104) and were found to be direct-acting (61) KCC-selective inhibitors without significant activity at NKCC1 (103). These compounds were important for demonstrating links between KCC2 inhibition and pathology, for example the link between KCC2 inhibition and spasticity after spinal cord injury (105). However, these compounds have a low potency for KCC2 (IC_{50} = 10 μM) and, likely owing to the large doses of compound used in experimental settings as a result of DIOA's low potency, cellular toxicity (103). Owing to the low potency of DIOA and toxicity associated with its use, this compound class is also not normally used to investigate KCC2 biology in light of the discovery of more potent, KCC-selective KCC2 inhibitors.

Benzyl prolinates, such as compound 2 and compound 13, were reported initially in 2010 by a group at *Union Chimique Belge* (UCB) (106). These benzyl prolinates were derived from

compounds discovered in a Rb^+ flux-based HTS campaign and were designed as selective inhibitors of KCC2 for use as tool compounds to investigate KCC2 biology. An initial medicinal chemistry effort, and subsequent follow up in 2012 to better define the benzyl prolinate pharmacophore (107), produced compounds with sub-micromolar potency (compound 13, IC_{50} = 400 nM) and selectivity for KCC2 over NKCC1 (compound 13, 35% inhibition at 100 μM on NKCC1). Furthermore, these compounds have the best pharmacokinetic properties reported for sub-micromolar KCC2 inhibitors, with compound 2 and compound 13 exhibiting a half-life ($t_{1/2}$) of 2.4 hours and 0.3 hours, respectively, together with a limited oral bioavailability (F) (compound 2 = 0.5%, compound 13 = 18%) (106). Despite the sub-micromolar potency and limited oral bioavailability of these compounds, they are rarely used in the literature. Use of these compounds is likely precluded by their lack of commercial availability.

ML077-like compounds, such as ML077 and VU0463271 (108), are selective and potent KCC2 inhibitors with widespread use throughout the literature. ML077 and its analogs have been used to investigate KCC2's physiological function in the nervous system (7, 46), together with demonstrating the pathological effect of KCC2 inhibition in a number of disease states, including epilepsy (46, 109), chronic pain (110), and spinal cord injury (16). This class of compounds was discovered through a Thallium (Tl^+) flux-based HTS campaign (75) and subsequent medicinal chemistry program (108) that were directed at finding selective and potent KCC2 inhibitors for use as probe compounds. These efforts yielded the first potent KCC2 inhibitors (VU0463271 IC_{50} = 61 nM) with >100-fold selectivity for KCC2 over NKCC1 (108). Subsequent studies illustrated direct binding between KCC2 and VU0463271 (59), and a recent cryo-EM structure has determined the binding mode of VU0463271 on a close KCC2 homolog, KCC1 (111). As seen by their widespread use, these compounds have been highly impactful on the KCC2 field and are excellent tool compounds for investigating *in vitro* KCC2 biology. However, the pharmacokinetic properties of these compounds limit their use *in vivo*. VU0463271, for example, has a serum $t_{1/2}$ of 9 minutes (108), which precludes its use as an *in vivo* probe, unless it is directly administered

to the target site (109). Because ML077-like compounds represent a significant advance for KCC2 inhibitor pharmacology and already have been instrumental in investigating KCC2 biology despite their lackluster pharmacokinetic properties, future studies aimed at improving their pharmacokinetics are warranted. ML077-like compounds with improved bioavailability and $t_{1/2}$ would be an asset to future studies aimed at investigating KCC2 activity.

KCC2 potentiator pharmacology

In contrast to KCC2 inhibitor pharmacology, KCC2 potentiator pharmacology is less firmly established. There have been promising advances in KCC2 potentiator pharmacology in recent years, but KCC2-selective and potent KCC2 potentiators that lack controversy are still highly sought-after in the field. The major classes of KCC2 potentiator are: alkylating agents, CLP257-like compounds, modulators of acute KCC2 regulators, and KCC2 expression–enhancing compounds (KEECs) (Figure 1.5).

Alkylating agents, such as NEM (90), were historically important in describing K^+-Cl^- in erythrocytes (112) and represent some of the first described small molecules capable of potentiating K^+-Cl^- cotransport. These compounds have pleotropic effects on cells, owing to their ability to nonspecifically alkylate certain functional groups, and are therefore not selective for KCC2 activity. NEM's activity at KCC2 is thought to be through its capacity to alkylate exposed thiols in kinases. The inhibition of these kinases is thought to induce a complicated change in KCC2 phosphorylation, driven in part by alterations in PKC and WNK phosphorylation, that produce the net effect of KCC2 potentiation (90, 113). Due to the highly nonspecific nature of alkylating agents such as NEM, these compounds are not useful chemical probes for investigating KCC2-specific biology.

CLP257-like compounds, such as CLP257 and CLP290 (10), are the first described compounds which are selective for KCC2 over other KCCs and NKCC1, have sub-micromolar
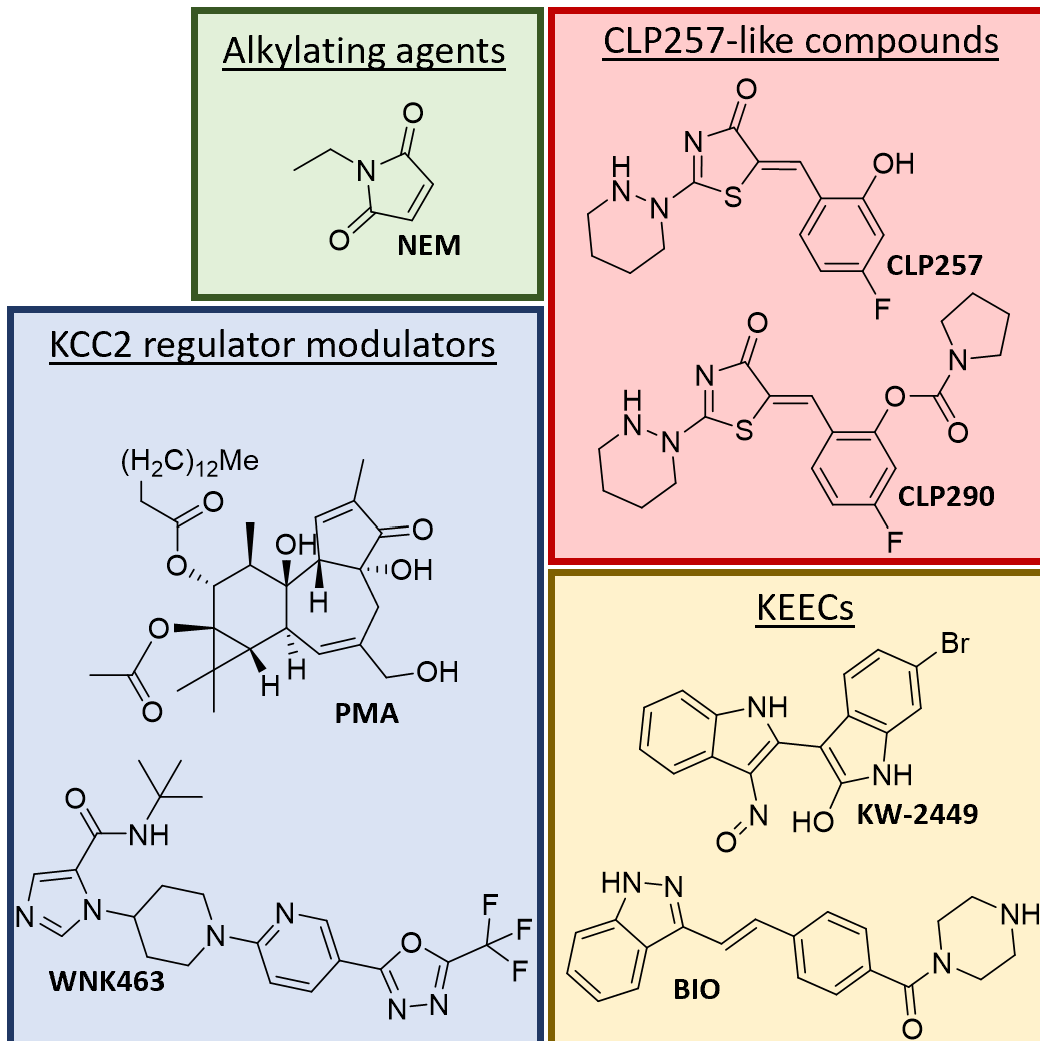
Figure 1.5. Major classes of small molecule KCC2 potentiator.

potency (CLP257 EC_{50} = 616 nM), and a pharmacokinetic profile suitable for *in vivo* use (10). These compounds were used in a number of studies supporting the therapeutic effect of KCC2 potentiation in chronic pain (10, 11) and paralysis after spinal cord injury (16, 114). However, these compounds have controversy surrounding their activity at KCC2. A letter with data supporting the conclusion that CLP257-like compounds act as $GABA_A$ potentiators, do not bind KCC2, and lack efficacy at KCC2 was published in the same journal as the CLP257 discovery paper (55), along with a rebuttal from the original authors (115). Therefore, there is doubt that these compounds are true KCC2 potentiators. A way to reconcile these pieces of contrasting data is that the CLP257 class may act indirectly on KCC2 through a currently undescribed KCC2 regulator. Regardless, while this compound still has some promise as a KCC2 potentiator, further research into its mechanism of action is required to mitigate concerns over its activity at KCC2.

Modulators of KCC2 acute regulators, such as the PKC-activating phorbol esters (66) and the WNK inhibitor WNK463 (116), can indirectly potentiate KCC2 activity through influencing KCC2 post-translational modification and PPIs. These indirect modulators have been important for establishing the regulatory network that KCC2 is embedded in and for demonstrating how alterations in KCC2 to regulation can affect KCC2 activity in different disease states. For example, small molecule modulation of PKC phosphorylation helped link PKC phosphorylation and KCC2 potentiation *in vitro* (66) and *in vivo* (45). Furthermore, receptor tyrosine kinase modulators, such as the TGFBR1/2 agonist TGF-β (91), can also act as indirect KCC2 potentiators through influencing PPIs which increase KCC2 activity. However, since all of the described KCC2 regulators to date also have pleotropic effects on cells outside of their actions on KCC2, these compounds are also not ideal for interrogating the effects of KCC2 ion transport on biological systems.

KEECs, such as the fms-like tyrosine kinase 3 (FLT3) inhibitor KW-2449 or glycogen synthase kinase 3β (GSK3β) inhibitor BIO (14), are compounds which indirectly promote increases in KCC2 expression. These compounds have recently been used to illustrate that

pharmacological increases in KCC2 expression are capable of ameliorating symptoms in a model of Rett syndrome (14). Moreover, these compounds, which are by and large repurposed drugs, also have exciting translational relevance: the safety and pharmacokinetics of these compounds have already been established in the clinic, thereby lowering the barrier required to translate these findings to a clinical setting. However, from a basic science perspective, these compounds are also not ideal as chemical probes. The targets they modulate, for example FLT3 and GSK3β, have multiple effects on hematopoiesis (117) and glycogen metabolism (118), respectively, and therefore have extensive effects on cells independent of their activity on KCC2. The KCC2-independent activity of these compounds complicates the interpretation of experiments where KEECs are used to increase KCC2 activity. Nonetheless, these compounds are important advances in KCC2 pharmacology and are useful for proof-of-concept studies.

Although these compounds represent excellent progress in the discovery of KCC2 potentiators, and illustrate proof-of-concept for the therapeutic potential of KCC2 potentiation in some disease areas, the discovery of selective, potent KCC2 potentiators is still warranted. Discovery of KCC2-selective potentiators is essential to better define if the therapeutic effects of KCC2 potentiation were due solely to KCC2 or if they were due, in part, to off-target liabilities of current KCC2 potentiators. Furthermore, the discovery of potentiators selective for different functions of KCC2 activity, i.e. its ion-transport and its scaffolding function, could help better define the mechanistic basis behind the therapeutic effects seen in studies using KCC2 potentiators. Lastly, the development of improved, selective KCC2 potentiators with adequate pharmacokinetic properties would directly aid the development of KCC2-directed therapeutics for debilitating diseases linked to deficits in KCC2 activity.

CHAPTER 2

SMALL MOLECULE KCC INHIBITION PROMOTES SEIZURE-LIKE ACTIVITY IN INSECTS[1]

Abstract

The insect nervous system, especially that of *Drosophila melanogaster*, is an important model system for the study of human health and disease. Fast inhibitory neurotransmission is a crucial regulator of electrical activity in the human central nervous system (CNS) that is readily modeled in insects. The effectors of fast inhibitory neurotransmission are ligand-gated Cl^- channels, such as the GABA receptor (GABA-R) in insects, which control the flow of Cl^- across the plasma membrane in neurons. In the mature nervous system, fast inhibitory neurotransmission requires a Cl^- gradient with low $[Cl^-]_i$, such that ligand-gated Cl^- channel activation results in an influx of Cl^- and neuronal hyperpolarization. In insects, the K^+-Cl^- cotransporter KCC is responsible for the efflux of Cl^- required to maintain low $[Cl^-]_i$. Hence, the interplay between KCC function, to maintain low $[Cl^-]_i$, and GABA-R function, to hyperpolarize neurons in response to inhibitory signaling, is critical for fast inhibitory neurotransmission, and is therefore critical for proper electrical regulation in the nervous system and proper nervous system function. Despite the centrally important role that the interplay between KCC and GABA-R function has to shaping neural activity patterns, the coupling between KCC and GABA-R function in insects has been understudied. To remedy this gap in knowledge in the field, we characterized KCC's function at the ion transport level, and used electrophysiological, genetic, and

---

[1] This chapter is adapted from the two publications that resulted from this work: Prael III et al. (135) and Chen et al. (146).

pharmacological methods to characterize KCC and GABA-R physiology in the insect nervous system. We discovered that (a) genetically and pharmacologically decreased KCC activity reduces the insect CNS response to GABA and leads to excess electrical activity in the insect CNS, and (b) submaximal KCC and GABA-R inhibition produces a synergistic effect that was consistent with perturbed inhibitory neurotransmission, which represent the first evidence directly supporting functional KCC-GABA-R coupling in the insect CNS. Additionally, beyond acting as a model system, insects also directly impact human health as vectors of human disease and as agricultural pests. Human disease vectors and agricultural pests are managed by insecticides, many of which function by causing unregulated electrical activity in the insect nervous system. However, growing insecticidal resistance is undermining control efforts. The discovery of new insecticidal mechanisms is therefore urgently needed. Building off of our fundamental study of KCC and GABA-R coupling in inhibitory neurotransmission, where our data suggested that KCC inhibition would cause unregulated electrical activity, we discovered that administration of a KCC inhibitor to a known vector of human disease, *Aedes aegypti*, is insecticidal. Together, our findings advance the basic understanding of CNS function in an important model system for human disease, and provide a new insecticidal mechanism which may be useful for control of vectors of human disease and agricultural pests.

Introduction

γ-aminobutyric acid (GABA) is the principal inhibitory neurotransmitter, and GABAergic signaling is responsible for shaping the neural activity patterns in insect and mammalian systems (119). Consistent with the importance of GABAergic signaling to normal central nervous system (CNS) function, drugs increasing the activity of the GABA receptors (GABA-R) and GABA-receptor-chloride-channel (GRCC) complexes are common therapeutics for a variety of human neurological disorders (120–124), and small molecules inhibiting GABA-R function are widely

used as insecticides, acaricides, and anthelmintics (125–129). Furthermore, the conservation of GABAergic signaling between humans and insects has made insect model systems, such as *Drosophila melanogaster*, important tools for the study of GABAergic signaling.

Cation-chloride cotransporters are critically important to GABAergic signaling, as they are essential for generating Cl^- gradients that $GABA_A$ receptors require to regulate electrical activity throughout the nervous system (73, 130). Furthermore, cation-chloride cotransporters are important to a multitude of biological processes outside of GABAergic signaling, including cell volume homeostasis and transepithelial fluid secretion (131). Despite cation-chloride cotransporter importance to GABAergic signaling (132, 133), and the utility of insects for modeling GABAergic signaling, cation-chloride cotransporters have received little attention within insect systems. In insects, KCC is a K^+-Cl^- cotransporter which uses the electrochemical gradient of K^+ for secondary active efflux of Cl^- across the plasma membrane (56, 134, 135). The limited studies on KCC biology in insects have shown that KCC inhibition decreases transepithelial fluid secretion in *Rhodnius prolixus* (136, 137), *Drosophila melanogaster* (138), and *Aedes aegypti* (135, 139) Malpighian tubules. In terms of GABAergic signaling, KCC has been shown to be expressed throughout the neuropil of adult *Drosophila*. Furthermore, functional studies have demonstrated that KCC is critical for neurotransmission as well: (i) in *Drosophila*, partial loss-of-function mutations to *kazachoc*, the gene that codes for KCC, increased seizure susceptibility in adult flies (140); and (ii) in *Aedes aegypti*, pharmacological inhibition of KCC with VU0463271, a small molecule KCC inhibitor, resulted in hyperexcitatory behavior and mortality in larval and adult female mosquitos (135). The seizure-like activity seen with genetic or pharmacological KCC inhibition was thought to be a result of a decrease in synaptic strength through reduced $GABA_A$ receptor-mediated hyperpolarization, which was shown to be the case for inhibition of the mammalian homolog of KCC, KCC2 (8, 141, 142). However, evidence illustrating a functional link between KCC and GABA-R in insects was currently lacking. Investing the functional link between

31

KCC and GABA-R is therefore important to deepen the understanding of GABAergic signaling in insects, which is critically important for their use as a model system.

In addition to the utility that insects have as a model system, insects can have a pathological effect on human wellbeing through their roles as vectors of disease and agricultural pests; insecticides are regularly used to control these deleterious interactions between agriculture/human health and insects. Ligand-gated Cl^- channels are of critical importance to insect control: ligand-gated Cl^- channel-directed insecticides represent the majority of molecules approved for the management of insect ectoparasites of companion animals (143). However, mounting insecticidal resistance is eroding our capacity to control insect vectors of disease and agricultural pests (144). The discovery of novel insecticides is therefore of paramount importance. Given the demonstrated efficacy of Cl^- channels for insect control, the critical importance KCC has for Cl^- channel function, and the link between KCC and seizure-like activity, inhibition of KCC is a promising new insecticidal mechanism that requires validation.

To further the basic understanding of the functional link between KCC and GABA-R in insects, together with investigate a promising new insecticidal mechanism, we used pharmacological and electrophysiological methods to study the effect of KCC inhibition on insect physiology. Using cell-based methods, we were the first to characterize the function of recombinant *Drosophila melanogaster* and *Aedes aegypti* KCC and developed an assay suitable for discovering new pharmacological inhibitors of KCC using high-throughput methods. Through our efforts, we discovered chemical probes useful for interrogating KCC activity *ex vivo* and *in vivo*. Using electrophysiological methods in *Drosophila melanogaster*, we demonstrated the functional dependency of GABA-R to KCC activity, established the synergistic link between KCC inhibition and GABA-R inhibition, and we illustrated the link between genetic and pharmacological perturbation of KCC activity to excess electrical activity in the insect CNS. Lastly, we demonstrated the insecticidal potential of KCC to a vector of human disease, *Aedes aegypti*, by demonstrating that pharmacological KCC inhibition disrupts KCC biology and induces dose-

dependent lethality in mosquitos. These data are consistent with previous observations of KCC in insects (134, 145), and expand these foundations by improving the molecular and electrophysiological contribution of KCC to nervous system function. Additionally, our results establish a new insecticidal mechanism, KCC inhibition, that can be used to sensitize insects to current insecticides at low doses and is insecticidal in its own right at higher doses. Our work with this novel insecticidal mechanism is critically important to circumvent mounting insecticidal resistance, and therefore to the control of insect vector borne disease and agricultural pests.

Methods

Compounds and compound synthesis

VU0463271 was acquired from Tocris Bioscience, and 44BD was synthesized as described previously (75) and solubilized in dimethyl sulfoxide (DMSO) (MilliporeSigma).

Insect stocks and rearing conditions

Five strains of *D. melanogaster* were used in this study. The wild type Oregon-R (OR) strain was provided by Dr. Jeffrey Bloomquist at the University of Florida, Gainsville, FL, and was originally donated by Doug Knipple, Cornell University, Ithaca NY. The cyclodiene-resistant (*rdl*-1675) strain was purchased from the Bloomington Drosophila Stock Center at Indiana University, Bloomington, IN. All GAL4-UAS fly strains were purchased from Bloomington Drosophila Stock Center. The GAL4-UAS strain 3739 expresses the Gal-4 pattern in the brain of third instars with strong expression throughout the CNS, but not in the disks. The strain 34584 expresses dsRNA for RNAi of KCC (FBgn0025698) under UAS control. The strain 41554 expresses hairpin RNA (hpRNA) under the control of UAS for RNAi of GFP and was used as a negative knockdown control. The genotypes of each strain are as follows: **3739**, P(w[+mW.hs]=GawB)c698a, w[1118];

34584, y[1] sc[*] v[1]; P{y[+t7.7] v[+t1.8]=TRiP.HMS01058-attP2; **41554**, y[1] sc[*] v[1]; P(y[+t7.7] v[+t1.8]=VALIUM20-EGFP.shRNA.2)attP2.

All fly strains were maintained in culture at Louisiana State University Agricultural Center (Department of Entomology) and were reared on standard medium in *Drosophila* tubes at 25 °C, 12 h/12 h photoperiod, and 55% relative humidity. For dissection, flies were anesthetized by chilling on ice and decapitated before dissecting out CNS in Schneider's medium (Invitrogen, Paisley, Scotland, UK).

An established colony of *Ae. aegypti* mosquitoes, Rockefeller strain, was reared and maintained in an environmental chamber at 28 °C and 70% relative humidity with a 12:12 dark and light cycle at Louisiana State University (Baton Rouge, LA, USA). Mosquitoes were originally provided by Dr. Todd Walker at the East Baton Rouge Mosquito Control and Abatement.

HEK-293 cell culture

Monoclonal, HEK293 cells were grown to 80%–90% confluence in TC-treated T75 flasks containing 1x α-MEM (Corning) 10% (v/v) fetal bovine serum (FBS) and 1x glutagro (Corning) [cell culture medium] with appropriate antibiotic selection (see Monoclonal cell line generation section below). Cells were passaged before they reached >90% confluence, for a maximum of 20 passages.

Molecular cloning

We created a vector suitable for stable expression of *Dm*KCC in human embryonic kidney 293 (HEK293) cells by cloning the ORF of *D. melanogaster* KCC variant B (NCBI Reference Sequence: NM_166632.2) into pcDNA3.1/Zeo(+) (ThermoFisher Scientific). A clone containing the KCC ORF was purchased from the *Drosophila* Genomics Resource Center (Bloomington IN; stock number: 4659). Polymerase Chain Reaction was used to amplify the ORF while adding 5′ XbaI and 3′ *Hin*dIII restriction sites for cloning into the pcDNA3.1/Zeo(+) backbone. The backbone

and the ORF PCR product were digested with XbaI and *Hin*dIII (New England Biolabs) and the ORF was ligated into the backbone using New England Biolabs Quick Ligation kit. The ligated DNA was transformed into chemically competent DH5α *E. coli*. The resulting plasmid DNA was purified (Qiagen) and the sequence was confirmed by Sanger sequencing (GenHunter).

We generated a vector suitable for stable expression of *Aa*KCC in human embryonic kidney 293 (HEK293) cells by cloning the ORF of *Aa*KCC1-A1 (147) (GenBank accession number HM125960.1) into pCMV6-A-Hygro (OriGene, Rockville, MD). The *Aa*KCC ORF was synthesized in gBlocks Gene Fragments (Integrated DNA Technologies, Skokie, Illinois) with appropriate ends for Gibson Assembly (148) into pCMV6-A-Hygro. The pCMV6-A-Hygro backbone was digested with *Asi*SI and *Mlu*I (New England Biolabs) and the *Aa*KCC fragments were cloned into the digested backbone using Gibson Assembly Master Mix (New England Biolabs). The assembled DNA was transformed into DH5α *E.coli* (Vanderbilt Molecular Cell Biology Resource Core). The resulting plasmid DNA (*Aa*KCC-pCMV6-A-Hygro) was purified with commercial kits and its sequence was confirmed by Sanger sequencing (GenHunter).

Monoclonal cell line generation

HEK293 cells (ATCC) were plated in a TC-treated T75 flask at 40% confluence and cultured in cell culture medium. The HEK293 cells were transfected with 7 µg of *Dm*KCC-pcDNA3.1/Zeo(+) DNA using Fugene6 (Promega) following the manufacturer's instructions. At 48 h after transfection, the cells were put under selection using 250 µg/mL Zeocin (ThermoFisher Scientific). After 2 weeks of Zeocin selection, the polyclonal cells were plated in 96 well plates at ~1 cell per well. The most promising monoclonal cell lines were selected based on the magnitude of KCC inhibitor-sensitive Tl$^+$ influx (see below) and proliferative capacity relative to untransfected HEK293 cells. These cell lines were expanded into TC-treated T25 flasks and retested for activity using Tl$^+$ flux and KCC inhibitors. The monoclonal cell line used in this paper (1D4) was selected based on its large KCC inhibitor-sensitive Tl$^+$ flux and robust growth characteristics. KCC

35

expression in the 1D4 monoclonal cell line was confirmed by Western blotting. After selection, the 1D4 cell line was cultured continuously in 250 µg/mL Zeocin

HEK293 cells were plated in a TC-treated T75 flask at 40% confluence in cell culture medium and transfected with 7 µg of *Aa*KCC-pCMV6-A-Hygro DNA using Fugene6 (Promega) following the manufacturer's instructions. Forty-eight hours after transfection, 250 µg/mL hygromycin (Corning) was added to the medium. After two weeks of hygromycin selection, the polyclonal cells were dislodged from the flask using TrypLE Express (ThermoFisher Scientific) collected, counted, and plated in 96 well plates at ~1 cell per well in 80 µL/well cell culture medium containing 250 µg/mL hygromycin. Monoclonal cell lines were assayed using Tl$^+$ influx (see below) and known KCC-family inhibitors, bumetanide and VU0463271 (75) to assess *Aa*KCC expression. The monoclonal cell line (1F4) was selected based on the magnitude of KCC inhibitor-sensitive Tl$^+$ influx relative to untransfected HEK293 cells. KCC expression in the 1F4 monoclonal cell line was confirmed by Western blotting. After selection, the 1F4 cell line was cultured continuously in the presence of 250 µg/mL hygromycin.

Tl$^+$ influx assay for insect KCC

Tl$^+$ flux assays were performed based on previously described methods (75). The day before the experiment, cells were plated in black-walled, clear-bottom, 384 well PureCoat amine-coated plates (Corning) at a concentration of 20,000 cells/well. On the day of the experiment, the HEK293 Cell Culture Medium was removed and replaced with 20 µL/well of Hank's Buffered Salt Solution (ThermoFisher Scientific) plus 20 mM HEPES-NaOH, pH 7.3 (Assay Buffer) containing 1.25 ng/µL Thallos-AM plus 0.02% (v/v) final Pluronic F-127 (MilliporeSigma) (Dye Loading Solution). Cells were incubated in Dye Loading Solution for 1 h at room temperature in the dark. After incubation, the Dye Loading Solution was replaced with 20 µL/well Assay Buffer. Compound serial dilutions were made in DMSO (MilliporeSigma) and then transferred to Assay Buffer at 2-fold above the final desired concentration. Tl$^+$ flux was measured using the Panoptic (Wavefront

Biosciences) kinetic imaging plate reader (1 Hz, excitation 480/40, emission 538/40). Following collection of 10 frames of baseline images, imaging continued with the addition of 20 µL/well of 2× compound solution. After four minutes of incubation with continuous imaging, 10 µL/well of 125 mM sodium bicarbonate, 12 mM thallium sulfate, 1 mM magnesium sulfate, 1.8 mM calcium sulfate, 5 mM glucose, and 10 HEPES-NaOH (pH 7.3) (MilliporeSigma) were added to the cells and imaging was continued for two additional minutes.

For analysis of Tl^+ influx studies, fluorescence values were normalized on a well-to-well basis by dividing the fluorescence values at each time point to the average of the baseline fluorescence values (F/F_0) for a given well. The slope of the fluorescence increase between 1 and 86 s after Tl^+ addition was used as a measure of Tl^+ flux. The slopes of the change in fluorescence in the absence of inhibitor were designated as 100% KCC activity and slopes obtained in the presence of a maximally effective concentration of 10 µM were designated as 0% KCC activity. To compare the effect of DMSO on DmKCC-mediated Tl^+ flux, a one-way ANOVA was performed with a Tukey's multiple comparison test. The potency of test compounds was determined by fitting slopes obtained at compound concentrations varying over a range of 10 µM to 0.03 nM using a four-parameter logistic equation with GraphPad Prism. For a given experiment, all conditions were tested in six wells per plate. Values reported are averages of those obtained from three independent experiments ± standard error of the mean (SEM).

Rb^+ influx

D. melanogaster KCC-expressing cells (1D4) were grown to confluence in 10 cm dishes with 10 mL of DMEM:F12 (Invitrogen) supplemented with 10% (v/v) FBS (Atlanta Biologicals), 180 U/mL penicillin + 180 U/mL penicillin + 250 µg/mL zeocin, at 37 °C 95% air, 5% CO_2. The day of the flux experiment, cells from 3 × 10 cm dishes were detached with trypsin and resuspended into 50 mL of complete medium, and 2 mL of homogeneous suspension was added to 24 × 35 mm dishes precoated with 0.1 mg/mL poly-l-lysine (MilliporeSigma). The cells were

allowed to attach for 2 h in the incubator. For the rubidium uptake experiment, the medium was aspirated and replaced with 1 mL isosmotic saline containing 140 mM NaCl (or *N*-methylglucamine Cl for Na$^+$-free solution), 5 mM KCl, 2 mM CaCl$_2$, 0.8 mM MgSO$_4$, 2 mM glucose, 200 µglouabain, 2.5 mM HEPES, pH 7.4, 310 mOsM, for a 15 min preincubation period. For the hypotonic saline, the concentration of NaCl (or NMDG-Cl) was reduced to 100 mM. After preincubation, the saline was aspirated and replaced with 1 mL of an identical solution containing 1 µCi/ml ^{86}Rb (PerkinElmer) for 15 min. After the uptake period, the medium was aspirated and the cells were washed three times with 1 mL of ice-cold saline. Following the rinse, the cells were lysed with 500 µL of 0.25 N NaOH for 1 h and then neutralized with 250 µL of glacial acetic acid. Aliquots of 300 µL in 5 mL of Biosafe-II liquid were utilized for β-scintillation counting using a Tri Carb 2910-TR, (PerkinElmer), and 20 µL for Bradford protein assay, respectively. Two aliquots of 5 µL of uptake solution were also counted per condition to transform the measured cpm into pmol K$^+$. The K$^+$ influx was expressed as pmol K$^+$ × mg protein^{-1} × min^{-1}.

Insect KCC Western blotting

HEK293, *Dm*KCC-expressing monoclonal HEK293 cells (clone 1D4), and *Aedes aegypti* KCC-expressing HEK293 cells (clone 1F4) were grown to 90% confluence in 150 mm TC-treated dishes (Corning) in cell culture medium. Cells were washed in ice-cold phosphate buffered saline (Corning), mechanically dissociated from the culture dishes, and transferred to prechilled conical tubes on ice. Cells were pelleted at 500 rcf for 2 min and resuspended in extraction buffer containing 50 mM HEPES, 10 mM dithiothreitol, 5 mM EDTA, 150 mM KCl, 1× Halt Protease Inhibitor Cocktail (TheromoFisher Scientific). Cells were triturated with a p1000 pipet to achieve a single-cell suspension and lysed by vortexing and sonication. The lysates were then clarified by centrifugation for 8 min at 3800 rcf at 4 °C. To isolate membranes, the supernatants from the previous step were ultracentrifuged at 132,000xg for 1 h at 4 °C. The pellets from the ultracentrifugation step were resuspended in ice-cold extraction buffer (membrane fraction) and

stored at −80 °C until use. Membrane fractions were diluted in Laemmli sample buffer (Bio-Rad) at room temperature to prevent protein aggregation and separated by SDS-PAGE on a NuPAGE Novex 4–12% Bis-Tris protein gel using the XCell SureLock Mini-Cell system (TheromoFisher Scientific) according to the manufacturer's instructions. Separated proteins were transferred to an Odyssey nitrocellulose membrane (LI-COR) using the XCell II Blot Module at 25 V for 1 h at RT, according to the manufacturer's instructions. Membranes were then rinsed in Tris buffered saline (TBS) (Corning) and blocked in 5% dry milk (w/v) (Bio-Rad) in TBS. Membranes were then rocked in a 1:2000 dilution of a rabbit anti-KCC antiserum in 5% dry milk (w/v) in TBS + 0.1% (v/v) Tween20 (TBS-T) (MilliporeSigma) at 4 °C overnight. Membranes were then washed 3× times in TBS-T, rocked in a 1:15,000 dilution of donkey anti-rabbit IRDYE800CW secondary antibody (LI-COR) for 1 h at room temperature and then washed 3× additional times in TBST. Finally, membranes were then rinsed in TBS and visualized on the Odyssey CLx near-infrared fluorescence imaging system (LI-COR). The anti-KCC antiserum was derived against a C-terminal KCC epitope conserved from *D. melanogaster* KCC to human KCC1–4 as previously described (134).

Electrophysiology on *Drosophila melanogaster* neural systems

Neurophysiological recordings were performed on the CNS of third instar *D. melanogaster* as described previously (149). Glass pipet electrodes were pulled from borosilicate glass capillaries on a P-1000 Flaming/Brown micropipet puller (Sutter Instrument). The CNS was excised from the larvae and placed in a separate dish with physiological saline (200 µL) containing 157 mM NaCl, 3 mM KCl, 2 mM CaCl$_2$, and 4 mM HEPES, pH = 7.25. The CNS was manually transected posterior to the cerebral lobes to disrupt the blood-brain barrier and enhance chemical penetration into the CNS (150, 151). Peripheral nerve trunks were drawn into a recording suction electrode and electrical activity was monitored from descending nerves originating from the CNS, with amplification by an AC/DC amplifier (Model 1700, A-M Systems). Descending electrical

activity was subjected to window amplitude discrimination and converted online into a rate plot, expressed in hertz (Hz), using LabChart7 Pro (ADInstruments). Noise (60 Hz) was eliminated using Hum Bug (A-M Systems). Activity was monitored for a 5 min time period to establish a constant baseline firing rate, as the spike frequency typically increased from 0 to 5 min before stabilization. After a baseline was established, the CNS preparation was directly exposed to test compounds by adding 200 µL of solution to the bath containing 200 µL of saline. The final concentration of solvent in the bath was 0.1% (v/v) DMSO. Frequencies were measured for 3–5 min for each concentration prior to the addition of the next drug concentration. Mean spike frequencies for each concentration were used to construct concentration–response curves to determine EC_{50} values were calculated by nonlinear regression (variable slope) using GraphPad Prism (GraphPad Software). Each drug concentration was replicated 5–10 times.

As with the CNS recordings, the sensory recordings were also performed on third instar *Drosophila melanogaster* with the same suction electrodes. The fat body, digestive system, and central nervous system were removed from the body to ensure nonsynaptic activity was recorded. After dissection was complete, a peripheral nerve trunk containing sensory nerve axons was drawn into a recording suction electrode. Activity was monitored for a 5 min time period to establish a constant baseline of spike activity. The inhibitors were applied directly to the larval body cavity and the final concentration of DMSO never exceeded 0.1%. (v/v) Each concentration was recorded for 3 min or until the spike frequency became constant. Mean spike frequencies for each concentration were analyzed identically to those of the CNS recordings.

Genetic knockdown of Drosophila melanogaster KCC

The GAL4-UAS system was used for tissue specific genetic ablation of KCC. The GAL4-UAS construct binds next to the gene of interest, which in this case is hairpin RNA (hpRNA) for KCC, to genetically enhance or decrease mRNA expression (152–154). The two components, GAL4 and UAS, are carried in separate *Drosophila* stocks that allow for hundreds of combinatorial

possibilities after a simple parental cross. In this study, we utilized a strain of fly that expressed the GAL4-UAS promoter only in the CNS of third instars, which is the lifestage analyzed using electrophysiological methods. These methods enabled the CNS-specific knockdown of KCC.

A schematic representation of the cross that enabled CNS specific knockdown of KCC is described by St. Johnston (155). Knockdown was achieved by crossing virgin females from the respective KCC RNAi strain (Bloomington stock 34584) with males from the CNS expressing GAL4-UAS strain (Bloomington stock 6870). The flies were given 96 h to mate and oviposit prior to removal from the growing medium. F_1 offspring were allowed to reach the wandering stage and these maggots were used in electrophysiological recordings.

RNA isolation and quantitative PCR

RNA isolation, cDNA synthesis and qRT-PCR were performed as described in our previous studies (149). Briefly, total RNA was isolated and extracted from 30 *Drosophila* larvae CNS using TRIzol Reagent (Life Technologies) and purified using the RNeasy kit (Qiagen). First-strand cDNA was synthesized from poly(A) RNA using the SuperScript III First-Strand Synthesis system for real-time quantitative PCR (qRT-PCR) (ThermoFisher Scientific) according to manufacturer instructions. qRT-PCR was then performed on an Qiagen Rotor Gene Q 2Plex Real-Time PCR system using the operating instructions. Relative quantification was carried out using the $2^{-\Delta\Delta CT}$ method (156), and β-actin was used as the reference gene. Appropriate controls, such as DNase and removal of reverse transcriptase, were performed to ensure the sample was not contaminated with genomic DNA. The *kcc* primers used in this study were identical to previous work (134) and were as follows: forward: 5′-CCAGAAGAGCATACCCATCG and reverse: 5′-AATGATGGCCATTCCCATAG. β-Actin was the housekeeping gene used as a standard, and actin primers were purchased from Life Technologies with primer reference numbers of Dm02361909_s1. Five biological replicates were conducted and each was analyzed in triplicate.

The graphed output displays average fold-change in mRNA levels relative to the wild type Oregon-R control CNS.

Aedes aegypti toxicology experiments

For topical toxicity assays of adult mosquitoes, the method of Pridgeon et al. (157) was used with slight modifications. Briefly, mosquitoes were chilled on ice for 3 min, during which 200 nL of chemical (dissolved in 95% (v/v) ethanol) was applied onto the pronotum using a handheld microapplicator (Hamilton Co.). For each chemical, 5 doses with 10 mosquitoes per dose was repeated 2–3 times using different batches of mosquitoes.

For injection toxicity assays of adult mosquitoes, chemicals were dissolved in DMSO and adult female mosquitoes were anesthetized on ice to enable manipulations. The mosquito was impaled through the metapleuron using a pulled-glass capillary attached to a Nanoliter2010 with Micro 2 T injection system (World Precision Instruments). Each mosquito received a single injection of 69 nL of solution containing the chemical or DMSO (control). The injection solution consisted of a calcium-free phosphate-buffered saline (ThermoFisher Scientific). DMSO concentrations did not exceed 1% (v/v) in the highest dose administered. After injection, mosquitoes were placed into 20 × 20 × 20 cm screen cages within a rearing chamber, and allowed free access to 10% (w/v) sucrose. Mortality was assessed at 24 h post injection. ID_{50} determinations were based on testing at least nine test compound doses that consisted of three replicates of 10 adults per concentration, which was repeated on three separate cohorts. Each concentration consisted of at least 90 individuals.

We used two distinct larval toxicity bioassays to assess pharmacokinetics of KCC modulators and toxicity. First, we employed a 24 h bioassay on intact larvae to determine if compounds could penetrate the integument to cause toxicity. Methods followed those described previously (158). Ten fourth instar larvae per treatment condition were placed in dishes containing a larval saline that consisted of: 154 mM NaCl, 2.7 mM KCl, 1.8 mM $CaCl_2$, 1.2 mM $NaHCO_3$,

(pH 6.9) plus DMSO or with test compound dissolved in DMSO. Larvae were observed after 1 h for any immediate toxic effects. Larvae were evaluated after 24 h of exposure by providing a mechanical stimulus to determine paralysis, which was determined by a body wall contraction or any movement. A lack of movement or contractility to the mechanical stimulus was scored as dead. LC_{50} determinations were based on testing at least six test compound concentrations that consisted of three replicates of 10 larvae per concentration, which was repeated on three separate cohorts. Mortality data for each concentration were pooled for each cohort and three LC_{50} values were determined and the average was determined between the 3 replicates. The LC_{50} was determined using GraphPad Prism (GraphPad Software). Each concentration consisted of at least 90 individuals.

For the second larval toxicity assessment we employed a headless larva bioassay to circumvent the problem of low cuticular penetration and provide a better estimate of the intrinsic toxicity of test compounds (159). These methods were performed as previously described in Islam and Bloomquist (159). Decapitation of 4th instar larvae was performed with forceps. The larvae were then placed into a test compound/vehicle/saline solution and observed for toxic effects every hour for a period of 5 h. Headless larvae show a strong bilateral contractile motion when probed and therefore, mortality was defined by no movement or a sluggish, unilateral contractility. Mortality was assessed at 1-, 3-, and 5- h after initial removal of the head. Vehicle controls were performed for each test compound concentration and data were discarded if control mortality exceeded 10%.

Aedes aegypti diuresis experiments

The excretory capacity of adult female *Ae. aegypti* (LVP strain) was measured as described previously (160, 161). Groups of 10 mosquitoes were injected with 200 nL of VU0463271 (1 µg/mg mosquito), 44BD (100 µg/mg mosquito), or 1% DMSO (v/v) 2 h before injecting the hemolymph of each mosquito with 69 nL of a potassium-enriched, phosphate-

buffered saline (K$^+$-PBS). The K$^+$-PBS consisted of the following (in mM): 92.2 NaCl, 47.5 KCl, 10 Na$_2$PO$_4$, and 2 KH$_2$PO$_4$ (pH 7.5). Each treatment group of mosquitoes was transferred into a separate graduated, packed-cell volume tube (MidSci) and incubated for 1 h at 28 °C. The volume excreted by the mosquitoes was measured visually *via* the graduated column at the bottom of the tube. For each treatment, 40 female mosquitoes were exposed to the chemical. These treatments were repeated on four separate broods. The mean volume excreted for each individual cohort was averaged and plotted. All mosquitoes were confirmed to be alive at the end of 1 h and any dead mosquitoes were discarded. The mean ($n = 4$) volumes excreted by vehicle-, VU0463271-, furosemide (MilliporeSigma)-, and 44BD-treated mosquitoes were analyzed using a one-way ANOVA with a Newman-Keuls *post hoc* analysis using GraphPad Prism.

Results

Coupling of KCC and GABA-R function in *Drosophila melanogaster*

We first sought to determine the inhibition potency of the mammalian KCC2 inhibitor VU0463271 and the structurally related analogue, 44BD (Figure 2.1) to *Drosophila melanogaster* KCC (*Dm*KCC). To quantify the activity of small molecules on *Dm*KCC, we developed a thallium (Tl$^+$) flux-based assay that measures *Dm*KCC ion transport across the plasma membrane (Figure 2.2.A.). Our assay uses a Tl$^+$-sensitive dye to measure the influx of Tl$^+$, a K$^+$ congener, to quantify the amount of KCC substrate transport in cells stably expressing KCC. We expressed *Dm*KCC isoform B, one of the most highly expressed KCC isoforms in the adult *Drosophila* nervous system, (134) in HEK293 cells. To increase the reproducibility of the assay, we isolated monoclonal cell lines stably expressing *Dm*KCC. Of the dozens of clones isolated, clone 1D4 had the largest basal Tl$^+$ flux, consistent with strongest overexpression of KCC (Figure 2.2.B). To verify that this

VU271

44BD
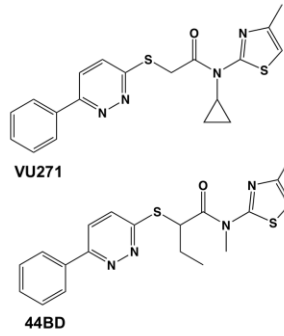
Figure 2.1. Chemical structures of pharmacological agents used in this study.
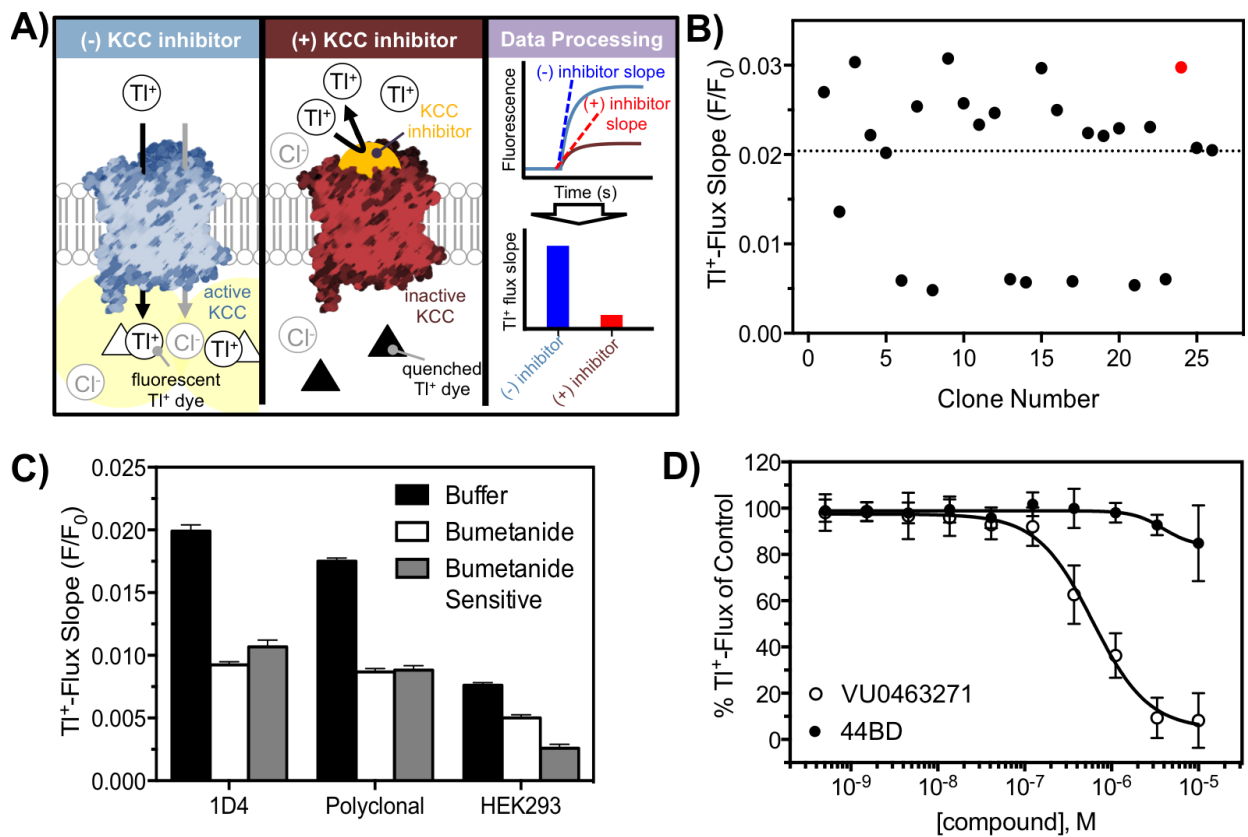
Figure 2.2. Development and use of an *in vitro* assay to quantify *Dm*KCC inhibition. (A) Scheme depicting assay design and data processing workflow. (B) Screening of monoclonal cell lines for increased Tl+ flux identifies cell line 1D4 (red highlighted data point). Tl+ flux slopes for individual cell lines are represented as points. The dotted line represents the Tl+-flux slope for the polyclonal cell line. (C) Bumetanide-sensitive response of monoclonal *Dm*KCC-expressing cell line 1D4, polyclonal *Dm*KCC cell line, and wild type HEK293 cells as detected by Tl+-flux ($n = 3$). *Asterisks represent statistical significance in each clone group at $P < 0.05$ as determined through a one-way ANOVA with Tukey's post-test. (D) Activity of specific KCC2 inhibitor VU0463271 (open circle) and structurally related, but less efficacious, analogue 44BD (closed circle) to *Dm*KCC as quantified by Tl+-flux ($n = 3$).

45

Tl$^+$ influx was KCC-mediated, we illustrated that the Tl$^+$ flux was sensitive to the nonspecific cation-chloride cotransporter inhibitor bumetanide (Figure 2.2.C) and verified KCC expression by Western blot (Figure 2.3.A). Although bumetanide is significantly more potent to NKCC than KCC, it has been shown that bumetanide is a weak inhibitor of KCC, and thus, we performed additional experiments to ensure the reduced flux observed in Tl$^+$ flux is indeed due to KCC inhibition. To do this, we performed ^{86}rubidium (^{86}Rb$^+$)-flux, and data show KCC activity was Na$^+$-independent and active under both hypotonic and isotonic conditions (Figure 2.3.B, C), which are characteristics that mirror K$^+$–Cl$^-$ coupled cotransport seen in mammalian neuronally expressed KCCs (56) and further indicate Tl$^+$-flux shown in Figure 2.2 is KCC-mediated. After validation of the *Dm*KCC expressing cell line, we sought to characterize the effect of the human KCC2-specific inhibitor VU0463271 and its structurally related control compound, 44BD on *Dm*KCC.

Using the Tl$^+$ flux assay, VU0463271 was shown to inhibit *Dm*KCC in a concentration-dependent manner with curve fits to varying concentrations of VU0463271, resulting in an IC$_{50}$ value of 608 nM (95% CI: 457–809 nM) and a Hill coefficient value of −1.4 (Figure 2.2.D). The potency of VU0463271 to *Drosophila melanogaster* KCC is similar to that of *Aedes aegypti* (135) but significantly reduced when compared to human KCC (162). This is not surprising given that *Dm*KCC and *Aedes aegypti* KCC share 88% amino acid sequence identity, but share approximately 50% amino acid identity with human KCC2. In an effort to identify a closely related inactive analogue of VU0463271 for use as a negative control in our toxicology studies, we assessed the potency of 44BD, which is a structural analogue to VU0463271 (Figure 2.1) and was previously shown to possess very low inhibitory activity at human KCC2 (75) and *Aedes aegypti* KCC (135). Indeed, in Tl$^+$-flux assays, 44BD was significantly less potent to *Dm*KCC when compared to VU0463271 with only a 15 ± 10% inhibition at 10 μM, which was the highest concentration tested (Figure 2.2.D). These data indicate that VU0463271 and 44BD are suitable pharmacological probes to test the physiological role of KCC in the *Drosophila* CNS. After
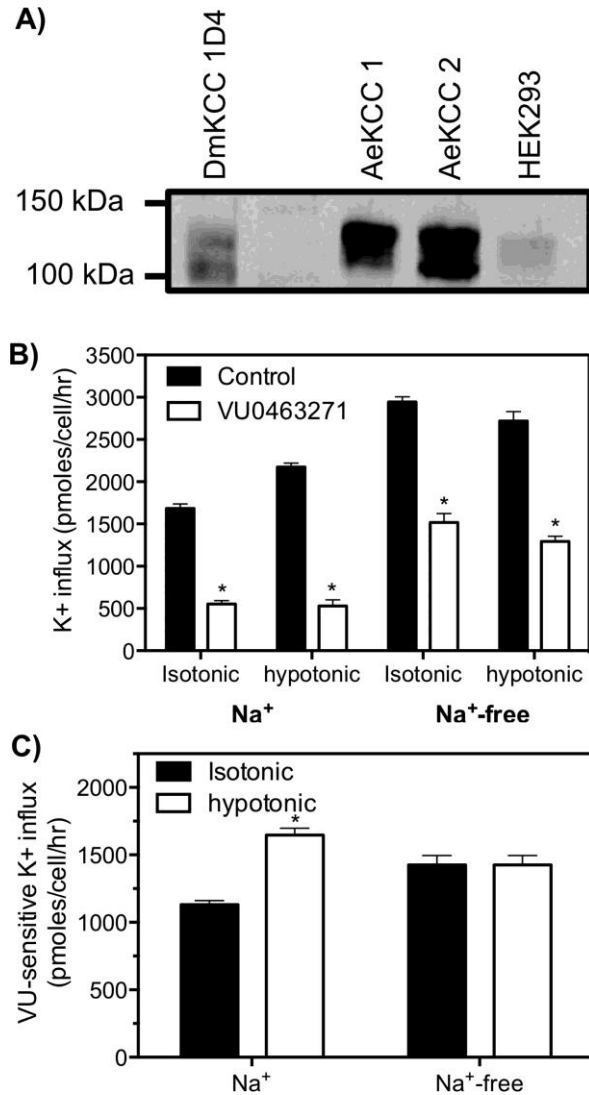
Figure 2.3. Validation of *Dm*KCC in the monoclonal HEK-293 cell line 1D4. (A) Western blotting illustrates increased immunoreactivity in 1D4 cells relative to HEK293 cells at a molecular weight corresponding to *Dm*KCC. *Aedes aegypti* KCC (*Ae*KCC) were run as a positive control for the anti-KCC primary antibody. Residual immunoreactivity in HEK293 cells is likely due to native, mammalian KCCs expressed in HEK293 cells that are inactive under isotonic conditions. (B) VU0463271-sensitive K^+ flux in the 1D4 cell line is active under both isotonic and hypotonic conditions in a Na^+-independent manner. (C) Quantification of VU0463271-sensitive K^+ flux from Figure 2.3.B. *Asterisks represent statistical significance between VU0463271 and control treatment groups at $P < 0.05$ as determined by an unpaired *t*-test.

validation that VU0463271 is potent against DmKCC and 44BD is a suitable "inactive" analogue, we performed *Drosophila* larval CNS recordings to test the initial hypothesis that DmKCC is an essential ion transport system that mediates proper neurotransmission in *Drosophila.* This is not an entirely new hypothesis as *Drosophila* KCC, encoded by *khazahoc,* has been speculated to contribute to inhibitory synaptic signaling of *Drosophila* central nervous systems (134) because it is related to mammalian KCC2, which is the principal extruder of Cl^- ions in mature neurons of mammals. To begin testing this hypothesis, VU0463271 was applied to the transected CNS preparation and resulted in a significant increase in firing rates of the *Drosophila* CNS with 1 μM VU0463271 resulting in a peak firing rate that was a 2.7- and 2.5-fold increase over baseline firing rate for OR and *rdl* strains, respectively (Figure 2.4.A). Importantly, 44BD did not alter firing rates of the *Drosophila* CNS at concentrations ranging up to 1 mM (Figure 2.4.C, E). For VU0463271, the concentration required to increase firing rate by 50% (EC_{50}) for OR was found to be 479 nM (95% CI, 281–679 nM; Hill slope, 1.6; r^2, 0.83) and the *rdl* strain was found to be near identical with an EC_{50} of 485 nM (95% CI, 313–695 nM; Hill slope, 1.4; r^2, 0.87). It is important to note that 10–100 nM VU0463271 resulted in approximately 20% reduction of CNS firing frequency within a small percentage of preparations. This inhibition was not concentration dependent and was considered to be an artifact of the dissection or recording, yet this observation warrants notation due to the dual action of dieldrin to cockroach neurons (163). These data mirror previous work in mammalian systems that have shown pharmacological inhibition of KCC2 increased spontaneous firing rates of cultured neurons and rat brain slices as well as increased membrane potential and input resistance, which were attributed to an increase in $[Cl^-]_i$ (7).

Importantly, the CNS recordings were performed on larval *Drosophila* preparations and it is currently unknown when the GABAergic switch occurs in this organism; thus, it was necessary to ensure the increased spike discharge frequency observed in Figure 2.4.A, B was not due to inhibition of NKCC prior to the developmental switch. We studied the influence of bumetanide, a
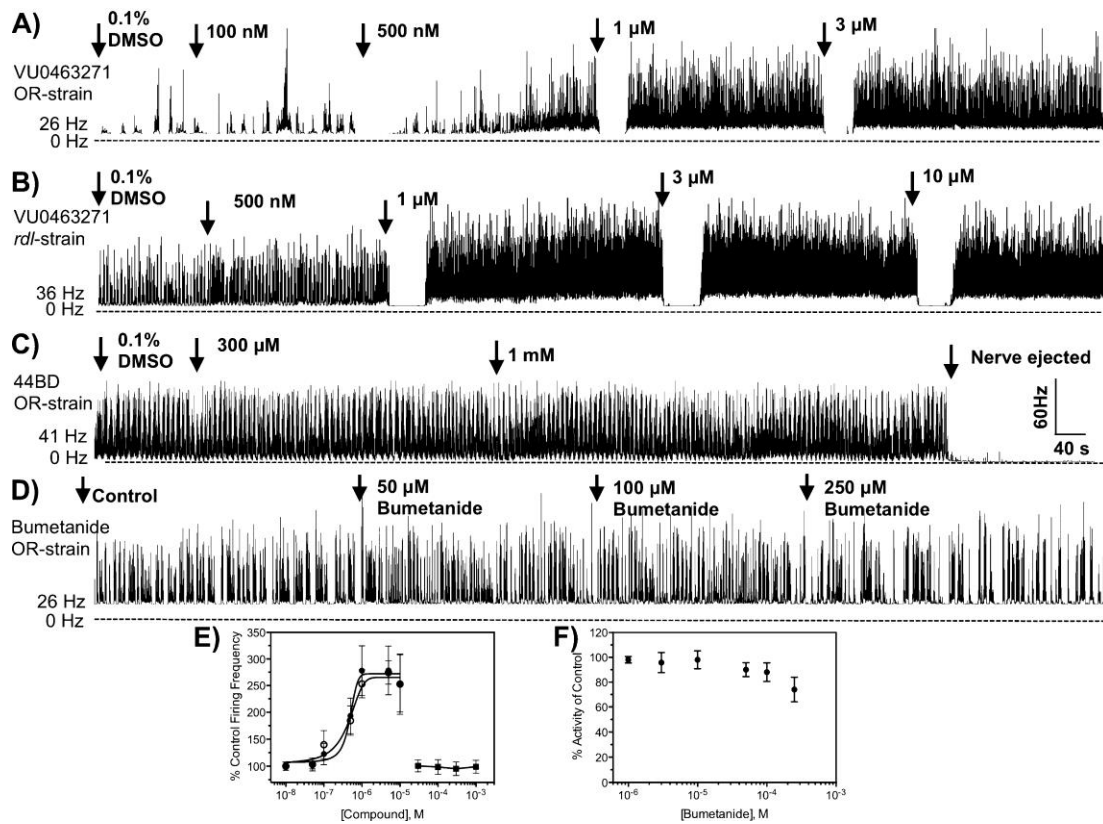
Figure 2.4. Neurophysiological recordings from the CNS of 3ʳᵈ instar *D. melanogaster*. Nerve discharges before and after VU0463271 treatment across the susceptible (OR) strain (A) and resistant (*rdl*) strain (B), as indicated. (C) Representative nerve discharge trace before and after 44BD treatment to OR strain. (D) Representative nerve discharge trace before and after bumetanide treatment to OR strain. Initial firing frequencies for (A)–(D) are shown in spikes/s (Hz) for each experiment and are given to the left of each representative trace. (E) Concentration–response curves for VU0463271 on CNS nerve discharge of OR strain (closed circles/squares) and *rdl* strain (open circles) of *D. melanogaster*. (F) Concentration–response curves for bumetanide on CNS nerve discharge of OR strain. Data points represent means from replicated recordings (*n* = 5–8 preparations per curve, with each concentration replicated a minimum of 4 times). Data points represent mean percentage increase of baseline firing rate, and error bars represent SEM.

validated NKCC inhibitor (164), to the firing rate of the *Drosophila* CNS. Bumetanide was found to have slight inhibitory actions to the firing rate of the *Drosophila* CNS with 250 μM (solubility limits in saline) resulting in 26 ± 9% reduced firing when compared to baseline (Figure 2.4.D). An EC_{50} of bumetanide was not determined due to the low inhibition at maximal concentrations (Figure 2.4.F). These data indicate that (1) the developmental switch from NKCC to KCC has occurred in the L3 lifestage because NKCC inhibition did not result in excitation and (2) VU0463271 is likely targeting KCC to induce the observed phenotype.

The data presented in Figure 2.4 indicate KCC provides an essential ion transport system in the fly central nervous system. Although the selectivity of VU0463271 has been shown to be highly specific for KCC2 (162) and our in vitro data (Figure 2.2 & 2.3) strongly support *Dm*KCC as the target of VU0463271, we reduced *kazachoc* mRNA levels specifically in the larval CNS by RNA-interference by using the GAL4-UAS system (152) to ensure a combination of proteins were not responsible for altered neuronal activity after VU0463271 exposure. Data show the CNS of the F_1 progeny expressed 69 ± 14% less *kazachoc* mRNA relative to the wild type (OR) and GFP dsRNA knockdown controls (Figure 2.5.A). Furthermore, *kazachoc* mRNA levels were not different from the carcass of control flies, indicating knockdown was CNS specific (Figure 2.5.A).

Due to the tight regulation of the nervous system, we tested if genetic ablation of *kazachoc* mRNA altered the baseline firing frequency of the *Drosophila* CNS. Significant changes were not detected in baseline firing frequencies were found between OR flies, GFP knockdown, or *kazachoc* knockdown with baseline firing frequency of 28 ± 11 Hz, 30 ± 9 Hz, and 34 ± 7 Hz, respectively (Figure 2.5.B). The lack of influence to baseline firing is potentially due to compensatory mechanisms through other cation-chloride cotransporters that are sufficient for maintaining a Cl⁻ gradient at rest or poor KCC protein reduction in the mRNA knockdown line that reduces the observed phenotype.

Next, we constructed concentration–response curves against OR, GFP knockdown, and
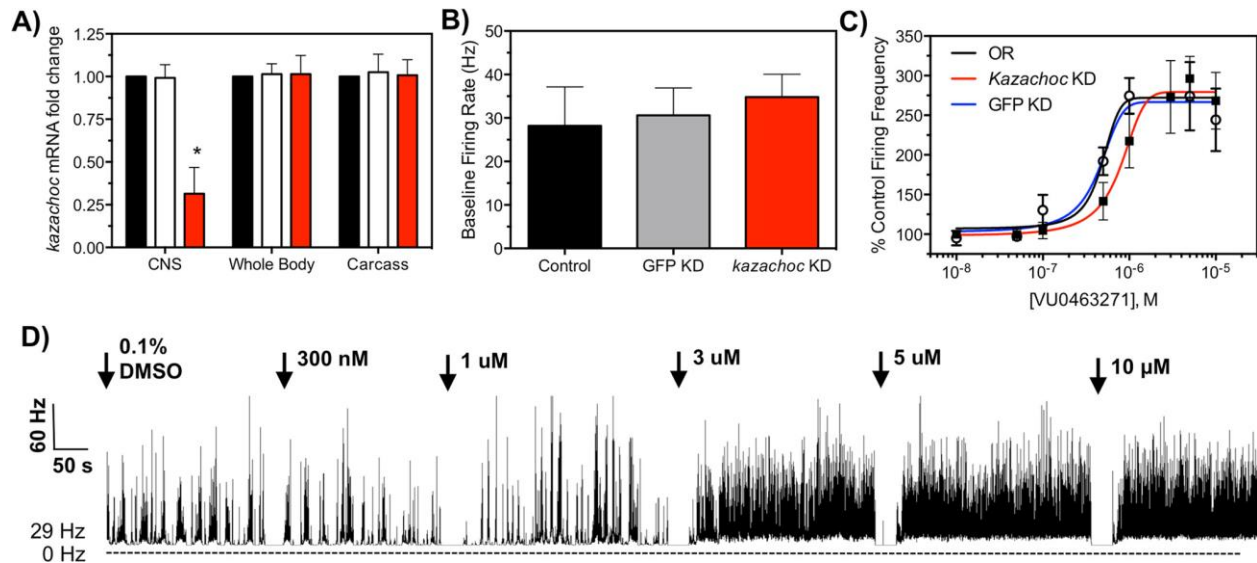
Figure 2.5. Effect of RNAi-mediated knockdown of *kcc* on VU0463271 sensitivity. (A) Quantitative RT-PCR analysis showing *Dm*KCC RNAi-based knockdown efficiency in the third instar CNS. Bars represent fold-difference in mRNA levels relative to β-actin control group. *Asterisk represents statistical significance at $P < 0.05$ as determined by a one-way ANOVA with a multiple comparisons post-test. (B) Baseline firing frequencies of control, knockdown control, and KCC knockdown flies, where bars represent mean ($n = 5$–8) frequencies and error bars represent SEM. (C) Concentration–response curve for VU0463271 on *D. melanogaster* CNS firing frequency with RNAi-mediated knockdown of KCC (solid squares) compared to wild type (solid line; CRC in Figure 2.2.B). (D) Representative neurophysiological recordings from the CNS of third instar *D. melanogaster* with RNAi-mediated tissue specific knockdown of KCC gene with exposure to VU0463271.

kazachoc knockdown flies (Figure 2.5.C) and data show a 3.2- and 2.7-fold reduction in VU0463271 potency in knockdown flies when compared to OR and GFP knockdown flies, respectively, with an EC_{50} value of 1237 nM (95% CI: 699–2189 nM; r^2: 0.85). A representative trace showing the loss of potency is shown in Figure 2.5.D. Interestingly, *kazachoc k*nockdown did not result in any obvious impact to the behavior of the third instar maggots. The loss of VU0463271 potency after CNS-specific knockdown of KCC mRNA supports our, and others' (134), hypothesis that neuroexcitation after VU0463271 exposure (Figure 2.4) is due to inhibition of KCC. However, the influence to CNS firing after genetic knockdown of KCC mRNA was significantly less than that of pharmacological inhibition, which may be due to compensatory mechanisms that negate the impact of KCC mRNA depletion, nontarget effects of VU0463271 on other Cl^- cotransporters, or that protein reduction was not correlative to mRNA reduction. If the latter is true, then it is important to note that the significant impact of VU0463271 to CNS firing may be due to nontarget inhibition and thus, must be interpreted cautiously.

Selective inhibition of KCC2 has been shown to cause a depolarizing shift of E_{Gly} and E_{GABA} within mammalian cultured neurons (7), validating functional coupling of KCC to ligand-gated Cl^- channel activity (LGCC) in an indirect manner within mammalian systems. Therefore, we aimed to determine whether KCC is similarly functionally coupled to LGCC in the *Drosophila* CNS. To do this, we studied changes in GABA-mediated inhibition of *Drosophila* CNS firing after exposure to VU0463271 and knockdown of *kazachoc*, both of which would alter $[Cl^-]_i$. As expected, exposure of the CNS to 5 mM GABA resulted in an immediate and complete cessation of spike activity (Figure 2.6.A). However, pre-exposure of the CNS to 3 µM VU0463271 followed by a cotreatment of 3 µM VU0463271 + 5 mM GABA resulted in partial inhibition of CNS spike activity, but the sensitivity of the CNS to 5 mM GABA was not altered by pretreatment of 500 µM 44BD. Representative recordings of these treatments are shown in Figure 2.6.A-C. GABA (5 mM) reduced spike discharge frequencies to an average of 0.5 ± 0.2 Hz from a baseline firing
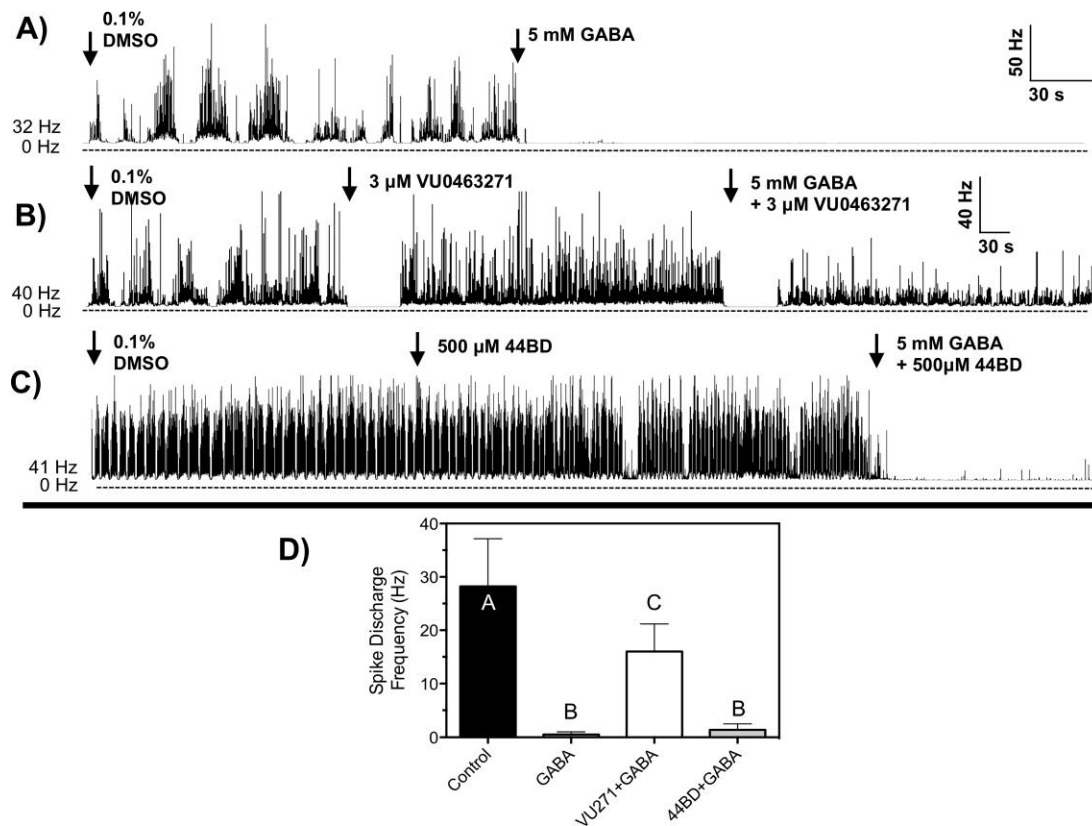
Figure 2.6. Influence of VU0463271 on GABA nerve sensitivity. (A) Representative neurophysiological recordings from the CNS of third instar *D. melanogaster* to GABA, (B) pre-exposure of 1 μM VU00463271 followed by 5 mM GABA, and (C) 500 μM 44BD followed by 5 mM GABA. (D) Initial firing frequencies in spikes/second (Hz) for each experiment are given to the left of each representative trace. Mean firing frequency of CNS nerve preparations of each treatment group. Bars represent mean ($n \geq 5$) spike discharge frequency and error bars represent SEM. Bars not labeled by the same letter represent statistical significance ($P < 0.05$) as determined by a one-way ANOVA with Tukey's multiple comparisons post-test.
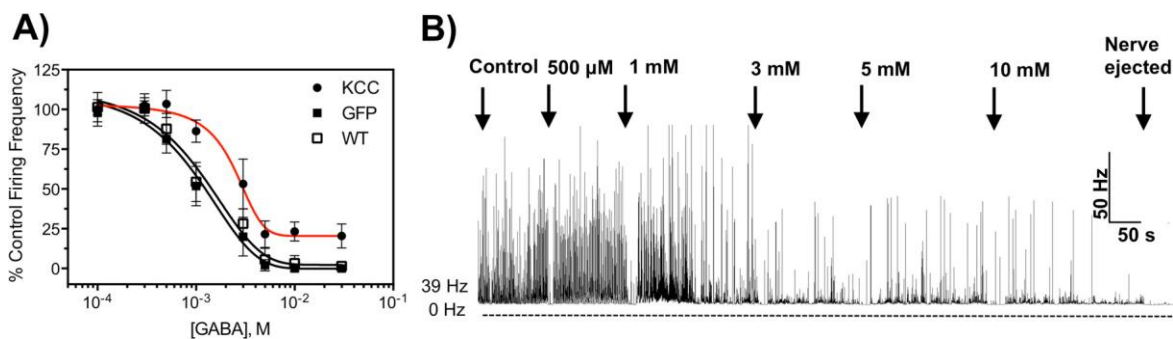
Figure 2.7. Effect of genetic knockdown of *kcc* on CNS GABA sensitivity. (A) Concentration–response curves of CNS firing frequency after exposure to GABA after RNAi-mediated knockdown of KCC (red line; closed circle), GFP (black line; closed square), and wild type (open squares). (B) Representative neurophysiological recordings from the CNS of third instar *D. melanogaster* after CNS specific knockdown of KCC.

frequency of 28 ± 11 Hz, which was a statistically significant ($P < 0.001$) reduction (Figure 2.6.D). The inhibitory effect of GABA was reduced when the CNS was pretreated with VU0463271 with an average firing rate 16 ± 5 Hz, which was significantly ($P < 0.01$) greater than GABA alone but was significantly ($P < 0.05$) reduced when compared to baseline firing rates. Importantly, the mean spike discharge frequency of CNS pretreated with 44BD followed by GABA was not significantly different when compared to baseline, suggesting that the reduced GABA sensitivity after pretreatment with VU0463271 is indeed due to KCC inhibition (Figure 2.6.D).

Despite the somewhat weak effect of KCC mRNA knockdown, genetic inhibition of KCC resulted in a significant reduction in GABA potency, which supports our pharmacological data collected in Figure 2.6 and the speculation that LGCC are functionally coupled to KCC in *Drosophila* CNS (134). The influence of *kazachoc* knockdown to GABA potency and CNS spike discharge frequency was studied through extracellular recordings of *Drosophila* CNS and GABA was shown to have an IC_{50} value of 1.1 mM (95% CI, 0.8–1.5 mM; Hill slope, − 1.5; r^2, 0.96) to OR flies, which was nearly identical to the IC_{50} value found for GFP knockdown flies (Figure 2.7.A). *Kazachoc* knockdown flies were shown to have a 2.2-fold reduction in GABA potency with an IC_{50} value of 2.3 mM (95% CI, 1.8–2.9 mM; Hill slope, − 2.1; r^2, 0.94). Interestingly, complete inhibition of CNS firing was never achieved in *kazachoc* knockdown flies with the greatest GABA-mediated inhibition reaching approximately 70% at concentrations ranging from 5 to 30 mM (Figure 2.7.A). These concentrations were found to completely eliminate all CNS activity in the OR and GFP-knockdown flies. All recordings were terminated with ejection of the descending nerves from the electrode to ensure the firing rate at these concentrations was not artifacts or extraneous noise signals, which is shown at the end of the representative trace in Figure 2.7.B. The reduced GABA sensitivity in *kazachoc* knockdown is shown in Figure 2.7.B and can be compared to GABA sensitivity for OR flies shown in Figure 2.6.A. The lack of effect of KCC mRNA knockdown to baseline firing rates (Figure 2.6.B) combined with incomplete inhibition of CNS activity at 10 mM GABA (Figure 2.7) indicates that cotransport of K^+ and Cl^- occurs very rapidly

and/or efficiently because only 25% of the KCC expression is necessary to maintain a proper Cl^- gradient and enable inhibitory neurotransmission. This is similar to work in mammalian systems that have shown that reduction of KCC2 protein in CA1 pyramidal neurons does not alter synaptic conductance (165) despite a depolarizing shift of E_{GABA} (166). Yet, our data (Figure 2.7) suggest that a continuous increase in the Cl^- extrusion deficit during prolonged synaptic activity increases the threshold for GABA-mediated inhibition and thus, prevents complete inhibition of CNS firing with high concentrations of GABA.

The functional relationship of KCC to GABA-gated chloride channels indicated by our data is consistent with a large amount of data supporting the critical role of KCC2 in affecting Cl^- homeostasis in human systems and the inhibitory function of synaptic Cl^- channels in mammalian and insect nervous systems (133, 141). Therefore, perturbing the function of KCC could synergize the activity of LGCC directed insecticides. To further investigate the hypothesis that KCC and GABA are functionally coupled proteins, we quantified the influence of partial inhibition of KCC and LGCC to the spike discharge frequency of the *Drosophila* CNS. In theory, if LGCC function is dependent on KCC function, then neural activity should be affected in a multiplicative fashion and not additive when an EC_{10} of each inhibitor is applied. Indeed, cotreatment of an EC_{10} of dieldrin, a known GABA-R inhibitor, and an EC_{10} of VU0463271 significantly ($P < 0.001$) increased the firing rate with a 70% and 110% increase over baseline at 0–5 min and 5–10 min postexposure, respectively (Figure 2.8). These firing rates are significantly ($P < 0.001$) greater than the expected 20% increase over baseline if the relationship was additive (dotted line; Figure 2.8.D). It is important to note that approximately 10% of the preparations did not respond to the cotreatment of dieldrin and VU0463271. These recordings were excluded from the data analysis and we speculate this lack of effect was due to high baseline firing rates that approached maximal firing frequencies (~60 Hz), increased rate of nerve mortality, or variability within the fly population. These data suggest that increased potency of Cl^- channel blockers,
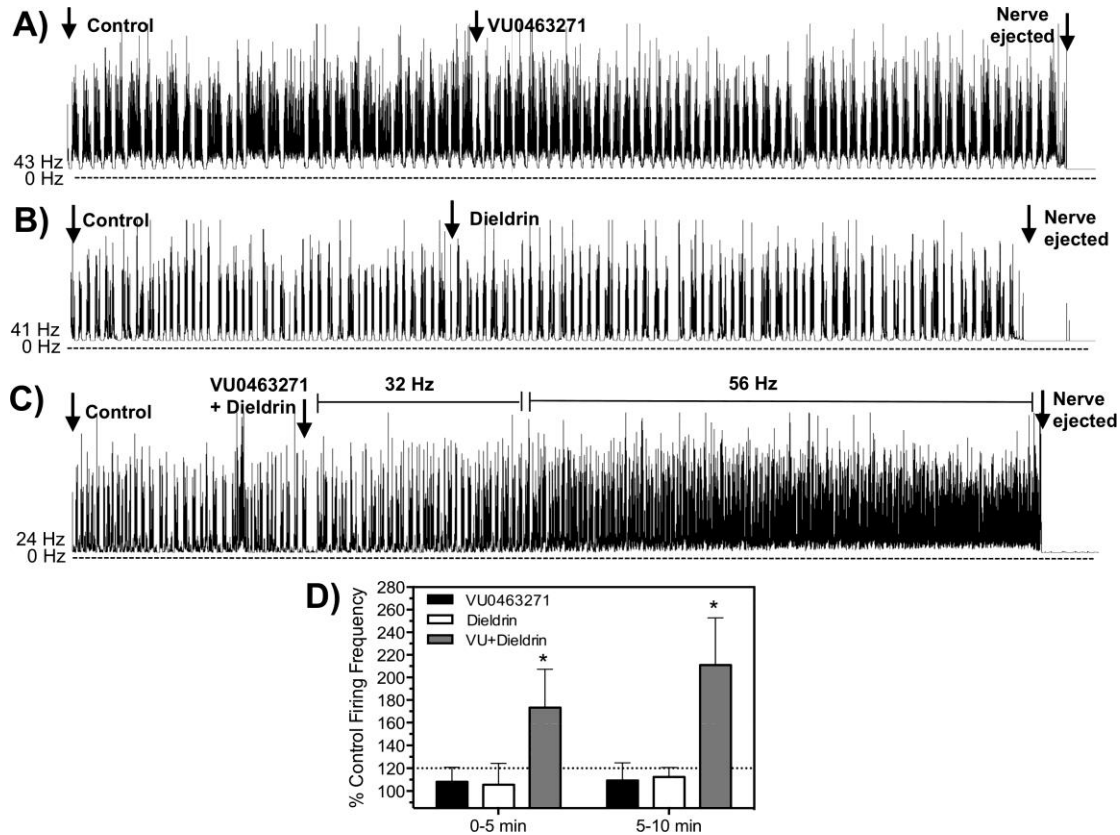
Figure 2.8. Evidence of functional coupling of KCC and GABA-R in the *Drosophila* CNS. (A) Representative traces of the effect of EC_{10} of VU0463271, (B) dieldrin, and (C) VU0463271 + dieldrin to the firing of *Drosophila* CNS. (D) Mean (n = 5–8) CNS firing rates after exposure to VU0463271 alone, dieldrin, and in combination with error bars representing SEM. Dotted line represents 20% increase over baseline, which is the expected additive firing rate. *Asterisks represent statistical significance at P < 0.001 as determined by an unpaired students *t*-test.
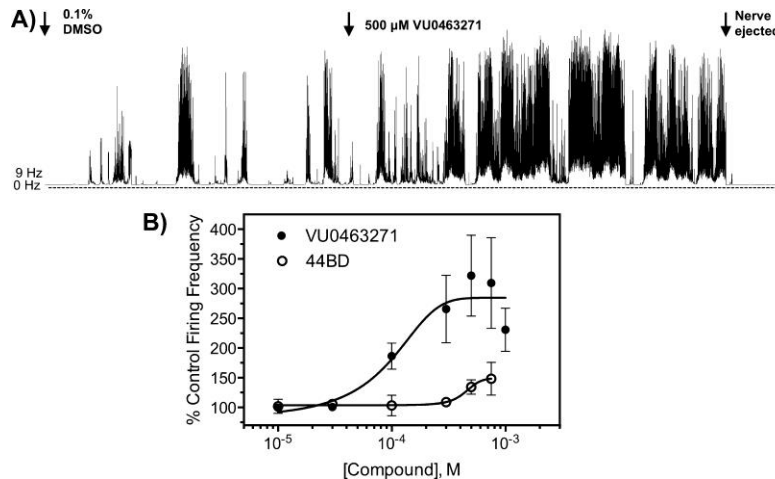
Figure 2.9. Sensory nervous system firing frequency recordings from *D.* melanogaster. (A) Representative traces of VU0463271 on the sensory nerves of third instar *Dm.* (B) Concentration–response curve for VU0463271 and 44BD on *D. melanogaster* PNS firing frequency where each data point represents mean (n = 5–8) PNS firing rates with error bars representing SEM.

such as dieldrin, can be obtained through simultaneous inhibition of KCC. However, these data contrast with previous work that showed the seizure-susceptibility of KCC^{DHS1} adult *Drosophila* is suppressed when they carry one null allele of the *rdl* GABA$_A$-R gene or are fed chemical inhibitors of GABA$_A$-R (134). These data are opposite of those shown in Figure 2.8 and could be due to unknown differences between third instar and adult CNS neural networks (167).

Lastly, we aimed to study the role of KCC in the peripheral nervous system of *Drosophila.* Disruption of mammalian KCC2 function has been primarily attributed to symptomology related to diseases of the central nervous system, such as epilepsy, whereas disruption of KCC3 and KCC4 function alters the activity of the central and peripheral nervous systems, resulting in psychosis and peripheral neuropathy. VU0463271 was found to have an excitatory influence on the peripheral nervous system of *Drosophila* with an EC$_{50}$ of 103 µM (95% CI, 63–169 µM; Hill slope, 2.1, r^2, 0.84), which is 215-fold less potent when compared to the CNS (Figure 2.9). Reduction of maximal nerve firing was observed at a VU0463271 concentration of 1 mM, but firing was still over 2-fold greater than that of baseline rates (Figure 2.9.B). As with the CNS response, 44BD was found to have limited influence to the firing rate of the sensory nerves with a maximal increase of firing rate being approximately 50% higher than baseline at 700 µM, consistent with its diminished activity at KCC (Figure 2.9.B). The significant difference in VU0463271 potency to central and peripheral nerves suggests that the KCC isoforms between the two nervous systems are different or the excitation observed in the peripheral nervous system is due to KCC-independent effects.

Insecticidal effect of KCC inhibition in *Aedes aegypti*

In order to facilitate *in vitro* characterization of the effects of test compounds on *Aa*KCC, we constructed a HEK293 cell line that stably expresses *Aa*KCC. Previously we developed a Tl$^+$ flux assay to measure the activity of human KCC (hKCC) (75). The Tl$^+$ flux assay reports the
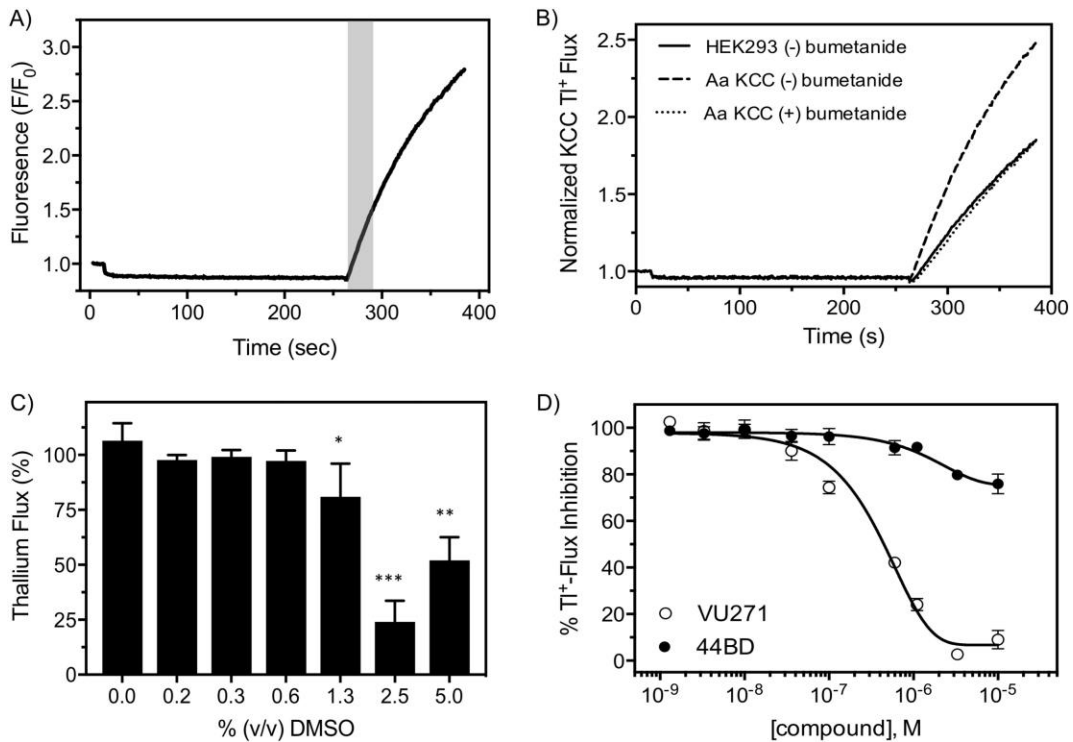
Figure 2.10. VU0463271 inhibits *Aa*KCC activity. (A) Representative Tl+-induced fluorescence of a single well of cells containing HEK293-AeKCC-expresing cells. The shaded box indicates the cell exposure to Tl+. (B) Representative Tl+-induced changes in fluorescence in the absence and presence of bumetanide. Treatments were: HEK293 cells exposed to bumetanide but not expressing AeKCC (solid line), HEK293 cells expressing AeKCC not exposed to bumetanide (dashed line), and HEK293 cells expressing AeKCC exposed to bumetanide (dotted line). (C) DMSO concentrations up to 5% v/v DMSO. Data are means (n = 6) and were compared to 0% DMSO via a one-way ANOVA. Statistical significance denoted by an asterisk where * represents $P < 0.05$, ** represents $P < 0.01$, and *** represents $P < 0.001$. (D) Concentration-response curve of VU0463271 (open circles) and 44BD (closed circles) derived from Tl+ flux assays. Data points are mean (n = 3) independent experiments performed in triplicate.

KCC-facilitated flux of the K^+ congener, Tl^+, across the plasma membrane using the intracellular Tl^+-sensitive fluorescent dye Thallos (WaveFront Biosciences). Figure 2.10.A shows a representative fluorescence trace recorded from an individual well of a 384-well plate containing AaKCC-expressing HEK293 cells in the absence of inhibitors. Addition of Tl^+ evoked a rapid fluorescence increase in untreated AaKCC-expressing cells that was inhibitable with small-molecule modulators (Figure 2.10.B). For instance, the addition of bumetanide, a non-selective inhibitor of mammalian KCC, decreased Tl^+ flux in AaKCC cells to the level of Tl^+ flux observed in wild-type HEK293 cells (Figure 2.10.B). These data demonstrate that our Tl^+ flux assay and AaKCC-expressing cell line are useful for measuring the effects of pharmacological modulators on AaKCC activity.

The assay was validated for *in vitro* screening by meeting a series of performance benchmarks. First, the assay was tested for its tolerance to the small-molecule vehicle DMSO at concentrations up to 10% v/v. As shown in Figure 2.10.C, the Tl^+-flux mediated by AaKCC is unaffected by DMSO concentrations up to 0.625% DMSO v/v as compared to the 0% DMSO control (one-way ANOVA, $P > 0.05$). A $20 \pm 15\%$ and $80 \pm 9\%$ inhibition of KCC-mediated fluorescence was observed at DMSO concentrations of 1.25% and 2.5% DMSO, which were statistically significant reductions ($P < 0.05$). Interestingly, 5% DMSO yielded greater $Tl+$−flux when compared to 2.5% DMSO with a $49 \pm 10\%$ inhibition of Tl^+-flux (Figure 2.10.C). KCC-mediated fluorescence was reduced at a concentration of 5% DMSO. The data indicate that the developed cell line and assay are robust and capable of generating reproducible data for *in vitro* screening of AaKCC modulators.

The non-selective nature and low potency of bumetanide make it unsuitable for exploring the toxicological potential of KCC inhibition. Therefore, we sought to determine whether a recently describe highly potent, highly selective hKCC inhibitor, VU0463271 (75, 162), is capable of inhibiting AaKCC. Using the aforementioned Tl^+ flux assays, VU0463271 was shown to inhibit AaKCC in a concentration-dependent manner. Curve fits to varying concentrations of VU0463271

yielded an IC_{50} of 1.3 µM (95% CI: 0.9–1.8 µM) and a Hill coefficient value of 1.3 (Figure 2.10.D). These data demonstrate that VU0463271 is in fact an inhibitor of *Aa*KCC. In contrast, VU0463271 did not show an appreciable effect on the Tl$^+$ flux in wild-type HEK293 cells.

In an effort to identify a closely related inactive analog of VU0463271 for use as a negative control in our toxicology studies, we chose a compound, 44BD, which was previously shown to possess very low inhibitory activity at hKCC (75). When we evaluated 44BD using our *Aa*KCC Tl$^+$ flux assay we observed a dramatic loss in potency when compared to VU0463271 with only a $25 \pm 10\%$ inhibition at 40 µM, which was the highest concentration tested (Figure 2.10.D). These data closely match what was observed with hKCC and verify that 44BD is a suitable "inactive" analog to act as a negative control in our *in vivo* studies exploring the physiological effects of VU0463271 on mosquitoes.

The toxicity of VU0463271 and 44BD was first assessed through topical bioassays. We observed <30% mortality after topical administration of VU0463271. Out of a concern of poor topical bioavailability, we bypassed the cuticular barrier –a lipophilic barrier in the insect exoskeleton that insecticides must penetrate when topically administered– by microinjection of VU0463271 and observed a concentration dependent effect to mortality with an ID_{50} of 56 ng/mg of mosquito (95% CI: 39–107 ng; Hillslope: 0.79; r^2: 0.93) (Figure 2.11.A). 44BD yielded appreciably lower mortality when compared to VU0463271 with approximately 20% mortality at 500 ng, which was the highest dose studied due to solubility limitations (Figure 2.11.A). These data are consistent with the dramatically lower potency and efficacy of 44BD compared to VU0463271 observed in our *in vitro* assays. In addition to the Rockefeller strain (susceptible), we also employed the Puerto Rico (PR) strain of *Aedes aegypti* which has been shown to possess target-site (*kdr*) resistance, which contrasts from another Puerto Rican strain that possesses elevated mRNA levels encoding CYP450 enzymes (168). Importantly, VU0463271 was insecticidal
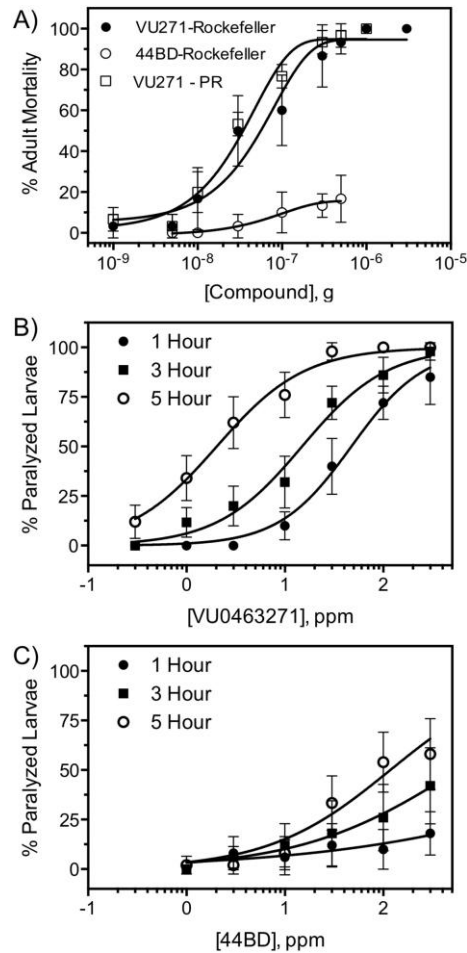
Figure 2.11. Toxicological characterization of *Aa*KCC inhibition in *Aedes aegypti*. (A) Toxicity of VU0463271 and 44BD to susceptible (Rockefeller; closed and open circles) and pyrethroid resistant (Puerto Rico; open square) strains of adult *Aedes aegypti* 24 h post-injection. Data points represent an n = 90 individual female mosquitoes. (B) Toxicity of VU0463271 to headless larvae at 1 h (closed circle), 3 h (closed square), and 5 h (open circle) post-exposure. Data points represent mean mortality where n = 30 individuals. (C) Toxicity of 44BD to headless larvae at 1 h (closed circle), 3 h (closed square), and 5 h (open circle) post-exposure. Data points represent mean mortality where n = 30 individuals.

in this insecticide resistant PR strain of *Aedes aegypti*. The ID_{50} of VU0463271 in the PR strain was 1.3-fold reduced when compared to the Rockefeller strain (Figure 2.11.A), which was not a statistically significant difference in toxicity (Figure 2.11.A).

Larval toxicity assays provided similar results when compared to adult toxicity in that mortality was not observed in intact larvae at concentrations up to 200 parts-per-million (ppm) (data not shown). To bypass the cuticular barrier once again, we performed the headless larval assay described in Islam and Bloomquist (159). Similar to the toxicity observed in adult mosquitoes, VU0463271 showed concentration-dependent lethality with an LC_{50} value of 47 ppm (95% CI: 39–56 ppm; Hillslope: 1.1; r^2: 0.94) at 1-h post exposure (Figure 2.11.B). We observed a 3.3-fold increase in toxicity at hour 3 (LC_{50} 14.9 ppm, 95% CI: 12–18; Hillslope: 1.0; r^2: 0.95) and a 23.5-

fold increase in toxicity at hour 5 (LC_{50} 2.0 ppm, 95% CI: 1.1–3.8; Hillslope: 0.97; r^2: 0.94) when compared to hour 1 (Figure 2.11.B). Importantly, 44BD was found to be non-toxic to intact larvae and was less toxic to headless larvae when compared to VU0463271 (Figure 2.11.C). We were unable to determine an LC_{50} due to lower than 50% lethality observed at the highest concentration tested. At 1- and 3-h post exposure, we observed a mean mortality of $18 \pm 48\%$ and $42 \pm 19\%$ at 300 ppm, respectively. Three-hundred ppm was the highest concentration tested due to solubility limits (Figure 2.11.C). At 5-h post 44BD exposure, we observed $58 \pm 16\%$ mortality at 300 ppm and estimated the LC_{50} to be approximately 230 ppm, which is a 115-fold decrease in toxicity when compared to the LC_{50} of VU0463271 at hour 5 (Figure 2.11.C). The toxicity profiled observed with VU0463271 and 44BD in the mosquito larvae assay corresponds to the potency and toxicity profiles observed for the *in vitro* and adult mosquito toxicity assays, respectively.

After treatment with lethal doses of VU0463271, *Aedes aegypti* mosquitoes were found to display hyperexcitatory tendencies. In adults, 20 min after treatment, the mosquitoes were observed to display an increased wing beat frequency, erratic and uncoordinated movements,
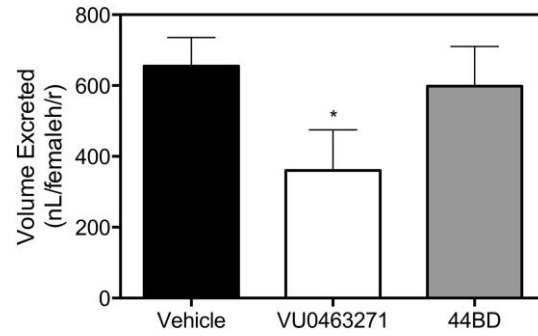
Figure 2.12. Effects of KCC inhibition on *Aedes aegypti* excretory capcity. Amount of urine excreted by mosquitoes 1 h after injection with 69 nL of the vehicle control or VU0463271/44BD solutions in K$^+$-PBS. Bars represent mean (n = 40) where error bars represent SEM. Statistical significance was denoted by the asterisk where * represents P < 0.05.

reduced climbing behavior, and increased leg contractions. Directed flight behavior did not occur. After approximately 10 s of hyperexcitation, the mosquitoes resumed lethargic behavior. Control mosquitoes had normal posture (legs not splayed away from the midline), would rest on the sides of the holding chamber *versus* the bottom, and upon agitation, the mosquitoes would immediately fly from their resting posture to a different location on the container and come to rest. Interestingly, slight excitatory tendencies were observed in about 20% of the mosquitoes injected with 44BD but were not to the same level of intensity when compared to mosquitoes treated with VU0463271. This modest efficacy is consistent with dramatically lower potency but not complete inactivity of 44BD against *Aa*KCC (Figure 2.10.D).

In addition to ecotoxicity in the nervous system, KCC inhibition can also be insecticidal from its ability to block fluid secretion in the mosquito Malpighian tubule. Fluid secretion in the Malpighian tubule is required during the process of taking a blood meal, and inhibition of this process has previously been shown to be insecticidal (161). Since KCC1-A, which is related to the mammalian KCC isoforms important for salt homeostasis in the kidney, has been shown to be a critical pathway that is essential for proper function of mosquito Malpighian tubules and fluid secretion from the isolated tubules (139), we evaluated the effects of VU0463271 on the excretory capacity of adult *Aedes aegypti.* Figure 2.12 shows the volume of urine excreted by mosquitoes 1 h after injection with vehicle, VU0463271, or 44BD. Compared to injection of the vehicle, VU0463271 significantly (P < 0.01) reduces the amount of excreted urine by 55%, whereas urine secretion in 44BD treated mosquitoes was not significantly different from animals treated with vehicle alone. These data highlight another potential insecticidal effect mediated by KCC inhibitors.

Discussion

Overall, our work (a) better defines the function of KCC within the insect nervous system and (b) uses this understanding to delineate a new insecticidal mechanism. (a) Our studies better

define insect KCC function by characterizing *Dm-* and *Aa*KCC flux on a molecular level, providing the first link between KCC function and electrical regulation on an electrophysiological level, and by demonstrating functional coupling between KCC and GABA-R function. (b) Our studies use this information to define a new insecticidal mechanism by demonstrating that KCC inhibition in a vector of human disease, *Aedes aegypti*, inhibits diuresis in adult mosquitos, and is insecticidal in adult and larval mosquito populations. Our findings are highly significant because they expand the understanding of a key regulator of inhibitory neurotransmission in a model system regularly used to study nervous system function, *Drosophila melanogaster*, and define a new insecticidal mechanism useful for the control of a vector of human disease, *Aedes aegypti*, that circumvents known resistance mechanisms.

Throughout our work, we used VU0463271 as a KCC inhibitor; VU0463271 was a useful tool compound for proof-of-concept studies to establish the insecticidal potential of KCC inhibition, however, VU0463271 is not ideal as an insecticide because it is an extremely potent inhibitor of human KCC2 (108), which has been linked to seizure-like activity in mammals (109). In addition to its potential for adverse effects in humans, VU0463271 does not readily cross the cuticular barrier in insects and is therefore not bioavailable upon topical administration, further precluding its use as an insecticide. To generate a practical insecticide targeting KCC, the discovery of new compounds better suited for KCC inhibition within insects is warranted. During our studies, we developed high-throughput compatible Tl$^+$ influx assays of *Dm*KCC and *Aa*KCC activity. Given the fact that Tl$^+$ influx has been used to discover KCC2 inhibitors by high-throughput screening previously (75, 169), these assays are an excellent starting point for high-throughput screening campaigns targeting insect KCC. The use of these assays either for a: chemistry-focused approach aimed at synthesizing VU0463271 analogs that maintain their activity at insect KCC while decreasing activity at human KCC2 and increasing topical bioavailability, or a high-throughput screening campaign aimed at discovering new chemical matter with KCC-selective

activity and topical bioavailability in insects, are two promising approaches to developing KCC inhibitors with practical use as insecticides going forward.

An unexpected finding during our knockdown experiments of KCC is that nervous system-specific KCC knockdown decreases potency of VU0463271. Based on reports of RNAi-mediated knockdown of the targets of other small molecule inhibitors (170), we anticipated that knockdown of KCC would increase VU0463271 potency because it would decrease KCC expression, and thus the amount of KCC which would be needed to be inhibited to reach a saturable effect. We believe that compensatory changes in response to KCC knockdown drove the decreased potency of VU0463271. While we focused on isotonic KCC-mediated Cl^- efflux in this work and its importance for GABAergic signaling, K^+-Cl^- cotransport has a host of functions, including cell volume homeostasis and transepithelial transport of Cl^- (130). Unlike in mammalian systems, where these essential functions are distributed over four distinct KCCs, in insects KCC is thought to be responsible for all of these critically important aspects of insect physiology. In agreement with KCC's essential function, KCC knockout is embryonic lethal (140). It is therefore conceivable that, in response to the stress originating from the loss of a host of physiological functions, that the insect nervous system upregulates alternate Cl^- efflux pathways that are VU0463271-insensitive. Increased VU0463271-insensitive Cl^- efflux would thus decrease VU0463271 potency. Elucidation of these molecular pathways could be important in understanding potential resistance mechanisms to insecticidal KCC inhibition. Regardless of the underlying mechanism, the change in VU0463271 potency in response to KCC knockdown demonstrates a functional link between the activity of KCC and VU0463271, and supports VU0463271's use as a tool compound to inhibit KCC function *in situ*.

A critical finding from our studies was observing coupling of KCC and GABA-R activity, as evidenced by synergistic, pro-seizure activity elicited by cotreatment of submaximal concentrations of dieldrin, a GABA-R inhibitor, and VU0463271 (Figure 2.8.D). These findings are important because they provide empirical evidence to the longstanding assumption that GABA-R

function depends on isotonic KCC activity in insects, and delineate a new insecticidal strategy where co-application of low dose KCC and GABA-R inhibitors can be used for insect control. However, this finding ostensibly contradicts previous work by Hekmet-Scafe et al., which showed that treatment of *kcc* knockdown flies with a high dose of a distinct GABA-R inhibitor, picrotoxin, decreased seizure-like activity (171). We believe we can reconcile these contrasting observations based on the level of KCC activity in each of these experimental systems. In the Hekmet-Scafe studies KCC activity was greatly diminished, stemming from a roughly 2.3-fold reduction in *kcc* transcript in their knockdown flies (134). Under these conditions of large and global KCC inhibition, it is likely that $[Cl^-]_i$ levels would increase and, coupled with steady Cl^- influx mediated by NKCC, produce a Cl^- gradient where GABA-R activation would actually produce Cl^- efflux and therefore depolarization. Under these conditions, GABA-R activation would produce seizures, and application of a GABA-R inhibitor would therefore attenuate seizure activity. In contrast, during our studies, an EC_{10} concentration of VU0463271 was used, producing limited KCC inhibition. The remaining KCC activity under these conditions is sufficient to produce a neuronal $[Cl^-]_i$ favoring influx or shunting inhibition, and not Cl^- efflux. Therefore, under these conditions, GABA-R activation would not produce an excitatory effect, and cotreatment of EC_{10} concentrations of KCC and GABA-R inhibitors produce the multiplicative, synergistic increase in seizure activity observed in our studies. Going forward it is important to verify these assumptions of depolarizing/hyperpolarizing GABA-R activity electrophysiologically, and test if the multiplicative levels of seizure activity detected *ex vivo* actually translate to comparable levels of lethality in an insecticidal setting.

DISCOVERY OF SMALL MOLECULE KCC2 POTENTIATORS THAT ATTENUATE SEIZURE-LIKE ACTIVITY IN NEURONS

Abstract

KCC2 is a K^+-Cl^- cotransporter with neuronal expression throughout the central nervous system. Deficits in KCC2 activity have been implicated in a variety of neurological disorders, including epilepsy, chronic pain, autism spectrum disorders, and Rett syndrome. Therefore, KCC2 potentiation is a promising conceptual approach to treatment of these disorders. From a translational perspective, it is important to establish if pharmacological potentiation of KCC2 could be therapeutic. However, studies investigating the effect of pharmacological KCC2 potentiation are limited because KCC2 potentiator pharmacology is underdeveloped. Herein, we describe the discovery and characterization of a new class of small molecule KCC2 potentiator, and the evaluation of its effect on *in vitro* seizure-like activity. This newly discovered class, exemplified by VU0500469 and VU0916219, exhibits KCC2-dependent activity, selectivity versus the structurally related NKCC1 transporter, a unique mechanistic profile relative to known small molecules which enhance KCC2 activity, and increases surface expression of KCC2. Furthermore, we demonstrate that small molecule KCC2 potentiation attenuates seizure-like activity in a neuronal-glial co-culture model of epilepsy. Together, our results provide a unique KCC2 potentiator class useful for deepening the field's understanding of KCC2 biology, and evidence that pharmacological KCC2 potentiation, by itself, is sufficient to attenuate seizure-like activity. These findings and chemical tools are important for evaluating the promise of KCC2 as a therapeutic target, and could lay a foundation for the development of KCC2-directed therapeutics for multiple

neurological disorders with significant unmet medical need. Note: the work for all sections of this chapter was completed by Prael III et al. and is currently under revision.

Introduction

Pathologically elevated levels of intracellular chloride ($[Cl^-]_i$) in neurons are implicated in a variety of neurological disorders, including: epilepsy (2, 19), neuropathic pain (172), autism spectrum disorders (12), and Rett syndrome (14). High levels of neuronal $[Cl^-]_i$ are thought to cause excessive neural activity that is a hallmark of these disorders (1, 173). Physiological levels of neuronal $[Cl^-]_i$ are typically low in the mature central nervous system. During pathological states, elevated $[Cl^-]_i$ is thought to cause excess neuronal excitability through blunting the activity of Cl^- channel effectors of fast inhibitory neurotransmission, namely $GABA_A$ and glycine receptors, which use the Cl^- gradient generated by low neuronal $[Cl^-]_i$ for their function. Loss of fast inhibitory neurotransmission thereby perturbs electrical regulation and subsequently causes excess neuronal activity (174). Therefore, mechanisms that increase neuronal Cl^- extrusion could be therapeutic in these diseases because they would decrease $[Cl^-]_i$, restore fast inhibitory neurotransmission, and subsequently counteract excess neuronal activity characteristic of these disorders.

KCC2 (*SLC12A5*) is a K^+-Cl^- cotransporter that has promise as a therapeutic target for diseases with pathologically elevated levels of $[Cl^-]_i$ (1, 173). KCC2's therapeutic potential stems from its function and expression profile: KCC2 uses the electrochemical gradient of K^+ to drive the efflux of Cl^- from cells (56), is critical for maintaining low neuronal $[Cl^-]_i$ in the mature nervous system (1), and has widespread neuronal expression (175). Therefore, potentiation of KCC2-mediated ion transport could counteract elevated levels of neuronal $[Cl^-]_i$ in the aforementioned diseases, and thus produce a therapeutic effect. In this study, we focused on epilepsy because

69

of the strong link between KCC2 and epilepsy, and the large unmet medical need people afflicted with epilepsy face (19, 25).

There is consistency between (i) clinical and (ii) preclinical evidence supporting KCC2 potentiation as a viable therapeutic strategy in epilepsy. (i) Clinically, over a dozen loss-of-function (LOF) KCC2 mutations in humans have been linked to epilepsy (37–40, 176), and resected tissue from epileptic patients has shown electrophysiological and protein expression-level abnormalities consistent with KCC2 LOF (26, 35). (ii) preclinically, pharmacological (7, 46, 54) or genetic (5, 6, 9, 87) inhibition of KCC2 activity exacerbates seizure-like activity across multiple epilepsy models. In contrast, genetically increasing KCC2 activity attenuates seizure-like activity in the same model systems, without overt side effects (6, 50, 177). Furthermore, TrkB modulators that increase KCC2 activity restore the efficacy of phenobarbital (PB), a GABA$_A$ positive allosteric modulator and antiepileptic drug, in PB-resistant seizure models (51–53). While some preliminary evidence exists linking pharmacological KCC2 potentiation to an antiepileptic effect (51–54), further validation of this effect is warranted, owing to limitations with current small molecule KCC2 potentiators.

To properly test if pharmacological KCC2 potentiation is antiepileptic we need small molecule KCC2 potentiators with adequate potency, efficacy, and selectivity. Recently described KCC2 potentiators represent excellent progress in the field, and have deepened the field's understanding of KCC2 in neurological disease (14). However, these probes are limited because they either act by inhibiting signaling pathways with pleotropic effects on cells (14, 66, 113, 116), thereby complicating the interpretation of their effects, or have some controversy surrounding their ability to potentiate KCC2 (10, 55, 115). Therefore, discovery of new, selective KCC2 potentiators would benefit the field.

In this chapter, we discovered a class of KCC2 potentiators that exhibit KCC2-dependent activity and preliminary selectivity. Furthermore, we demonstrated that this potentiator class has a unique mechanism-of-action relative to known KCC2 potentiators, improved the

pharmacological properties of this class by medicinal chemistry, and determined that this potentiator class increases KCC2 plasma membrane expression. Finally, we established that these KCC2 potentiators attenuate seizure-like activity in cortical neuronal-glial co-cultures. Together, these results describe a new KCC2 potentiator class with KCC2 selectivity, and provide evidence supporting the hypothesis that pharmacological KCC2 potentiation alone is sufficient to attenuate seizure-like activity.

Methods

HEK-293 Cell Culture.

HEK-293 cells were cultured up to 80%-90% confluence in T75 flasks (TPP) containing HEK-293 medium [α-MEM (Corning) supplemented with 10% (v/v) FBS (Gibco), 1x glutagro (Corning)] and appropriate antibiotics for selection (*vide infra*) at 37°C and 5% CO_2. Cells were passaged before they reached 90% confluence using 1x TrypLE (Gibco) up to a maximum of 20 passages.

Antibodies for Western Blotting and Immunofluorescence.

Primary antibodies used for Western blotting were: 1:1000 rabbit Anti-K^+/Cl^- Cotransporter (KCC2) Antibody (MilliporeSigma 07-432) and 1:500 mouse Transferrin Receptor Monoclonal Antibody (H68.4) (ThermoFisher Scientific 13-6800). Secondary antibodies used for Western blotting were: 1:15,000 goat anti-Rabbit IRDye 800CW (LI-COR 926-32211) and 1:10,000 goat anti-Mouse IgG IRDye 680RD (LI-COR 926-68070). Primary antibodies used for immunofluorescence were: 1:100 mouse anti-KCC2/SLC12A5 Antibody (S1-12) (Novus Biologicals NBP2-59337) and 1:50 rabbit anti-GAD65/GAD67 (Thermo Fisher Scientific PA5-36080). Secondary antibodies used for immunofluorescence were: 1:500 goat anti-Mouse IgG

71

IRDye 680RD (LI-COR 926-68070) and 1:500 Goat anti-Rabbit Alexa Fluor 555 Secondary Antibody (ThermoFisher A-21428). Cell nuclei were imaged using Hoechst 33342 at 1 μg/mL.

Reagents for Pharmacological Experiments.

Compounds were sourced from the following companies: Go6983 (Tocris), WNK463 (Selleckchem), Bumetanide (MilliporeSigma), and VU0463271 (Tocris). All other compounds were either synthesized in house (see Synthesis sections below) or purchased from Life Chemicals Inc.

Molecular Cloning.

The most widely expressed KCC2 isoform in the adult mammalian brain (KCC2b) was subcloned from the pCITF-KCC2 vector (Addgene plasmid #61404) into pcDNA4/TO (ThermoFisher Scientific) between the AflIII and NotI restriction sites using Gibson Assembly (New England Biolabs) for inducible expression of KCC2b. SuperClomeleon (178) was subcloned into the pENTR1A no ccDB (w48-1) (Addgene #17398) Entry Vector (179) using Gibson Assembly. The SuperClomeleon ORF was subsequently recombined into the pLenti CMV Puro DEST (w118-1) (Addgene #17452) destination vector for lentiviral transduction and constitutive SuperClomeleon expression using LR Clonase II Enzyme Mix (ThermoFisher Scientific). The SuperClomeleon-pLenti-CMV-puro vector was propagated in NEB® Stable Competent E. coli (New England Biolabs) to prevent homologous recombination of long terminal repeats. All sequences were verified by Sanger Sequencing (GenHunter) before cell line generation.

Polyclonal Cell Line Generation for the Cl⁻ Flux Assay.

Two polyclonal cell lines were created for use with the Cl⁻ flux assay (a) one expressing KCC2 and (b) one lacking KCC2 expression. (a) Generation of a KCC2-expressing polyclonal cell line: to allow for inducible expression of KCC2, T-REx-293 cells (ThermoFisher Scientific)

seeded at 40% confluence in a T75 flask were transfected with the pcDNA4/TO-KCC2 construct using FuGENE6 (Promega), according to the manufacturer's instructions. One day after transfection, the cells were treated with 5 µg/mL blasticidin, to select for the tetracycline repressor protein in T-REx-293 cells, and 250 µg/mL zeocin, to select for KCC2. Cells remained under selection for two weeks to ensure stable KCC2 expression. To generate a stable T-REx-293-KCC2-SuperClomeleon cell line, SuperClomeleon-containing lentivirus was produced in HEK-293T cells through transfection of the pLenti-CMV-puro-SuperClomeleon transfer vector, the pCMV-VSV-G (Addgene #8454) envelope plasmid, and the pMDLg/pRRE (Addgene #12251) and pRSV-Rev (Addgene #12253) packaging plasmids using FuGENE6. The T-REx-293-KCC2 polyclonal cell line was then seeded at 40% confluence in a T75 flask and transduced with SuperClomeleon-containing lentivirus as described in Campeau et al. (179). One day after transduction, the virus-containing medium was removed, and the cells were washed with fresh HEK-293 medium. Cells were treated with 5 µg/mL blasticidin, 250 µg/mL zeocin, and 3 µg/mL puromycin roughly 24 hours after removal of the virus to generate the polyclonal T-REx-293-KCC2-SuperClomeleon cell line. (b) Generation of a control cell line lacking KCC2 expression: The T-REx-293-SuperClomeleon polyclonal cell line was generated by transducing T-REx-293 with SuperClomeleon-bearing lentivirus as described above. A clone was selected whose YFP and CFP fluorescence levels matched those of uninduced 4p2.F7 cells used for screening (*see below*) to control for baseline SuperClomelon expression.

Monoclonal Cell Line Generation for HTS.

The T-REx-293-KCC2-SuperClomeleon polyclonal cell line was cell-sorted based on highest YFP and CFP fluorescence into individual wells of a 96-well TC-treated plate (Corning) using a BD FACSAria IIIu. After allowing the cells to proliferate to near confluence in the presence of antibiotic selection, the ~200 resulting monoclonal cell lines were screened using the Cl⁻ flux assay (described below) ± 100 µM KCC2 potentiator N-Ethylmaleimide (NEM) (MilliporeSigma)

and ± KCC2 induction with 1 µM tetracycline (MilliporeSigma). The six cell lines having the highest KCC2 induction-dependent activity in response to treatment with NEM, as determined by the highest Area Under the Curve (AUC) of the YFP/CFP ratio in treated vs. untreated cells, were then tested for (a) suitability for HTS by Z' value calculation (*see below*), and (b) for predicted KCC2 pharmacology by testing a panel of known KCC2 modulators (Fig. S1*A*). The cell line, 4p2.F7, which had the highest Z' value and exhibited pharmacology consistent with KCC2 expression was subsequently used for HTS.

Cl⁻ Flux Assay.

The Cl⁻ flux assay functioned by monitoring $[Cl^-]_i$ levels via a the genetically-encoded Cl⁻ sensor, SuperClomeleon (178), and, after compound treatment, using the changes in $[Cl^-]_i$ as a surrogate for changes in KCC2 Cl⁻ transport activity. The SuperClomeleon Cl⁻ sensor functions by Förster resonance energy transfer (FRET) between a Cl⁻-sensitive Yellow Fluorescent Protein (YFP), whose fluorescence is quenched upon Cl⁻ binding, and a Cl⁻-insensitive Cyan Fluorescent Protein (CFP), which is used as a control for SuperClomeleon expression. The corresponding changes in FRET ratio are then used to quantify changes in $[Cl^-]_i$. The day before the experiment, HEK-293 cells were counted and plated at 20,000 cells/well in black-walled, amine-coated, 384 well plates (Corning) at 20 µL/well in HEK-293 medium supplemented with 10 ng/mL tetracycline to induce KCC2 expression. After incubation for approximately 24 hours at 37°C and 5% CO_2, cell culture medium was removed by centrifugation in the Blue Washer (BlueCatBio) under the GentleSpin setting, and 20 µL/well Assay Buffer [1x Hank's Buffered Salt Solution (ThermoFisher) + 20 mM HEPES (Corning) (pH 7.3)] was added to each well. Compound plates were made in polypropylene, v-bottom, 384-well plates (Greiner) with compounds dissolved at 2x relative to the desired concentration in Assay Buffer; DMSO concentrations were kept below 0.8% (v/v) final. Cell plates were incubated at 37°C within the Panoptic plate reader (WaveFront Biosciences) for at least 30 minutes prior to the beginning of the run to allow for temperature equilibration to 37°C.

To measure Cl⁻ flux, fluorescence was recorded at 1 Hz (excitation at 440/40 nm and emission alternating between 480/17 nm [CFP] and 536/40 nm [YFP FRET]) for 20 seconds, then 20 µL of the 2x compound solution was added and fluorescence was recorded for an additional 20 minutes. For data analysis, a YFP/CFP FRET ratio was calculated by taking the YFP fluorescence intensity value and, to account for the temporal offset between CFP and YFP recordings, interpolating CFP values to match the YFP timepoints. The YFP values were then divided by the interpolated CFP values to generate a YFP/CFP FRET ratio to quantify Cl⁻ extrusion (Fig. 1*A*). The FRET ratio traces were subsequently normalized by dividing each fluorescence trace by the trace's average FRET ratio before compound addition. To quantify Cl⁻ Flux over the course of the run, average vehicle control-treated traces were subtracted from each trace to reveal the signal dependent on presence of an active test compound, and AUC for each FRET trace was calculated using the trapezoidal rule.

Z' Calculation.

Z' values were calculated as in Zhang et al. (180) using the following formula:

$$Z' = 1 - \left(\frac{3\sigma_{c+} + 3\sigma_{c-}}{|\mu_{c+} - \mu_{c-}|} \right)$$

Where σ_{c+} is the standard deviation (SD) of positive control (KCC2 potentiator)-treated wells, $3\sigma_{c-}$ is the standard deviation (SD) of the vehicle-treated wells, μ_{c+} is the mean of positive control-treated wells, and μ_{c-} is the mean of the positive control-treated wells.

Thallium (Tl⁺) Influx Assay.

The day before the experiment, HEK-293 derived cell lines were resuspended in HEK-293 medium supplemented with 100 ng/mL tetracycline to induce KCC2 expression, counted, and plated at 20,000 cells/well in black-walled, amine-coated, 384-well plates at 20 µL/well. On the day of the experiment, a 5x Tl⁺ stimulus solution [125 mM sodium bicarbonate, 12 mM thallium

sulfate, 1 mM magnesium sulfate, 1.8 mM calcium sulfate, 5mM glucose, and 10 mM HEPES-NaOH (pH 7.3)] was prepared and pipetted into a polypropylene v-bottom 384-well plate. Compounds were prepared at a 2x concentration in Assay Buffer in a separate polypropylene, v-bottom, 384-well plate, with a final DMSO concentration below 0.8% (v/v). The stimulus and 2x compound plates were sealed and incubated for at least 30 minutes at 37°C within the Panoptic plate reader before assaying. After approximately 24 hours of induction, the cells were loaded with the Tl^+-sensitive dye, Thallos AM (ION Biosciences): the cell culture medium in the cell plate was removed and replaced with 20 µL/well Assay Buffer containing 2.5 µg/mL Thallos, and cells were dye-loaded for 45 minutes at 37°C. After dye loading, the dye-loading solution was removed and replaced with 20 µL/well Assay Buffer pre-warmed to 37°C. The cell plate was then incubated for 10 additional minutes at 37°C in the Panoptic before assaying. After incubation, fluorescence intensity values were recorded at 1 Hz (482/35 nm excitation and 536/40 nm emission) for 10 seconds prior to compound addition. 20 µL of 2x compound solution was added to the cells and incubated for 10 minutes followed by the addition of 10µL of the 5x thallium stimulus solution and an additional 1 minute of data collection. Data for each well were normalized by dividing data at each time point for a given well by the average of its own pre-compound addition baseline fluorescence (F/F_0) and Tl^+ influx was quantified by the maximum fluorescence after Tl^+ stimulus addition. The T-REx-293-KCC2 monoclonal cell line, TK2D2, and untransfected T-REx-293 cells were used for all Tl^+ influx experiments. The TK2D2 cell line was generated from the T-REx-293-KCC2 polyclonal cell line described in the "Polyclonal Cell Line Generation for the Cl^- Flux Assay" section by serial dilution and subsequent clonal selection based on maximum Tl^+ influx that was sensitive to the KCC2 inhibitor VU0463271.

High-throughput Screening.

80 nL of 10 mM (nominal) test compound dissolved in DMSO was transferred from the Vanderbilt Institute of Chemical Biology (VICB) Discovery Collection to 384-well, v-bottomed,

polypropylene plates (Greiner) using an Echo 555 Acoustic Liquid Handler (Labcyte) and diluted to a concentration of 20 µM by addition of 40 µL/well Assay Buffer using a Multidrop Combi Reagent Dispenser (ThermoFisher Scientific). The compound plates were mixed on a plate shaker (ThermoFisher Scientific) for at least 2 minutes, sealed and bath sonicated (Branson) for approximately 1 minute. Compound plates and cell plates were incubated at 37°C for at least 30 minutes before assaying. The 4p2.F7 T-REx-293-KCC2-SuperClomeleon cell line was prepared and assayed at 37°C, at final compound concentration of 10 µM (nominal), as described in the Cl⁻ flux assay section. Z-scores were calculated relative to the YFP/CFP ratio AUCs of vehicle-treated wells on a plate-by-plate basis. Potentiator Hits were defined as compounds with a Z-score > 3. The first 9,000 compounds were screened at random from the VICB Discovery Collection. The final 14,000 compounds were iteratively screened, in batches of approximately 3,000 compounds, to enrich for compound classes which could accommodate chemical variation while still potentiating KCC2-dependent Cl⁻ extrusion in four steps. First, hits were selected and re-tested in the Cl⁻ flux assay, with or without KCC2 expression, to gauge reproducibility and KCC2-dependence. Second, hits were tested in the Tl⁺ influx assay to test if their activity was consistent across disparate assays of KCC2 ion transport. Third, hits that exhibited reproducible and consistent activity at KCC2 were enriched in the next round of screening by selecting plates from the compound library containing structurally similar compounds, together with random compounds to continue a broad sampling of the chemical library throughout the screen. Compounds of similar structure were selected using chemical similarity searching in Python, using the RDKit library: chemical fingerprints for the entire compound library were generated using RDKit fingerprints, and similarity was quantified between hits and the rest of the VICB Discovery Collection by Tanimoto coefficient calculation (181). The highest Tanimoto coefficients were interpreted as the most chemically similar compounds. Fourth, compound plates containing the enriched compound set was then screened, and the process repeated after hit determination.

[83]Rb^{+}/K^{+} Influx Assay.

Wild-type or KCC2-expressing HEK-293 cells were grown in 10-cm dishes in DMEM/F12 medium supplemented with 5% (v/v) FBS and 1% penicillin/streptomycin (v/v). For K^{+} influx experiments, cells were plated (2 ml/dish) for 2 hours in 35-mm dishes pre-coated with poly-L-Lysine (0.1 mg/ml, Sigma). Medium was then aspirated and replaced with 1 ml appropriate saline for a 10 min preincubation period. For KCC2-mediated K^{+} influx measurements, cells were rinsed and pre-incubated with a Na^{+}-free solution containing in mM: 132 N-methyl-D-glucamine (NMDG)-Cl, 5 KCl, 2 CaCl$_2$, 0.8 MgSO$_4$, 1 glucose, 5 HEPES, pH 7.4. For NKCC1-mediated K^{+} influx measurements, the solution contained in mM: 132 NaCl, 5 KCl, 1 CaCl$_2$, 0.8 MgSO$_4$, 1 glucose, 60 sucrose, 5 HEPES, pH 7.4 with NaOH. Following the preincubation period, the medium was aspirated and replaced with identical solutions containing 200 mM ouabain and 0.5 mCi/ml [83]Rb. After 3 rapid washes in ice-cold solution, the cells were lysed with 0.5 ml 0.5N NaOH for 1 hour then neutralized by adding 0.25 ml glacial acetic acid. Aliquots were then collected for protein assay (Bio-Rad) and b-scintillation counting. K^{+}-influx was calculated based on [83]Rb uptake and expressed in pmole K^{+} mg protein^{-1} * min^{-1}.

Surface Biotinylation.

Our surface biotinylation protocol was based on previously published work by Friedel et al. (182), with modifications to accommodate compound treatment. The day before the experiment, 4p2.F7 T-REx-293-KCC2-SuperClomeleon cells were plated in 10 cm, TC-treated cell culture dishes containing HEK-293 medium supplemented with 1 µg/mL tetracycline to achieve 90% confluence during surface biotinylation. After approximately 24 hours, cells were washed in Assay Buffer and treated with test compounds dissolved in Assay Buffer that had been warmed to 37°C. After 15 minutes at 37°C, the cells were washed once in Assay Buffer, and incubated with the compound-containing Assay Buffer solution supplemented with 0.4 mg/mL EZ-

link Sulfo-NHS-SS Biotin (Pierce 89881) at 20°C for 30 minutes. The biotinylation reaction was subsequently quenched with lysine using PBS/Ca/Mg [PBS containing 0.1 mM $CaCl_2$ and 1 mM $MgCl_2$ (pH 7.3)] that had been supplemented with 100 mM lysine and adjusted to final osmolality of 300 mOsm with H_2O. Cells were then washed three times in ice-cold PBS/Ca/Mg and harvested by cell scraping. Cell pellets were generated by centrifugation at 500 xg for 2 minutes, the supernatant solution was removed by aspiration, and the cells were transferred in ice-cold Lysis Buffer [50 mM NaCl, 1% (v/v) Triton X-100, 0.5% (v/v) deoxycholate, 0.1% (v/v) SDS, 50 mm Tris-HCl, 10 mM iodoacetamide, and protease inhibitors (ThermoFisher Scientific 78430) (pH 8)] to a microcentrifuge tube, and lysed with gentle agitation at 4°C for 30 minutes. Iodoacetamide is added to the lysis buffer to prevent the formation of SDS-insoluble KCC2 aggregates and allow for the visualization of monomeric and oligomeric populations of KCC2 by Western blot (182). Lysates were centrifuged at 1,200 xg at 4°C for 5 minutes, and the clarified lysates were transferred to a new microcentrifuge tube. Protein concentrations were determined by BCA assay (Pierce) using BSA (MilliporeSigma) as a standard. Lysate containing 20 µg of protein were set aside at 4°C overnight, for use as a control of total protein levels, and lysate containing 400 µg of protein was incubated with streptavidin-conjugated agarose beads (Pierce 89881) overnight at 4°C with gentle agitation. The next day, the agarose beads with bound biotinylated proteins were washed three times in ice-cold lysis buffer, and one time in ice-cold PBS/Ca/Mg supplemented with 10 mM iodoacetamide. Protein was eluted from agarose beads in 40 µL of Loading Buffer [65.8 mM Tris-HCl, 26.3% (w/v) glycerol, 2.1% SDS (v/v), 5% β-mercaptoethanol (v/v) (pH 7)] pre-heated to 95°C. The 20 µg total protein sample (above) and 40 µL of the eluted protein from the streptavidin beads were then loaded separately onto an SDS-PAGE gel for Western blotting and quantification as described below.

SDS-PAGE and Western Blot.

HEK-293 cells were lysed and protein concentrations quantified as described in the Surface Biotyinlation section. 20 µg of lysate, unless otherwise specified, was diluted 1:1 in Loading Buffer that was preheated to 95°C, immediately loaded onto a NuPAGE Bis-Tris 4%-12% SDS-PAGE gel (ThermoFisher Scientific) and separated using the XCell SureLock Mini-Cell system (ThermoFisher Scientific). Proteins were transferred to a PVDF membrane using the iBlot2 transfer system (ThermoFisher Scientific), incubated in Intercept Blocking Buffer (LI-COR) for one hour at room temperature to inhibit non-selective antibody binding, and incubated in primary antibody overnight. The blots were washed three times in TBS-T [150 mM NaCl, 25 mM Tris-HCl, 0.05% (v/v) Tween 20 (pH 7.4)] for 5 minutes each time, incubated with secondary antibody for one hour at room temperature, washed three times in TBS-T, and rinsed in TBS. All blots were imaged using the Odyssey CLx system (LI-COR) and quantified using the Image Studio acquisition software (LI-COR). Consistent with previous reports, KCC2 had a multiband pattern (182). We interpreted the lower band at approximately 120 kDa, the predicted molecular weight for full length KCC2, as monomeric KCC2. We interpreted the bands at approximately 240 kDa and above as dimeric- and higher-order oligomers of KCC2. For quantification of the amount of KCC2 in each sample, values for monomeric and oligomeric bands were pooled. For surface biotinylation experiments, the amount of endogenous transferrin receptor (TfR) expression was used to normalize for loading differences in the total- and surface-fractions of KCC2. For surface/total protein quantification, the KCC2 signal from surface and total fractions were normalized to their respective TfR levels, and then the normalized KCC2 surface values were divided by normalized KCC2 total values.

Rat Husbandry.

Time-pregnant Sprague Dawley dams were purchased from Taconic Biosciences. Experiments involving animals were approved by and adhered to the guidelines of the Vanderbilt Institutional Animal Care and Use Committee (protocol # M1900117-00).

Neuronal-glial Co-culture.

Brain cortices were isolated from E18 Sprague Dawley rat embryos and placed in ice-cold PBS and prepared as described in Pacico and Mingorance-Le Meur (183). Cortices were dissociated in 0.25% (w/v) Trypsin (Gibco) at 37°C for 20 minutes. The trypsin reaction was quenched by addition of neurobasal complete medium (NbC)[1x Neurobasal (Gibco), 1x B-27 supplement (Gibco), 1x glutamax (Gibco), 100 U/mL penicillin-streptomycin (Gibco)] supplemented with 10% (v/v) horse serum (NbC+HS)(Gibco). The tissue was then pelleted at 100 xg for 5 minutes, the supernatant solution was removed by aspiration, and a single-cell suspension was generated by trituration in NbC+HS medium. The cells were then counted, diluted to 500 cells/µL in NbC+HS, and 100 µL of this suspension was plated in black-walled, poly-L-lysine-coated, 96-well plates (Greiner) for a final density of 50,000 cells/well. The neuronal-glial co-cultures were then incubated at 37°C and 5% CO_2 for 4 hours, and the serum-containing NbC+HS medium was then replaced with serum-free NbC medium. The neuronal-glial co-cultures were maintained until at least 14 days *in vitro* (DIV) at 37°C and 5% CO_2 before assaying. Half of the medium was exchanged with fresh NbC medium every 3-4 days.

Synchronized Neuronal Ca^{2+} Oscillation Assay.

Neuronal-glial co-cultures were assayed between 14 DIV and 18 DIV using a protocol adapted from Pacico and Mingorance-Le Meur (183). The medium was removed from the co-cultures and the co-cultures were loaded with Fluo-8 AM (AAT Bioquest) by incubation in 90 µL/well dye-loading solution [1x HBSS (Corning), 20 mM HEPES (MilliporeSigma), 1 µg/mL Fluo-8 AM, 1 mM probenecid, 3 mg/mL BSA (MilliporeSigma) (pH 7.3)] for 30 minutes at 37°C. The dye-loading solution was then removed and replaced with 180 µL/well Neuronal Assay Buffer [1x Ca^{2+}- and Mg^{2+}-free HBSS (Corning) + 2 mM $CaCl_2$ + 3 mM $MgCl_2$ + 20 mM HEPES (pH 7.3)] that was pre-warmed to 37°C. The co-cultures were then immediately loaded into the Panoptic

plate reader and assayed. Cultures were continuously imaged at 5 Hz (482/35 nm excitation and 536/40 nm emission) at 37°C throughout the run. After a 3-minute reading to establish a Ca^{2+} oscillation baseline, 20 µL of a 10x compound solution was added to the co-cultures using the Panoptic. Co-cultures were subsequently imaged for 12 minutes to quantify the effect of compounds on the Ca^{2+} oscillation rate. Ca^{2+} oscillation rates were quantified in Python. Our data analysis workflow consisted of: (a) correction for baseline drift, (b) peak counting, and (c) oscillation rate normalization. (a) correction for baseline drift: fluorescent traces were corrected by calculating a smoothened version of each trace and then subtracting the smoothened trace from the original trace. Traces were smoothened by a mean filter generated by iterative convolutions of a 100-frame and a 200-frame averaging kernel over the timeseries data; afterward, the smoothened trace was subtracted from the overlapping region of the original trace. (b) peak counting: peaks were counted separately in the pre-compound addition and post-compound addition segments by counting peak-to-peak local maxima using a manually set threshold value and minimum distance between peaks to prevent over/under counting of peaks. (c) oscillation rate normalization: oscillation rates were calculated by dividing Ca^{2+} oscillation counts by time. Lastly, post-compound addition oscillation rates were normalized as a percentage of the baseline oscillation rate to yield a "% baseline oscillation rate". All edge wells in the 96 well plate (Rows A and H, together with columns 1 and 12) were omitted from data analysis owing to differences in signal observed in those wells relative to the rest of the plate.

Immunofluorescence.

Immunofluorescence staining of cortical co-cultures was performed after 14 DIV as described above for Ca^{2+}-imaging experiments. NbC medium was removed and cells were washed 3 times with PBS and fixed with 4% (w/v) paraformaldehyde in 1x HBSS for 20 minutes at room temperature. Cells were then washed with PBS and subsequently permeabilized with 0.3% (v/v) Triton X-100 (MilliporeSigma) in PBS for 15 minutes. Permeabilized cells were blocked

in 10% (w/v) BSA (MilliporeSigma) in PBS for 45 minutes cells were washed 3 times with PBS. Cells were treated with mouse anti-KCC2/SLC12A5 antibody (S1-12) and rabbit anti-GAD65/GAD67 in 1% BSA (v/v) in PBS at 4 °C overnight. Cells were washed 3 times with PBS prior to being incubated with goat anti-mouse and goat anti-rabbit AF555 secondary antibodies for 45 minutes at room temperature. Cells were washed 3 times with PBS and stained with Hoechst (1:5,000, ThermoFisher Scientific, H3570). Images were recorded using the ImageXpress Micro XLS system (Molecular Devices).

Statistical Tests of Significance.

Statistical tests of significance were conducted in R and Python. All tests with a two-sided $p < 0.05$ were considered statistically significant. Assumptions of normality were tested using the Shapiro-Wilk test. For two samples of normally distributed data, the Welch's unequal variances t-test was used for hypothesis tests using independent data, and the paired t-test was used for dependent data. To test if one, normally distributed sample was statistically significant from a single value, a one sample t-test was used. For two samples of data that were not necessarily normally distributed, the Mann-Whitney U test was used. For hypothesis testing of linear regression models containing normally distributed inputs, the Wald test was used with a t-distribution of the test statistic.

Synthesis General Procedure.

All non-aqueous reactions were performed in flame-dried or oven-dried round-bottomed flasks under an atmosphere of argon. Stainless steel syringes or cannula were used to transfer air- and moisture-sensitive liquids. Reaction temperatures were controlled using a thermocouple thermometer and analog hotplate stirrer and monitored using liquid-in-glass thermometers. Reactions were conducted at room temperature (approximately 21-23 °C) unless otherwise

noted. Flash column chromatography was conducted using silica gel 230-400 mesh. Reactions were monitored by analytical thin-layer chromatography, using Silica Gel 60 F254 glass-backed pre-coated silica gel plates (MilliporeSigma). The plates were visualized with UV light (254 nm) and stained with potassium permanganate or *p*- anisaldehyde-sulfuric acid followed by charring. Yields were determined by weight of isolated, spectroscopically pure compounds.

Materials.

Solvents and chemicals were purchased from Sigma-Aldrich, Acros Organics, TCI and/or Alfa Aesar and used without further purification. Solvents were purchased from Fisher Scientific. Dry dichloromethane (CH_2Cl_2) was collected from an MBraun MB-SPS solvent system. Dichloroethane (DCE) was distilled from calcium hydride and stored over 4 Å molecular sieves. Triethylamine, N,N-dimethylformamide (DMF) and dimethyl sulfoxide (DMSO) were used as received in a bottle with a Sure/Seal. N,N-diisopropylethylamine was distilled from calcium hydride and stored over KOH. $BF_3 \cdot Et_2O$ was distilled prior to use from calcium hydride. Deuterated solvents were purchased from Cambridge Isotope Laboratories.

Instrumentation.

Preparative reverse phase HPLC (Gilson) was performed using a Phenomenex Gemini column (5 micron, 110 Å, 50 x 21.20 mm, flow rate 30 mL/min) with UV/Vis detection. Low-resolution mass spectra were performed on an Agilent 1200 series system with UV detection at 214 and 254 Low-resolution mass spectra were obtained on an Agilent 6130 single quad mass spectrometer with electrospray ionization (ESI) in positive mode. LC-MS experiments were performed with the following parameters: Accucore C18 column 2.6 μm, 2.1 mm × 30 mm column) at 40 °C; an acetonitrile/water with 0.1% trifluoroacetic acid gradient 7-90 % ACN (method 1) for 1.5 min and 40-90% ACN (method 2) for 1.5 min; flow rate of 1.5 mL/min. ^{1}H NMR spectra were recorded on Bruker 400 or 600 MHz spectrometers and are reported relative to internal chloroform

(^{1}H, δ 7.26), methanol (^{1}H, δ 3.31), and DMSO (^{1}H, δ 2.50). Data for ^{1}H NMR spectra are reported as follows: chemical shift (δ ppm), multiplicity (s = singlet, d = doublet, t = triplet, dd = doublet of doublet, ddd = doublet of doublet of doublet, m = multiplet, br=broad), coupling constants (Hz), and integration. ^{13}C NMR were recorded on Bruker 100 or 150 MHz spectrometers and are reported relative to internal chloroform (^{13}C, δ 77.1), methanol (^{13}C, δ 49.2), and DMSO (^{13}C, δ 40.3).

Scheme 1: Synthesis of **VU0500469**
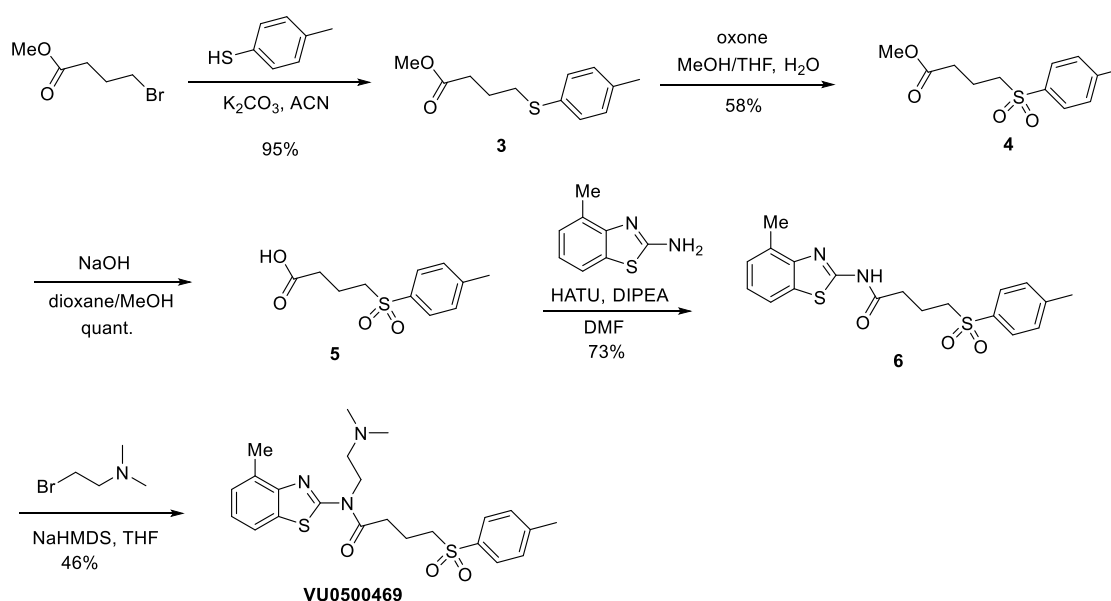
Methyl 4-(p-tolylthio)butanoate 3. A mixture of methyl 4-bromobutanoate (2.19 g, 12.07 mmol), 4-methylbenzenethiol (1.0 g, 8.05 mmol), and potassium carbonate (2.22 g, 16.10 mmol) in acetonitrile (24 mL) was stirred for 3 h and solvent was removed in vacuo. The crude residue was dissolved in EtOAc (30 mL), washed with sat. ammonium chloride (30 mL), extracted with

EtOAc (3 x 30 mL), and dried over MgSO$_4$. The solvent was removed under reduced pressure and the residue was purified by column chromatography (0 to 30% hexane/EtOAc gradient) to afford sulfide **3** as a yellow oil (2.46 mg, 95 %). LCMS (ESI) R$_t$ 1.14 min, *m/z*: 225.2 [M+H]$^+$.

Methyl 4-tosylbutanoate 4. To a solution of ester **3** (1.0 g, 4.46 mmol) in MeOH/THF (22 mL / 66 mL) was added a solution of Oxone (31.2 mL, 1.0 M in water). The reaction mixture was stirred for 20 h and concentrated in vacuo. The crude mixture was diluted with water (50 mL), extracted with EtOAc (3 x 50 mL), and dried over MgSO$_4$. The solvent was removed under reduced pressure and the residue was purified by column chromatography (0 to 50% hexane/EtOAc gradient) to afford sulfone **4** as a yellow oil (0.66 g, 58 %). LCMS (ESI) R$_t$ 0.86 min, *m/z*: 257.1 [M+H]$^+$.

4-tosylbutanoic acid 5. To a solution of sulfone **4** (0.66 g, 2.57 mmol) in dioxane/MeOH (10 mL / 5 mL) was added NaOH (6.43 mL, 1.0 M solution). The reaction mixture was stirred for 3 h at 40 °C, acidified to pH 2 with HCl (1.0 N solution), extracted with EtOAc (3 x 20 mL), and dried over MgSO$_4$. The crude product was used without further purification. ^{1}H NMR (DMSO-d_6, 400 MHz) δ 7.76 (d, *J* = 8.0 Hz, 2H), 7.48 (d, *J* = 8.0 Hz, 2H), 3.32-3.27 (m, 2H), 2.43 (s, 3H), 2.33 (t, *J* = 7.2 Hz, 2H), 1.75-1.67 (m, 2H); LCMS (ESI) R$_t$: 0.72 min, *m/z*: 243.1 [M+H]$^+$.

N-(4-methylbenzo[d]thiazol-2-yl)-4-tosylbutanamide 6. To a solution of 4-tosylbutanoic acid **5** (100 mg, 0.61 mmol) in DMF (3 mL) was added DIPEA (0.43 mL, 2.44 mmol), followed by 1-[Bis(dimethylamino)methylene]-1H-1,2,3-triazolo[4,5-b]pyridinium 3-oxide hexafluorophosphate (HATU, 0.35 g, 0.92 mmol). After stirring for 30 min at 0 °C, 4-methylbenzo[d]thiazol-2-amine (148 mg, 0.61 mmol) was added to reaction mixture. The reaction mixture was stirred 12 h, diluted with water (5 mL), and resulting precipitate collected and washed with water (3 x 10 mL). Amide **6** was obtained as a white solid product (174 mg, 73%) by filtration.

^{1}H NMR (DMSO-d_6, 400 MHz) δ 7.78 (dd, J = 8.8, 8.4 Hz, 3H), 7.48 (d, J = 8.0 Hz, 2H), 7.24 (d, J = 8.0 Hz, 1H), 7.19 (t, J = 8.4 Hz, 1H), 3.37-3.33 (m, 2H), 2.60 (t, J = 7.2 Hz, 2H), 2.56 (s, 3H), 2.42 (s, 3H), 1.86 (q, J = 7.2 Hz, 2H); LCMS (ESI) R_t 1.09 min , m/z: 389.3 [M+H]$^+$.

N-(2-(dimethylamino)ethyl)-N-(4-methylbenzo[d]thiazol-2-yl)-4-tosylbutanamide (VU0500469, KK-29-132). To a solution of N-(4-methylbenzo[d]thiazol-2-yl)-4-tosylbutanamide (**6**) (50 mg, 0.128 mmol) in THF (3 mL) was added sodium bis(trimethylsilyl)amide (0.384 mL, 1M solution in THF) at 0 ^{o}C. After stirring for 10 min a solution of 2-bromo-N,N-dimethylethan-1-amine (60 mg, 0.26 mmol) in THF (0.8 mL) was added, the mixture was allowed to room temperature stirred for 12 h and quenched with sat. ammonium chloride (10 mL). The quenched reaction was extracted with EtOAc (3 x 10 mL), and dried over MgSO$_4$. The solvent was removed under reduced pressure and the residue was purified by column chromatography (0 to 10 % DCM/MeOH gradient) to afford **VU0500469** as a white solid (33 mg, 46 %). ^{1}H NMR (MeOH-d_4, 400 MHz) δ 7.83 (d, J = 8.0 Hz, 2H), 7.64 (d, J = 8.0 Hz, 1H), 7.46 (d, J = 8.0 Hz, 2H), 7.24-7.18 (m, 2H), 4.37 (t, J = 7.2 Hz, 2H), 3.37 (t, J = 7.2 Hz, 2H), 3.00 (t, J = 8.0 Hz, 2H), 2.95 (t, J = 6.8 Hz, 2H), 2.78 (t, J = 8.0 Hz, 2H), 2.62 (s, 3H), 2.46 (s, 3H), 2.42 (s, 6H), 2.10 (t, J = 7.2 Hz, 2H); LCMS (ESI) tR: 1.01 min , m/z: 460.4 [M+H]$^+$.

Scheme 2: Synthesis of **VU0500458** and **VU0916219.**
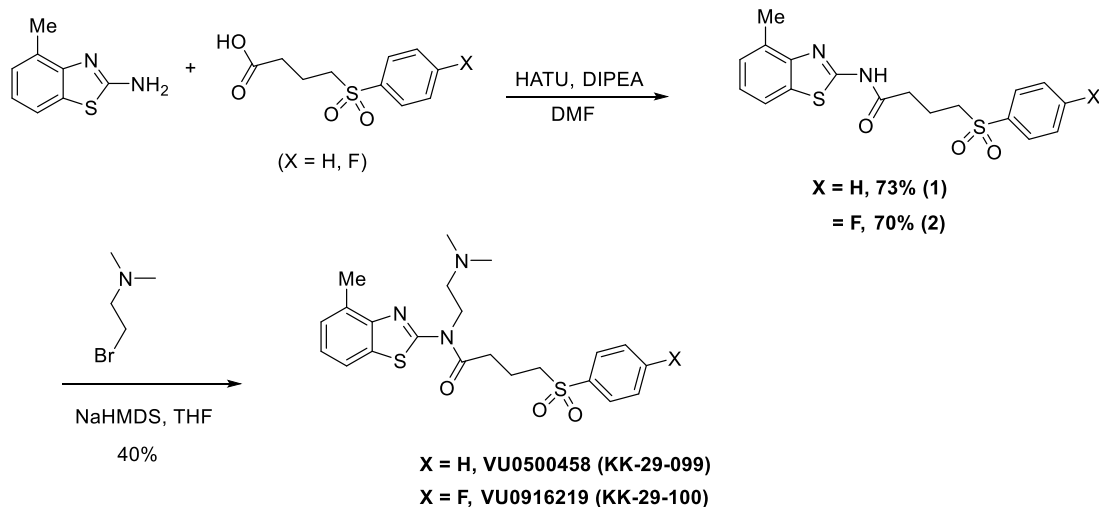
N-(4-methylbenzo[d]thiazol-2-yl)-4-(phenylsulfonyl)butanamide (1). To a solution of 4-(phenylsulfonyl) butanoic acid (68 mg, 0.3 mmol) in DMF (2 mL) was added DIPEA (0.21 mL, 1.2 mmol), followed by 1-[Bis(dimethylamino)methylene]-1H-1,2,3-triazolo[4,5-b]pyridinium 3-oxide hexafluorophosphate (HATU, 171 mg, 0.45 mmol). After stirring for 30 min at 0 °C, 4-methylbenzo[d]thiazol-2-amine (49 mg, 0.3 mmol) was added to reaction mixture. The reaction mixture was stirred 12 h, diluted with water (3 mL), and the resulting precipitate collected and washed with water (3 x 10 mL). The crude amide (**1**) was obtained as a white solid (82 mg, 73%) and used next step without further purification. LCMS (ESI) tR: 1.06 min , *m/z*: 375.3 [M+H]⁺.

4-((4-fluorophenyl)sulfonyl)-N-(4-methylbenzo[d]thiazol-2-yl)butanamide (2). Amide **2** was obtained as a white solid (82 mg, 70%) following the procedure described above except using 4-((4-fluorophenyl)sulfonyl)butanoic acid (74 mg, 0.3 mmol) as the coupling partner. LCMS (ESI) tR: 1.07 min, *m/z*: 393.2 [M+H]⁺.

N-(2-(dimethylamino)ethyl)-N-(4-methylbenzo[d]thiazol-2-yl)-4-(phenylsulfonyl)butanamide (VU0500458, aka KK-29-099). To a solution of N-(4-methylbenzo[d]thiazol-2-yl)-4-(phenylsulfonyl)butanamide (33 mg, 0.088 mmol) in THF (2 mL) at

0 °C was added a solution of sodium bis(trimethylsilyl)amide (0.26 mL, 1M solution in THF). After maintaining the reaction mixture at0 °C for 10 min, 2-bromo-N,N-dimethylethan-1-amine (41 mg, 0.18 mmol) in THF (0.5 mL) was added. The reaction mixture was allowed to warm to room temperature, maintained for 12 h, and quenched with sat. ammonium chloride (5 mL). The quenched reaction was extracted with EtOAc (3 x 10 mL), and dried over MgSO₄. The solvent was removed under reduced pressure and the residue was purified by column chromatography (0 to 10 % DCM/MeOH gradient) to afford **VU0500458** as a yellow solid (16 mg, 41 %). ^{1}H NMR (MeOH-d_4, 400 MHz) δ 7.97 (d, J = 9.2 Hz, 2H), 7.75 (t, J = 8.4 Hz, 1H), 7.67 (d, J = 8.4 Hz, 2H), 7.65-7.63 (m, 1H), 7.25-7.18 (m, 2H), 4.42 (t, J = 7.2 Hz, 2H), 3.40 (t, J = 7.2 Hz, 2H), 2.98 (t, J = 6.8 Hz, 2H), 2.86 (t, J = 7.6 Hz, 2H), 2.63 (s, 3H), 2.48 (s, 6H), 2.14 (q, J = 7.6 Hz, 2H); LCMS (ESI) R$_t$ 0.97 min , m/z: 446.4 [M+H]$^+$.

N-(2-(dimethylamino)ethyl)-4-((4-fluorophenyl)sulfonyl)-N-(4-methylbenzo[d]thiazol-2-yl) butanamide (VU0916219, aka KK-29-100). VU0916219 was prepared using same method with VU0500458. ^{1}H NMR (MeOH-$_{D4}$, 400 MHz) δ 8.01 (dd, J = 8.8, 5.2 Hz, 2H), 7.65 (d, J = 7.2 Hz, 1H), 7.38 (t, J = 8.4 Hz, 2H), 7.27-7.19 (m, 2H), 4.4 (t, J = 7.2 Hz, 2H), 3.40 (t, J = 7.2 Hz, 2H), 3.00 (t, J = 6.0 Hz, 2H), 2.88 (t, J = 7.6 Hz, 2H), 2.63 (s, 3H), 2.50 (s, 6H), 2.15 (t, J = 7.6 Hz, 2H); LCMS (ESI) R$_t$0.98 min , m/z: 464.3 [M+H]$^+$.

Results

Discovery of KCC2 Potentiators by High-Throughput Screening.

To identify small molecule KCC2 potentiators, we used a human embryonic kidney 293 (HEK-293) cell line with induction-dependent human KCC2 expression and constitutive expression of the Cl$^-$ sensor SuperClomeleon (178) for high-throughput screening (HTS). This

cell line formed the basis for the Cl⁻ flux assay, which uses intracellular Cl⁻ levels as a surrogate for KCC2 activity (Figure 3.1.A). Throughout the paper, data are normalized to the FRET ratio between the Cl⁻-sensitive YFP and Cl⁻-insensitive CFP (YFP/CFP ratio) of SuperClomeleon, where an increase in this ratio is consistent with an increase in KCC2 activity.

To determine if the Cl⁻ flux assay was suitable for HTS, we demonstrated that the Cl⁻ flux assay (i) measures KCC2 activity and (ii) has an adequate separation in signal between vehicle-treated and KCC2 potentiator-treated wells for HTS. (i) We determined that the Cl⁻ flux assay reports KCC2 activity by demonstrating that the assay responds to a panel of known KCC2 modulators, consisting of indirect KCC2 potentiators and a direct-acting KCC2 inhibitor (Figure 3.2.A), and exhibits induction-dependent KCC2 expression (Figure 3.2.B, C). (ii) We determined that the assay was suitable by HTS, defined by reproducibility and an adequate separation in signal between vehicle-treated and KCC2 potentiator-treated wells, by calculation of its Z' value over the course of a week. For Z' value calculation, we treated every other well on the 384-well plate with either WNK463 (116), a WNK inhibitor that indirectly potentiates KCC2, or vehicle-treated control. These experiments yielded a Z' value of 0.69 ± 0.03 (Figure 3.1.B-C), consistent with a well-to-well separation of vehicle- and KCC2 potentiator-treated wells adequate for HTS (180).

Having demonstrated that the Cl⁻ flux assay was suitable for HTS, we used it to screen ~23,000 compounds from the Vanderbilt Discovery Collection in search of compounds that can potentiate the capacity of KCC2 to promote Cl⁻ extrusion (Figure 3.1.D). Compounds with a Z-score > 3 were considered hits and subject to further testing. To test for reproducibility and KCC2-dependence, hits were re-tested in the Cl⁻ assay in the absence or presence of KCC2 expression. To investigate hit activity in a mechanistically distinct assay of KCC2, hits were additionally tested in the Thallium (Tl⁺) influx assay, which measures the inward flux of a K⁺ congener –Tl⁺– via a Tl⁺-sensitive dye to quantify KCC2 activity (75, 184). Hits that were reproducible, KCC2 expression-

90
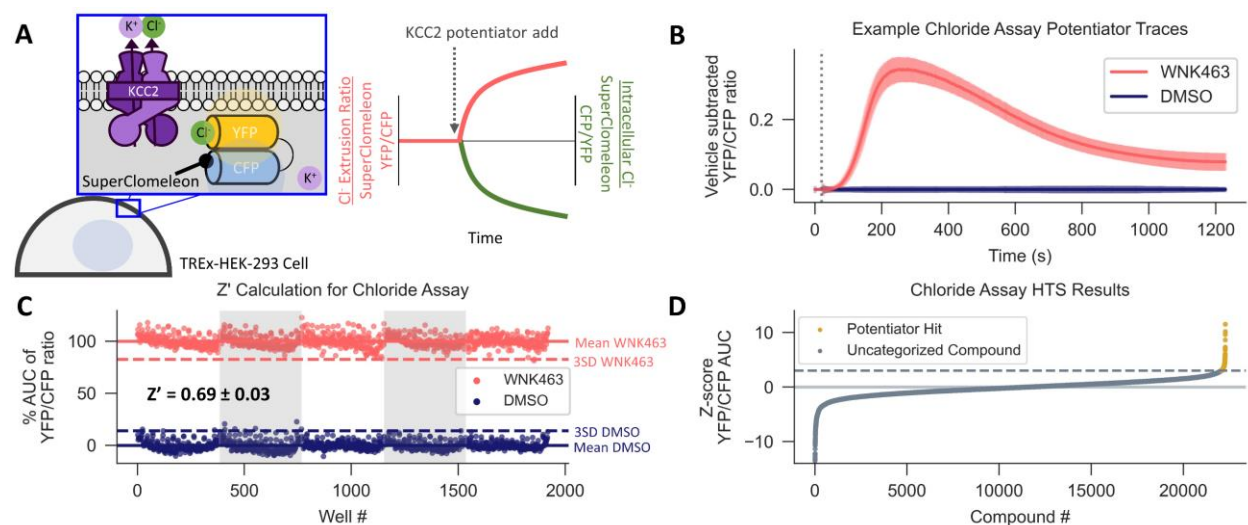
Figure 3.1. Discovery of KCC2 Potentiators by High-throughput Screening. (*A*) Cl⁻ flux assay schematic and data normalization. KCC2 activity is approximated by measuring intracellular Cl⁻ using HEK-293 cells overexpressing KCC2 and the Cl⁻ sensor SuperClomeleon. Data are normalized as a YFP/CFP ratio, such that an increase in KCC2 activity registers as an increase in value. (*B, C*) Calculation of Z' for the Cl⁻ flux assay. (*B*) Vehicle control subtracted and averaged traces from the Cl⁻ flux assay used for Z' calculation. Cells were treated with either the KCC2 potentiator WNK463 or DMSO control. Error bars represent standard deviation of the mean (SD). (*C*) Percent Area Under the Curve (AUC) of Cl⁻ flux assay traces in (*B*). The mean AUC (solid line) and 3 x SD away from mean AUC (dotted line) are displayed for each treatment. [N=5 independent experiments with 192 technical replicates per condition]. (*D*) Results of screening approximately 23,000 unique compounds at a concentration of 10 µM in the Cl⁻ flux assay. Data are presented as Z-scores relative to vehicle control values on each plate. A Z-score of 3 (dotted line) was used as a cut off for separating potentiator hits (gold) from uncategorized compounds (gray). All experiments ran at 37°C.

A Activity of Known KCC2 Modulators on HEK293-KCC2-SC Cell Line

B

C Western blot Quantification

D Chloride Assay HTS Results
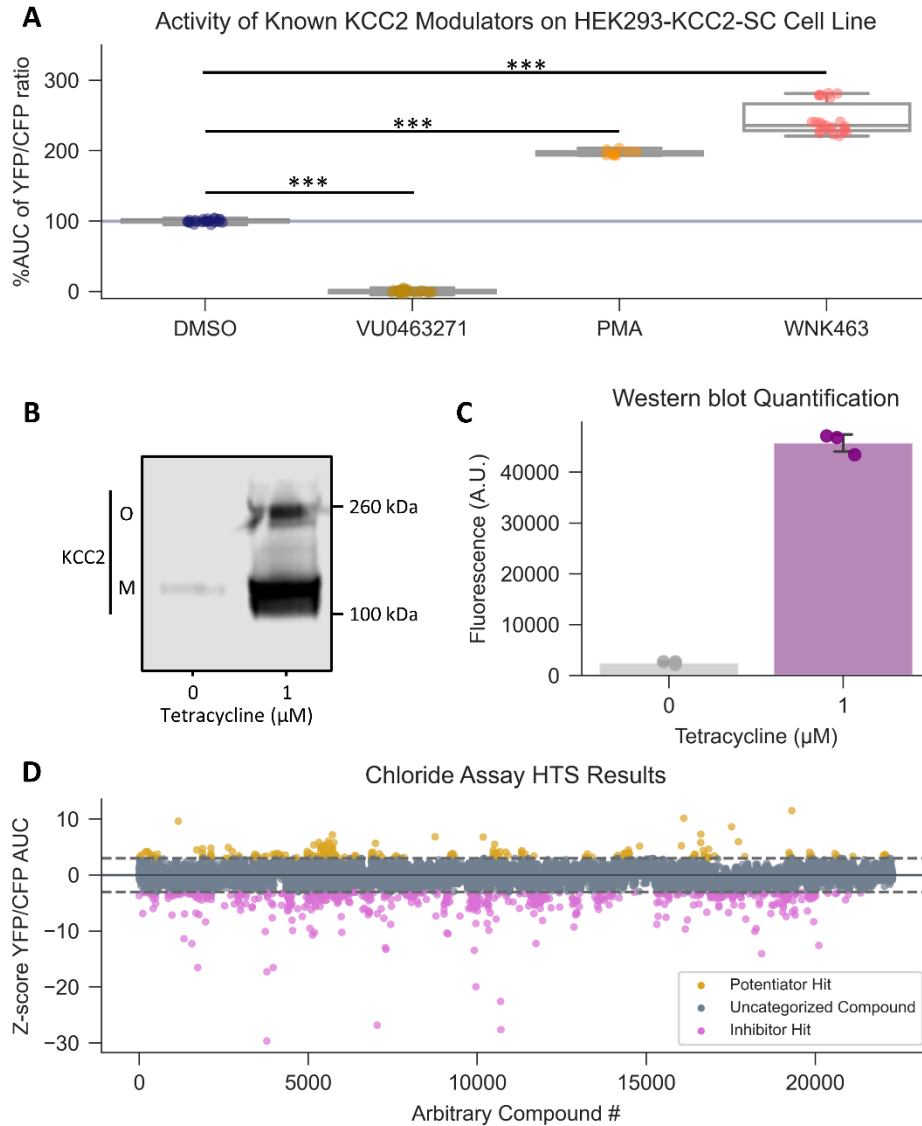
Figure 3.2. The HEK-293-KCC2-SC Cell Line [4p2.F7] used for screening exhibits KCC2-dependent pharmacology, and induction-dependent expression of KCC2. (*A*) Activity of a panel of known KCC2 modulators on YFP/CFP ratio in the HEK-293 cell line used for high-throughput screening [N=2 independent experiments with at least 9 technical replicates per experiment]. (*B*) Detection of KCC2 in HEK-293-KCC2-SC cell line [4p2.F7] lysates by immunoblotting, with or without induction by tetracycline. (*C*) Quantification of signal from (*B*) [N=3]. (D) Unsorted HTS results with potentiator and inhibitor hits labeled. Solid line represents vehicle-treated mean. Dotted lines represent 3*SD above or below the vehicle-treated mean. All experiments ran at 37°C. *** = $p < 0.001$ by Mann Whitney *U* test. Error bars represent SD.

dependent, and increased Tl$^+$ influx were considered "validated hits" and were prioritized for further study. Of the validated hits we discovered, VU0500469 (Figure 3.3.A) stood out based on its unique pharmacological profile which is described in detail below (Figure 3.3, 3.4).

VU0500469's Activity is Consistent and Selective Across Distinct Assays of KCC2.

To further validate that VU0500469 (Figure 3.3.A) was not an artifact of the Cl$^-$ flux assay, we tested the compound in two additional mechanistically distinct KCC2 activity assays using HEK-293 cells: the ^{83}Rb$^+$-measured K$^+$ influx (^{83}Rb$^+$/K$^+$ influx) assay (Figure 3.3.B), the Cl$^-$ flux assay (Figure 3.3.C, D), and the Tl$^+$ flux assay (Figure 3.3.E, F). The ^{83}Rb$^+$/K$^+$ influx assay uses radioactive detection of an influx of a K$^+$ congener, ^{83}Rb$^+$, to measure KCC2 activity. Consistent with an increase in KCC2 activity, treatment with 30 µM VU0500469 produced a statistically significant 2.7-fold increase in ^{83}Rb$^+$/K$^+$ influx (24,883 ± 807 pmol/mg/min) over vehicle-treated control (9141 ± 107 pmol/mg/min) (Figure 3.3.B$;$ $p<0.001$). The Cl$^-$ flux assay and the Tl$^+$ flux assay mirrored the outcome of the ^{83}Rb$^+$/K$^+$ influx assay, producing statistically significant increases in the Area Under the Curve (AUC) of the SuperClomeleon YFP/CFP ratio (Figure 3.3.C$;$ $p<0.001$), and fold-increase in Tl$^+$-sensitive dye fluorescence (Figure 3.3.E$;$ $p<0.001$), respectively, which also are in agreement with KCC2 potentiation.

To investigate whether the activity of VU0500469 was dependent on KCC2, we tested VU0500469 in HEK-293 cells lacking KCC2 activity. In the ^{83}Rb$^+$/K$^+$ influx assay, we pharmacologically inhibited KCC2 by co-treating VU0500469 with a maximally effective concentration of the selective KCC2 inhibitor ML077 (108). ML077 co-treatment blocked the increase in ^{83}Rb$^+$/K$^+$ influx seen with VU0500469 treatment alone (Figure 3.3.B$;$ $p < 0.001$), demonstrating sensitivity of VU0500469 to KCC2 inhibition. In the Cl$^-$ flux assay and the Tl$^+$ influx assay, we evaluated KCC2-dependence by conducting the experiments in the absence of KCC2 overexpression. Without KCC2 overexpression, there was no significant difference between

93
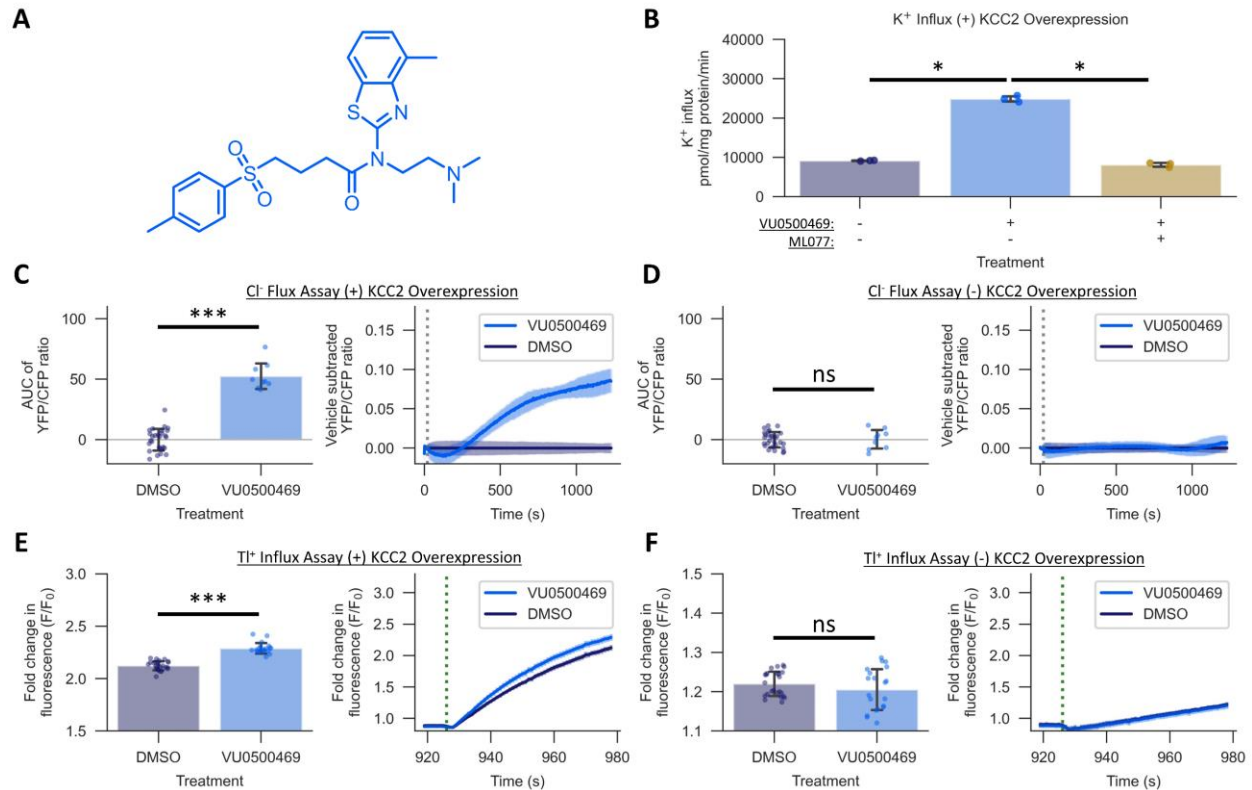
Figure 3.3. VU0500469 potentiates KCC2-mediated ion transport across mechanistically distinct assays of KCC2 activity in HEK-293 cells. (*A*) VU0500469 structure. (*B*) Effect of 30 µM VU0500469 on ^{83}Rb$^+$ influx in cells overexpressing KCC2 in the absence or presence of KCC2 inhibitor ML077 [N=3]. (*C, D*) Effect of 15 µM VU0500469 on Cl$^-$ flux in the absence or presence of KCC2 overexpression. (*C*) Cl$^-$ Flux Assay in cells overexpressing KCC2. Left: AUC of the YFP/CFP Cl$^-$ efflux ratio. Right: Vehicle control subtracted and averaged traces of the YFP/CFP Cl$^-$ efflux ratio. Dotted line represents time of compound addition [N = 2 independent experiments with a total of $\geq$ 9 technical replicates per condition]. (*D*) Cl$^-$ Flux Assay in cells lacking KCC2 overexpression. Data generated and presented as in (*C*). (*E, F*) Effect of 15 µM VU0500469 on Tl$^+$ influx in the absence or presence of KCC2 overexpression. (*E*) Tl$^+$ influx in cells overexpressing KCC2. Left: maximum fold increase in Tl$^+$-sensitive dye fluorescence. Right: fold increase in Tl$^+$-sensitive dye fluorescence over time. Dotted line represents time point of Tl$^+$ addition [N = 2 independent experiments with a total of $\geq$ 20 technical replicates per condition]. (*F*) Tl$^+$ influx in cells lacking KCC2 overexpression. Data generated and presented as in (*E*). All experiments ran at 37°C. Error bars represent SD. Statistical significance calculated by Welch's *t*-test (*B*) and Mann–Whitney *U* test (*C-F*): * = $p < 0.05$, *** = $p < 0.001$, ns = $p > 0.05$.
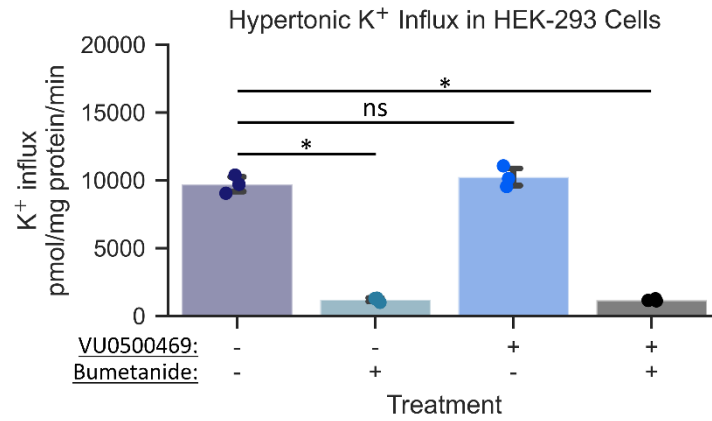
Figure 3.4. VU0500469 does not affect NKCC1 activity. Hypertonic ^{83}Rb$^+$ flux in HEK-293 cells without KCC2 overexpression were used to measure NKCC1 activity. Experiment was conducted in the absence or presence of the NKCC1 inhibitor bumetanide [N=3]. Statistical significance calculated by Welch's *t*-test: ** = $p < 0.01$, *** = $p < 0.001$, ns = p > 0.05. Error bars represent 95% CI.

vehicle control-treated cells and VU0500469-treated cells in either the Cl^- flux assay (Figure 3.3.D; $p > 0.05$) or the Tl^+ flux assay (Figure 3.3.F; $p > 0.05$). These observations further support the KCC2-dependent nature of VU0500469 activity.

To assess whether VU0500469's activity had KCC2 selectivity, we used the $^{83}Rb^+/K^+$ influx assay to measure the effect of VU0500469 on Na^+-K^+-Cl^- Cotransporter 1 (NKCC1), another member of the SLC12 transporter family. We tested NKCC1 because of the high amino acid identity between the two transporters, and because some small molecule inhibitors of KCC2 inhibit NKCC1 and KCC2 indiscriminately – consistent with the presence of a shared small molecule binding site on both transporters. Using hypertonic conditions in HEK-293 cells lacking KCC2 to potentiate NKCC1-mediated ion transport, we established that we could measure NKCC1 activity through the use of the NKCC1 inhibitor, bumetanide. Treatment of the cells with 10 µM bumetanide yielded a strong inhibition of $^{83}Rb^+/K^+$ influx assay, relative to vehicle-treated cells (Figure 3.4; $p < 0.05$). In contrast, $^{83}Rb^+/K^+$ influx under these conditions during 30 µM VU0500469 treatment was indistinguishable from vehicle-treated controls (Figure 3.4; $p > 0.05$), consistent with VU0500469 having selectivity for KCC2 over NKCC1.

VU0500469 Exhibits a Unique Pharmacological Profile.

Confident that the activity of VU0500469 was KCC2-dependent, we next sought to evaluate whether VU0500469 was acting through an established KCC2 regulatory mechanism, or a novel one (Figure 3.5, 3.6).

There are many signaling pathways that influence KCC2 activity (185). Based on the rapid onset of VU0500469's ability to potentiate Cl^- efflux, we reasoned that VU0500469 could act through one of three Cl^- homeostasis regulatory pathways expressed in HEK-293 cells: PKC (66), the WNK-SPAK/OSR1 pathway (67), and NKCC1 (75) (Figure 3.5.A). To test if VU0500469 affected these regulatory pathways, we first used a pharmacological co-treatment approach using
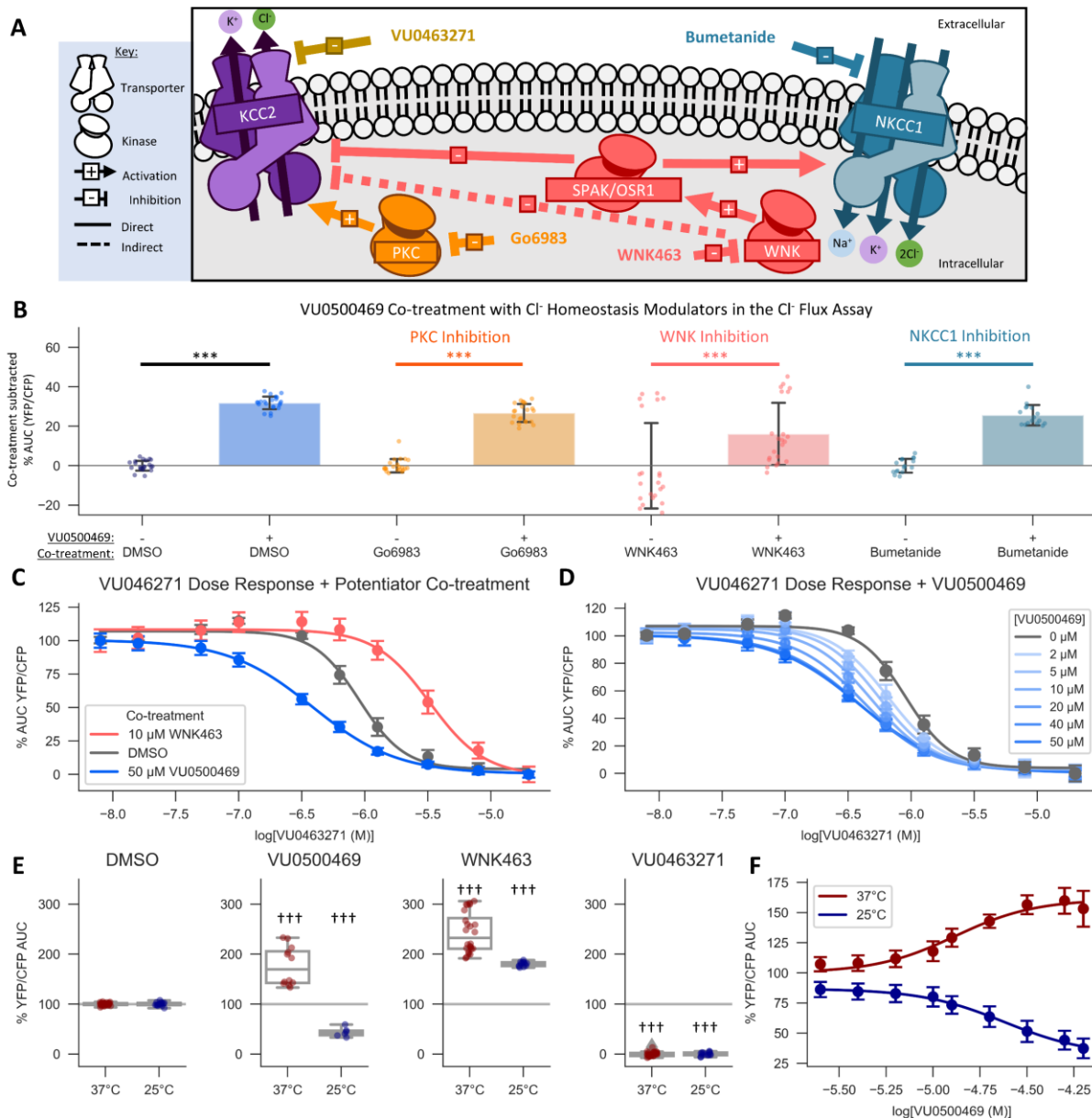
Figure 3.5. VU0500469 potentiates KCC2 by a unique mechanism. All experiments conducted using the Cl⁻ Flux Assay in HEK-293 cells overexpressing KCC2 at 37°C, unless otherwise noted. (*A*) Schematic depicting investigated small molecule targets known to regulate Cl⁻ homeostasis. (*B*) Co-treatment of modulators of Cl⁻ homeostasis from (*A*) with or without VU0500469. (*C, D*) VU0500469 increases the potency of KCC2 inhibitor VU0463271. (*C*) VU0463271 dose-response curve with co-treatment of constant VU0500469, WNK463, or vehicle control at each point. (*D*) VU0463271 dose-response curve with increasing concentrations of VU0500469. Note that the two dose-response curves with the highest concentrations of VU0500469 are overlaid on one another, indicating saturation of the effect. (*E, F*) The mode of VU0500469 activity is temperature dependent. (*E*) Comparison of temperature dependence of vehicle control, VU0500469, WNK463, and VU0463271 at 37°C (red) and 25°C (blue). (*F*) Dose-dependent effect of VU0500469 at indicated temperatures. Error bars represent SD. [N=2 independent experiments with a total of ≥ 8 technical replicates per condition] for all data. Statistical significance calculated by Mann–Whitney *U* test: *** = $p < 0.001$, ††† = $p < 0.001$ relative to corresponding vehicle control.

97
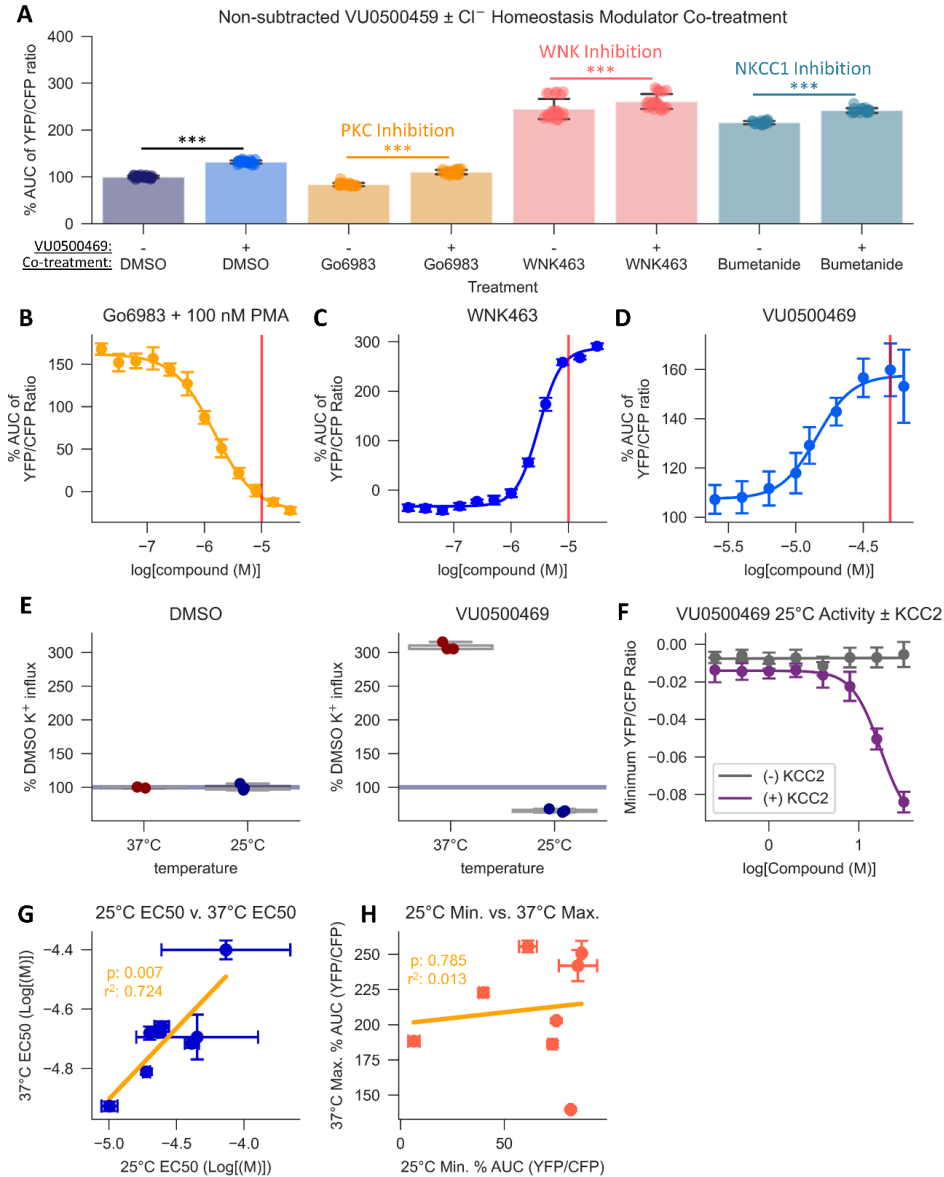
Figure 3.6. Additional validation data for unique KCC2 potentiation mechanism by VU0500469. All data generated in HEK-293 cells overexpressing KCC2 at 37°C, unless otherwise noted. (*A*) Data from VU0500469 co-treatment experiments without control subtraction. Experiment used 10 μM of indicated modulator of Cl$^-$ homeostasis ± 20 μM VU0500469. *** *p* < 0.001, Mann Whitney *U* test. (*B-D*) Dose-response curves for PKC inhibitor Go6983, WNK inhibitor WNK463, and VU0500469 to calculate the dose needed for maximal efficacy in the Cl$^-$ flux assay. Red line indicates maximum concentration used in co-treatment experiments. (*E*) Effect of temperature variation on VU0500469's efficacy in ^{83}Rb$^+$ Influx Assay. (*F*) Effect of varying KCC2 expression on VU0500469's inhibitory activity at 25°C in the Cl$^-$ flux assay. (*G-H*) Correlations between fits of dose-response curves in the Cl$^-$ flux assay for compounds with similar structure to VU0500469. (*G*) Correlation between the EC$_{50}$ at 25°C and 37°C. *p* = 0.007 by Wald Test, r^2 = 0.724. (*H*) Correlation between inhibition at 25°C and potentiation at 37°. *p* = 0.785 by Wald Test, r^2 = 0.013. Error bars represent SD in (*A-F*) and SEM in (*G, H*). [N=3] for Rb$^+$ influx experiments, all other experiments where [N=2 independent experiments with $\geq$ 8 technical replicates per condition].

regulatory pathway inhibitors, together with the Cl$^-$ flux assay, in KCC2 overexpressing HEK-293 cells. We observed that 20 µM VU0500469 retained its ability to potentiate Cl$^-$ efflux (Figure 3.5.B, S3A; $p < 0.001$) despite treating cells with saturating inhibitor concentrations of either PKC (Go6983), WNK (WNK463), or NKCC1 (bumetanide) (Figure 3.6.B, C), suggesting that VU0500469 acts independent of these regulatory mechanisms. Furthermore, we reasoned that VU0500469 acts by a distinct mechanism relative to compounds which increase KCC2 activity on the timescale of hours to days, such as CLP257 (10), owing to its rapid onset on the scale of minutes, and that VU0500469 works independent of pathways that increase KCC2 expression, such as KCC2 expression-enhancing compounds (KEECs) (14), because VU0500469 does not alter total protein expression of KCC2 (Figure 3.9.D).

To gain further insight into VU0500469's pharmacological mechanism, we investigated what phenotype the co-treatment of a direct-acting KCC2 inhibitor, VU0463271 (59, 108), would have with KCC2 potentiators. Using the Cl$^-$ flux assay in HEK-293 cells overexpressing KCC2, when Cl$^-$ efflux was potentiated by 10 µM WNK463 treatment, we observed a rightward shift in the potency of the VU0463271 dose response curve (Figure 3.5.C). Surprisingly, 50 µM VU0500469 co-treatment caused a leftward shift in the VU0463271 dose response curve (Figure 3.5.C), consistent with increasing the KCC2 inhibitor's potency. Moreover, this potency increase is dose-dependent (Figure 3.5.D) and saturates at the same concentration that VU0500469's ability to potentiate Cl$^-$ efflux saturates (Figure 3.6.D), establishing a stronger link between VU0500469's ability to potentiate KCC2 activity and its effect on VU0463271 potency. These findings further distance VU0500469's activity from WNK inhibition, and emphasize its unique pharmacological mechanism.

During our characterization of VU0500469, we discovered that the pharmacological mode of the compound's activity in the Cl$^-$ flux assay is temperature dependent: at 37°C VU0500469 acts as a KCC2 potentiator (Figure 3.5.E; $p < 0.001$), while at 25°C the compound acts as a KCC2 inhibitor (Figure 3.5.E; $p < 0.001$). Additionally, the temperature-dependent effects of VU0500469

are dose-dependent (Figure 3.5.F), are reproducible in the $^{83}Rb^+/K^+$ influx assay (Figure 3.6.E), and are KCC2 expression-dependent (Figure 3.6.F), further strengthening the link between VU0500469's pharmacological activity and KCC2. Conversely, WNK463 and VU0463271 either potentiate or inhibit KCC2, respectively, independent of the temperature tested (Figure 3.5.E; $p < 0.001$). The temperature-dependence of VU0500469 further underscores the novelty of this compound's pharmacology.

Collectively with VU0500469's activity in the presence of known inhibitors of Cl^- homeostasis (Figure 3.5.B, Figure 3.6.A-C), its ability to increase the potency of VU0463271 (Figure 3.5.C, D), and its temperature-dependent effect (Figure 3.5.E, F; Figure 3.6.E, F), we conclude that VU0500469 works via a previously unreported mechanism to potentiate KCC2 activity.

Improvement of VU0500469's Pharmacological Properties to Yield VU0916219.

While we were encouraged by the first-in-class KCC2 potentiator activity that VU0500469 possesses, the compound exhibited lower potency (EC$_{50}$, 14.2 ± 0.7 µM; Figure 3.6.D) and efficacy (E$_{max}$, 158 ± 2%; Figure 3.6.D) than we desired. Starting from the VU0500469 lead compound we sought to improve these properties by further screening of the in-house compound library and direct synthetic modification of the VU0500469 scaffold (Figure 3.7, 3.8).

We began by screening 200 compounds from the Vanderbilt Discovery Collection with structural similarity to VU500469 to develop a structure activity relationship (Figure 3.8.A). Structural similarity to VU0500469 was quantified by Tanimoto coefficient (Tc) calculation after chemical fingerprinting (181, 186) of the Vanderbilt Discovery Collection. Compounds with the highest Tc were selected for screening with or without KCC2 overexpression to assess KCC2-dependence. From this screen, we discovered inactive analogs with high structural similarity to VU0500469 (VU0500693 Tc = 0.82, VU0500849 Tc = 0.79) which are suitable as inactive control
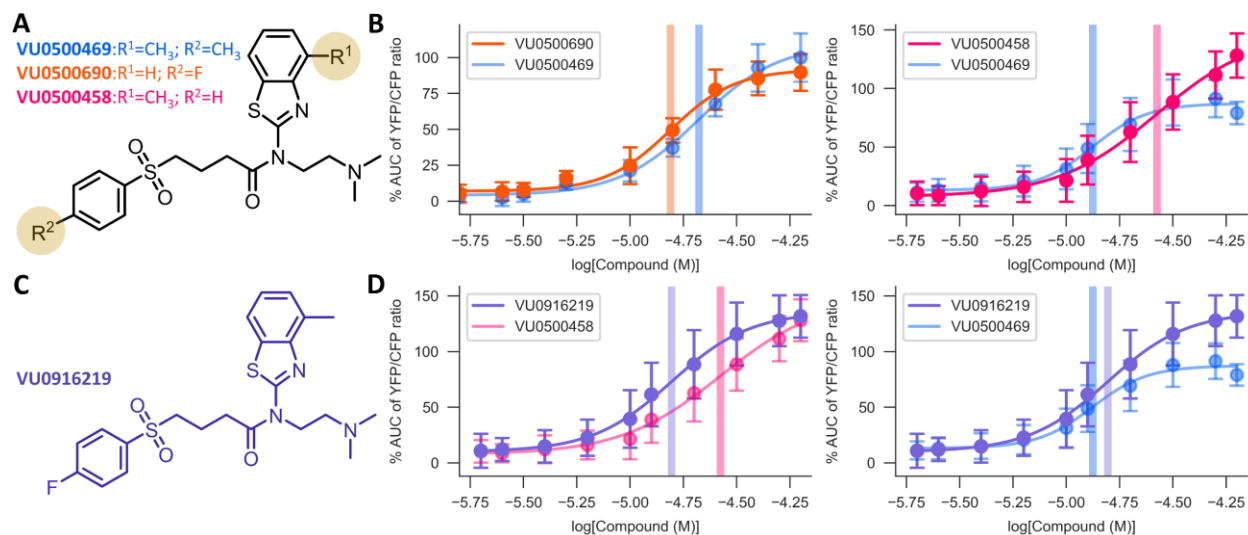
Figure 3.7. Development of VU0916219, a KCC2 potentiator with improved efficacy. Experiments conducted at 37°C, using the Cl⁻ Flux Assay in HEK-293 cells overexpressing KCC2. Data are normalized to maximum VU0500469 activity being 100%. (*A*) Structures of the most potent and efficacious VU0500469 analogs. (*B*) Comparison of VU0500469 dose-response curve to: most potent (left panel) and efficacious (right panel) compounds. (*C*) Structure of VU0916219. (*D*) Comparison of VU0916219 to the most efficacious compound (left panel), and VU0500469 (right panel). [N = 2 independent experiments with a total of ≥ 6 technical replicates per condition]. Error bars represent SD.
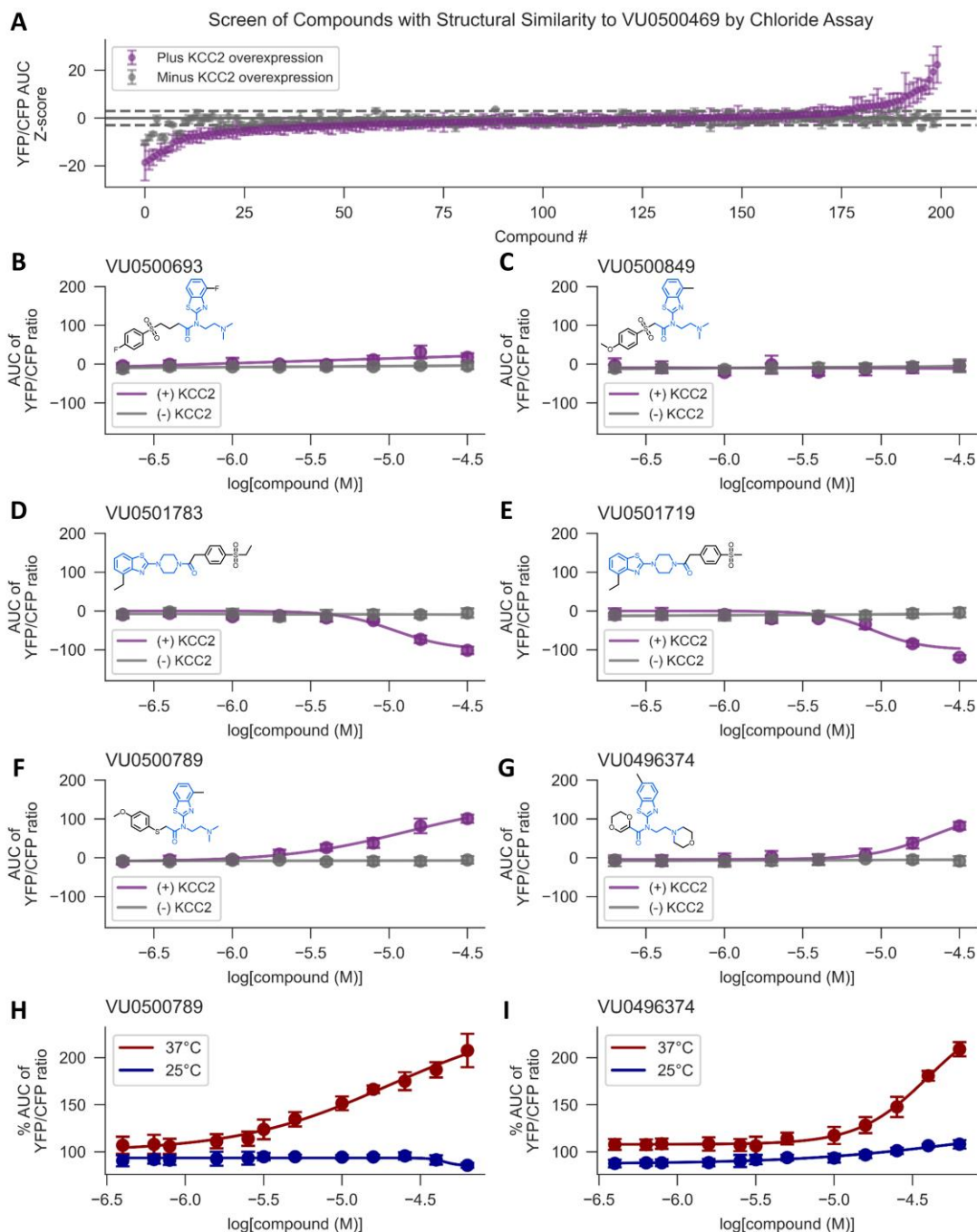
Figure 3.8. Representative VU0500469 analogs from SAR studies with multiple activity modes on KCC2. Data generated in HEK-293 cells overexpressing KCC2 at 37°C using the Cl⁻ flux assay, unless otherwise indicated. (*A*) Screening results of 200 compounds with similar structure to VU0500469 ± KCC2 overexpression. (*B-G*) Dose response curves ± KCC2 overexpression for VU0500469 analogs with distinct activity and structure. *Inset*: structures of compounds used in the dose response curves, with similar structural regions between compounds highlighted. (*H, I*) Effect of varying temperature on the activity of VU0500789 and VU0496374, VU0500469 analogs with distinct structural elements that retained KCC2 potentiator activity at 37°C. [N=2 independent experiments with at least 4 total technical replicates per data point]. Error bars represent SD.

compounds (Figure 3.8.B, C). Additionally, we discovered VU0500469 analogs, which featured the tertiary amine and amino groups embedded in a piperazine ring (VU0501719 Tc = 0.76, VU0501783 Tc = 0.79), that exhibited KCC2-dependent inhibition at 37°C (Figure 3.8.D, E), indicating that changes to the class's structure can switch its pharmacological mode. Importantly, we discovered multiple KCC2-dependent Cl$^-$ efflux potentiators with either improved potency (VU0500690 Tc =0.87) or efficacy (VU0500458 Tc =0.99) relative to VU0500469 (Figure 3.7.A*, B*). We also discovered VU0500469 analogs, while sharing the central benzthiazole moiety and retaining KCC2 potentiator activity, that had appreciable differences in structure through the rest of the molecule (VU0496374 Tc = 0.55, VU0500789 Tc = 0.73) (Figure 3.8.F, G). From these data, we conclude that VU0500469 analogs can tolerate structural changes while maintaining its ability to potentiate KCC2 activity.

To confirm that the activities of VU0500469 and VU0500458 were due to the chemicals registered in our chemical library, and not impurities or mislabeled compounds, we resynthesized VU0500469 (Scheme 1) and VU0500458 (Scheme 2). We then validated that the resynthesized compounds (Figure 3.7.B, D) retained the same activity as the stocks from the chemical library (Figure 3.3.C) in the Cl$^-$ flux assay.

To improve upon the pharmacological properties of VU0500469, we sought to combine the unique features of the most potent compound we had discovered, the fluorophenyl group from VU0500690 (Figure 3.7.A, B *Left*), and the most efficacious compound, the 4-methyl-benzthiazole from VU0500458 (Figure 3.7.*A, B Right*) into a single structure, VU0916219 (Figure 3.7.C). We synthesized VU0916219 using a similar synthetic route to VU0500458 (Scheme 2). VU0916219 retained the same efficacy (E_{max}, 202 ± 5%; Figure 3.7.D) as our most efficacious compound, VU0500458 (E_{max}, 213 ± 13%; Figure 3.7.D), however, VU0916219 had a notable increase in potency (EC_{50}, 17.1 ± 1.2 μM; Figure 3.7.D) relative to VU0500458 (EC_{50}, 28.8 ± 4.2 μM; Figure 3.7.D). While VU0916219's potency (EC_{50}, 17.1 ± 1.2 μM; Figure 3.7.D) was still slightly less than VU0500469's (EC_{50}, 14.2 ± 0.7 μM; Figure 3.7.D), VU0916219 had a greater efficacy than

VU0500469 at all concentrations tested (Figure 3.7.D). That overall increase in activity, coupled with VU0916219's increased maximum efficacy (E_{max}, 202 ± 5%; Figure 3.7.D) relative to VU0500469 (E_{max}, 158 ± 2%; Figure 3.7.D), represent improvements in *in vitro* pharmacological properties over VU0500469. Furthermore, these data indicate that the VU0500469 structural class is suitable for future medicinal chemistry efforts to further improve its pharmacological properties.

VU0916219 Increases KCC2 Surface Expression.

Given the effect of temperature on the VU0500469 structural class's activity at KCC2 and the known effect of temperature on transporter trafficking, we investigated the possibility that KCC2 potentiators from the VU0500469 structural class affected KCC2 surface expression.

To better detect subtle changes brought about by pharmacological changes in KCC2 cell surface expression, we decided to use our most efficacious compound, VU0916219, for cell surface expression experiments. VU0916219 is a suitable compound to draw conclusions about the VU0500469 structural class because it is a close chemical analog to VU0500469 (Figure 3.7.A, C, Tc = 0.82), and has the same pharmacological profile as VU0500469, namely: (i) KCC2-dependent activity (Figure 3.10.A), and (ii) temperature-dependent pharmacological mode switching (Figure 3.10.B).

To measure changes in KCC2 surface expression, we used surface biotinylation (187) in HEK-293 cells overexpressing KCC2. We isolated surface fractions using streptavidin affinity purification, and we subsequently quantified surface and total KCC2 expression levels by immunoblot. Treatment with either 100 nM phorbol 12-myristate 13-acetate (PMA), a PKC agonist previously shown to increase KCC2 surface expression (66), or 60 μM VU0916219 caused a statistically significant increase in KCC2 surface levels relative to vehicle-treated controls (Figure 3.9.A, B; $p < 0.05$). In contrast, total KCC2 levels were statistically indistinguishable from vehicle
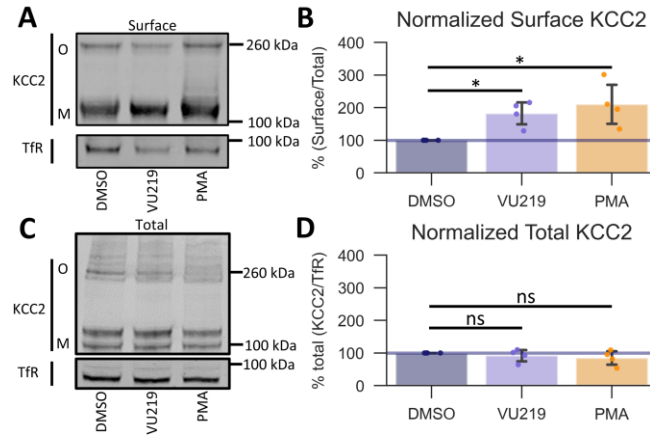
Figure 3.9. VU0916219 (VU219) increases surface expression of KCC2 without affecting total KCC2 levels in HEK-293 cells. (*A*) Representative Western blot of biotinylated surface fraction from cells treated with vehicle (DMSO), VU219, or the positive control phorbol 12-myristate 13-acetate (PMA). Band intensity was normalized to Transferrin Receptor (TfR) levels. O = oligomeric KCC2, M = monomeric KCC2. (*B*) quantification of (*A*) as Surface KCC2/Total KCC2 normalized to TfR levels. (*C*) Representative Western blot of total protein fraction from cells treated as in (*A*). (*D*) Quantification of (*C*) as total KCC2 normalized to TfR levels. [N=4]. Error bars represent SD. Statistical significance calculated by paired *t*-test: * = $p < 0.05$; ns = $p > 0.05$.
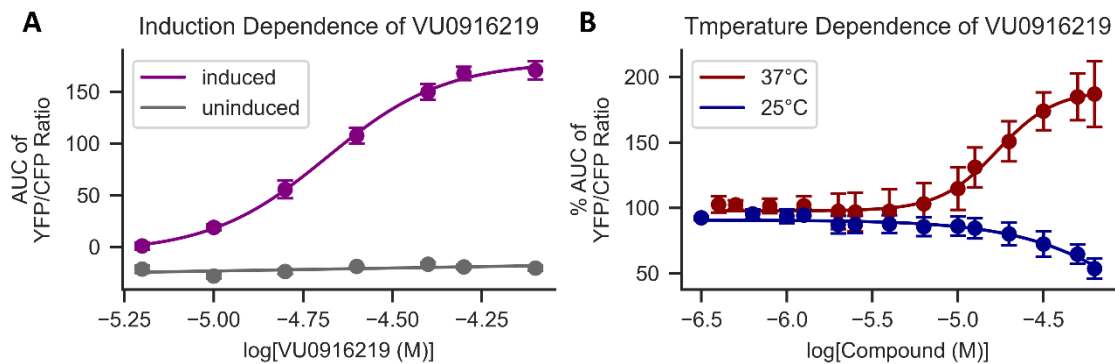
Figure 3.10. VU0916219 has a similar pharmacological profile to VU0500469. All data generated in HEK-293 cells overexpressing KCC2 using the Cl⁻ flux assay at 37°C, unless otherwise indicated. (*A*) Dose-dependence of VU0916219 activity in presence or absence of KCC2 induction. (*B*) Dose-dependent potentiator activity of VU0916219 at 37°C or inhibitory activity at 25°C. [N=2 independent experiments with at least 6 technical replicates per data point]. Error bars represent SD.

treated controls for both PMA and VU0916219 (Figure 3.9.C, D; $p > 0.05$). Taken together, these data are consistent with the conclusion that the VU0500469-like compounds increase KCC2 surface expression without affecting total KCC2 expression.

VU0500469 Prevents Synchronized Ca^{2+} Oscillations in Neuronal-Glial Co-cultures.

To evaluate if VU0500469 could affect an epilepsy-relevant process in a more native system, we applied a previously described neuronal-glial co-culture seizure model (183) (Figure 3.11.A). This model is based on the observation that high-density neuronal-glial rat cortical cultures undergo synchronous Ca^{2+} oscillations that mirror synchronous electrical activity during seizure events. The rate of these Ca^{2+} oscillations are reduced when the cultures are treated with antiepileptic drugs, such as carbamazepine (CBZ) (Figure 3.11.B, C; $p < 0.01$), and elevated when treated with convulsant agents, such as 4-aminopyridine (4-AP) (Figure 3.11.C; $p < 0.001$).

To validate the suitability of this system for modeling KCC2 activity during seizure-like events, we demonstrated that (i) KCC2 is expressed in neuronal populations via immunofluorescence (Figure 3.12.A), and (ii) KCC2 is functional in these neurons as seen by the increased Ca^{2+} oscillation rates generated by VU0463271-mediated KCC2 inhibition (Figure 3.11.C; $p < 0.01$), and reduced Ca^{2+} oscillation rates generated by diazepam-mediated positive allosteric modulation of GABA$_A$ receptors, which relies on the Cl$^-$ gradient established by KCC2 for its activity (Figure 3.11.C; $p < 0.01$) (1).

Treatment of these neuronal-glial co-cultures with VU0500469 caused a dose-dependent decrease in Ca^{2+} oscillations (Figure 3.11.D-F). In contrast, treatment with a close structural analog to VU0500469 which is largely inactive in the Cl$^-$ flux assay, VU0500693 (Figure 3.8.B), did not produce a dose-dependent decrease in Ca^{2+} oscillation rate (Figure 3.11.G-I). Moreover, there was a statistically significant correlation between increased KCC2 activity in the HEK-293 cell-based Cl$^-$ flux assay and a decrease in neuronal Ca^{2+} oscillation rate, strengthening the

Figure 3.11. VU0500469 inhibits seizure-like, synchronous Ca2+ oscillations in cultured rat cortical neurons. (*A*) Cartoon description of the synchronous Ca^{2+} oscillation assay, which uses neuronal Ca^{2+} oscillations from high density neuronal-glial cocultures to model epileptiform activity. (*B, C*) Validation of the synchronous neuronal Ca^{2+} oscillation assay's ability to report anti-epileptic and KCC2-dependent activity. (*B*) Example Ca^{2+} oscillation trace treated with the antiepileptic drug carbamazepine (CBZ). Segments before and after compound addition are highlighted to better show neuronal Ca^{2+} oscillations in the absence and presence of compound, respectively. Timepoint of compound addition denoted by the red line. Oscillations recognized by a spike counting algorithm are marked by a red "X". (*C*) Quantified % pre-addition oscillation rate for CBZ, the $GABA_A$ positive allosteric modulator diazepam, vehicle control, the convulsant 4-AP, and the KCC2 inhibitor VU0463271 [N=3]. (*D-F*) VU0500469 dose-dependently prevents seizure-like Ca^{2+} oscillations. (*D*) VU500469 structure. (*E*) Example trace treated with 20 μM VU0500469, annotated as in (*B*). (*F*) Dose-dependent effect of VU0500469 on Ca^{2+} oscillation rate. (*G-I*) VU0500693, a structurally related analog of VU0500469 without significant activity in the Cl^- flux assay, does not affect seizure-like Ca^{2+} oscillations. (*G*) VU0500693 structure. (*H*) Example trace treated with 20 μM VU0500693, presented as in (*B*). (*I*) Dose-dependent effect of VU0500693 on % pre-addition oscillation rate. Error bars represent SD. [N=2 independent experiments with 10 total technical replicates]. Statistical significance calculated by one sample *t*-test (*6B*, to illustrate DMSO is statistically significant from 0%), and Welch's *t*-test for all other samples: ** = $p < 0.01$, *** = $p < 0.001$.

Figure 3.12. Additional validation of compound activity on KCC2 in the synchronous neuronal Ca2+ oscillation assay. (*A*) KCC2 immunoreactivity colocalizes with immunoreactivity from an inhibitory neuronal marker, GAD. Representative immunofluorescence images from neuronal-glial cocultures used in the synchronous neuronal Ca^{2+} oscillation assay. (*B*) Plot of compound activity at 30 µM in the Cl⁻ flux assay against compound effect on % baseline oscillation rate at 6 µM in the neuronal Ca^{2+} oscillation assay [N=2 independent experiments with 4 total technical replicates per data point]. Error bars represent SD. p = 0.013, Wald Test with t-distribution of the test statistic; r^2 = 0.667.

relation between VU0500469's effect on Cl⁻ extrusion and the anti-seizure effect seen in the epilepsy model (Figure 3.12.B). Collectively, these results support the conclusion that VU0500469 decreases seizure-like activity in cultured neurons.

Discussion

Taken together, we have detailed the discovery and characterization of a new KCC2 potentiator class, exemplified by VU0500469 and VU0916219, and demonstrated the ability of these compounds to prevent seizure-like, synchronous Ca^{2+} oscillations in neurons. The KCC2-dependence, consistency in potentiator activity across disparate assays of KCC2, selectivity versus a closely related transporter, and unique mechanism of VU0500469-like compounds support the conclusion that these compounds represent a new KCC2 potentiator class. The discovery of a new KCC2 potentiator class is significant because these compounds deepen our understanding of KCC2 potentiation, and are useful for investigation of KCC2's therapeutic potential in a host of neurological disorders with tremendous unmet medical need (1). Furthermore, our discovery that the VU0500469 class prevents seizure-like events further validates the antiepileptic promise of KCC2 potentiation, and provides evidence that pharmacological KCC2 potentiation, alone, is sufficient to produce an antiepileptic effect.

Our results indicate that active members of the VU0500469 structural class potentiate KCC2 via a unique mechanism. We did not directly test a number of mechanisms capable of increasing KCC2 activity that are upstream of PKC (188), since we show that VU0500469 functions independent of PKC. Furthermore, we also did not directly test SPAK/OSR1 modulators, given our data which indicate that VU0500469 acts independent of the WNK signaling pathway, and the fact that SPAK/OSR1 inhibitors have been shown to inhibit NKCC1 (189, 190), whereas VU0500469 has no discernable effect on that transporter. In addition to the mechanisms we

110

Table 3.1. Structural information for VU0500469-class KCC2 potentiators.

Compound	SMILES	Similarity (Tc)
VU0500469	CC1=CC=C(C=C1)S(=O)(=O)CCCC(=O)N(CCN(C)C)C2=NC3=C(C=CC=C3S2)C	1.000
VU0500454	CC1=CC2=C(C=C1)N=C(S2)N(CCN(C)C)C(=O)CCCS(=O)(=O)C3=CC=CC=C3	0.945
VU0500789	CC1=C2C(=CC=C1)SC(=N2)N(CCN(C)C)C(=O)CSC3=CC=C(C=C3)OC	0.726
VU0496374	CC1=CC2=C(C=C1)N=C(S2)N(CCN3CCOCC3)C(=O)C4=COCCO4	0.546
VU0500690	CN(C)CCN(C1=NC2=CC=CC=C2S1)C(=O)CCCS(=O)(=O)C3=CC=C(C=C3)F	0.869
VU0500458	CC1=C2C(=CC=C1)SC(=N2)N(CCN(C)C)C(=O)CCCS(=O)(=O)C3=CC=CC=C3	0.995
VU0500465	CC1=CC=C(C=C1)S(=O)(=O)CCCC(=O)N(CCN(C)C)C2=NC3=CC=CC=C3S2	0.940
VU0500456	CN(C)CCN(C1=NC2=C(S1)C=C(C=C2)F)C(=O)CCCS(=O)(=O)C3=CC=CC=C3	0.862
VU0916219	FC1=CC=C(S(=O)(CCCC(N(C2=NC3=C(C)C=CC=C3S2)CCN(C)C)=O)=O)C=C1	0.956

Table 3.2. Dose-response estimation of pharmacological properties of VU469-class potentiators.

Compound	Emax (% VU0500469)	Hill Coefficient	Log[EC50(M)]
VU0500469	100 ± 5.9	2.3 ± 0.3	-4.68 ± 0.03
VU0500454	70.1 ± 4.9	2.4 ± 0.4	-4.66 ± 0.04
VU0500789	115.8 ± 23.1	0.9 ± 0.2	-4.69 ± 0.19
VU0496374	122.7 ± 17.9	1.9 ± 0.3	-4.4 ± 0.08
VU0500690	83.7 ± 3.4	2.9 ± 0.5	-4.81 ± 0.03
VU0500458	170.6 ± 22.7	1.9 ± 0.4	-4.58 ± 0.08
VU0500465	72 ± 6.5	2.1 ± 0.4	-4.68 ± 0.06
VU0500456	32.3 ± 1.8	5 ± 1.9	-4.93 ± 0.04

tested, other compounds that increase KCC2 activity on longer timescales have also been reported (10, 14, 51). These include compounds that act on the timescale of hours, such as CLP257 (10) and TrkB antagonists (51, 81), or days, in the case of KEECs (14). The VU0500469 chemical class is distinguished from these reported KCC2 potentiators by its rapid onset of activity, and in the case of KEECs and TrkB antagonists, by the lack of effect the VU0916219 has on total KCC2 protein expression. Together, these findings are consistent with the VU0500469 structural class being a first-in-class KCC2 potentiator.

During our mechanistic studies, an interesting finding was that the co-treatment with VU0500469 and the direct KCC2 inhibitor VU0463271 increased VU0463271's potency. Recently, a structure of VU0463271 bound to KCC1, another SLC12 family member with 66.3% sequence identity to KCC2, was published; this structure reported VU0463271 bound to the ion permeation path on the extracellular face of the transporter, where it stabilized an outward-open state of the transporter (191). It is therefore conceivable that VU0500469 treatment could lower an energetic barrier to promote an outward-open confirmation of the transporter, thereby favoring the formation of an VU0463271-KCC2 complex and driving an increase in VU0463271 potency. Interestingly, the transition from an inward-facing to outward-facing state is the rate-limiting step in multiple SLC transporters, including SERT (192) and EAAT2 (193), and is also rate-limiting in K^+-Cl^- cotransport in erythrocytes (194). Furthermore, facilitating this reorientation is thought to be the mechanism by which the allosteric EAAT2 potentiator, Parawixin1, exerts its effects (193). Hence, facilitation of the reorientation of the transporter to an outward-open state may also underlie the potentiator activity of the VU0500469 structural class. Future mechanistic studies, however, are required to evaluate this hypothesis.

Another intriguing finding from our studies characterizing VU0500469 was its temperature-dependent activity. While all compounds tested had lower activity at 25°C than 37°C, of particular note was the temperature-dependent switch between potentiation and inhibition for some VU0500469 class members. We observed a statistically significant correlation between the IC_{50}

of the inhibitory activity at 25°C and EC$_{50}$ of the potentiator activity at 37°C (Figure 3.6.G, Table 3.1 & 3.2), which may indicate a mechanistic relationship between the observed inhibition and potentiation. However, we did not find a statistically significant correlation between the magnitude of the inhibitory activity at 25°C and the magnitude of potentiator activity at 37°C (Figure 3.6.H, Table 3.1 & 3.2), which suggests that the inhibitory activity at 25°C is not indicative of potentiator activity at 37°C. Moreover, the most efficacious members of this chemical class, VU0500458 and VU0916219, had less inhibitory activity at 25°C than other VU0500469 structural class members, indicating that the inhibitory activity at 25°C may decrease potentiator efficacy at 37°C. Finally, the most chemically distinct member of the VU0500469 class of compounds, VU0496374, lacked inhibitory activity altogether at 25°C. We therefore conclude that the temperature-dependent switch between potentiation and inhibition is not necessary for this chemical class's activity as a KCC2 potentiator.

Given the VU0500469 structural class's unique pharmacological profile, it would be informative to discover its molecular target. It is conceivable that the VU0500469 structural class may be a direct-acting KCC2 potentiator, given VU0500469's effect on the potency of the KCC2 inhibitor VU0463271: the saturable increase in the potency of VU0463271 by VU0500469 is a hallmark of an allosteric interaction (195, 196), and given VU0463271's direct interaction with KCC2 (59), may indicate an allosteric interaction between the two chemical classes. Alternatively, this chemical class may be targeting a yet undescribed KCC2 regulator, or interacting with a known regulator in a novel way. Regardless, the elucidation of the target of VU0500469 would deepen our understanding of how small molecules can potentiate KCC2 and should be the focus of future studies.

Although we have improved some pharmacological properties of VU0500469, further improvement and investigation of its pharmacological properties is needed. The most optimized member of this chemical class is still lacking in potency. Its micromolar potency may preclude *in vivo* studies owing to the large projected dose needed to observe effects on KCC2. Furthermore,

the pharmacokinetic properties of this chemical class are currently unknown. Pharmacokinetic studies are warranted to evaluate if the VU0500469 structural class is suitable for *in vivo* use. Regardless, we have shown that the chemical class can maintain activity at KCC2 after chemical modification, and established a preliminary SAR. Based on these findings, we conclude that the VU0500469 structural class represents an excellent starting point for KCC2 potentiator discovery and is a superb candidate for future medicinal chemistry work.

CHAPTER 4

CONCLUSIONS AND FUTURE DIRECTIONS

Conclusions

This work deepens the field's understanding of neuronal K^+-Cl^- cotransport, an important physiological process implicated in a host of neurological diseases, and provides needed tool compounds to facilitate future work in this area. This work's contributions can be broken down into two major parts: in **Chapter 2**, we investigated the epileptogenic effects of KCC2 inhibition in the insect nervous system, and in **Chapter 3**, we investigated the antiepileptic effects of KCC2 potentiation in mammalian systems.

In **Chapter 2**, our main conclusions are: (a) that insect K^+-Cl^- cotransporter KCC and the insect Cl^- channel GABA-R are functionally coupled in the *Drosophila* nervous system, and that (b) KCC inhibition is insecticidal for a vector of human disease, *Aedes aegypti*. Our claim that (a) KCC and GABA-R function is coupled is evidenced by the increase in seizure-like activity produced by KCC inhibition by VU0463271, the effect blunted effect of GABA-mediated signaling in the presence of small molecule KCC inhibition or KCC knockdown, and by the synergistic effect sub-maximal doses of KCC inhibition and GABA-R inhibition had on seizure-like activity. These findings are significant because *Drosophila* is a widely used model system for studying neurotransmission, and our work validates a key functional relationship within this process. The functional coupling of K^+-Cl^- cotransport is well established in mammalian systems, however, this validation was lacking in insect systems. By demonstrating this relationship can also be modeled in insect systems, our work supports the use of *Drosophila* for studies investigating this key aspect of inhibitory neurotransmission. Furthermore, they provide mechanistic context to our findings that

KCC inhibition is insecticidal. Our claim that (b) KCC inhibition is insecticidal is evidenced by our data demonstrating that administration of the KCC inhibitor VU0463271 is toxic to adult female mosquitos and mosquito larvae, while decreasing mosquito excretory capacity. These findings are significant because insecticides are essential for managing agricultural pests and vectors of human disease, and because rising insecticide resistance is eroding our ability to control these deleterious interactions with insects. Therefore, our findings contribute to the discovery of new insecticides useful for combatting agricultural pests and vectors of disease that are increasingly becoming resistant to current approaches.

In **Chapter 3**, our main conclusions were that we: (a) discovered a new class of small molecule KCC2 potentiator, and (b) small molecule KCC2 potentiation can attenuate seizure-like activity. Our claim that (a) we discovered a new class of small molecule KCC2 potentiator is evidenced by the activity of our lead class across multiple assays of KCC2 activity, the ability of our compounds to increase KCC2 surface expression, and the unique pharmacological profile our compounds have relative to any described KCC2 potentiator in the literature. These findings are significant because KCC2 pharmacology is limited, and the lack of drug-like probes capable of potentiating KCC2 activity is precluding studies investigating the functions of KCC2 in human physiology and disease. Our discovery of a new KCC2 potentiator class therefore helps lay the foundation for future studies investigating the biology and therapeutic potential of KCC2 potentiation. Our claim that (b) small molecule KCC2 potentiation can attenuate seizure-like activity is evidenced by the ability of our compounds to prevent synchronous Ca^{2+} oscillations in a neuronal-glial co-culture model of epilepsy, and the correlation between activity of analogs of in the Cl^- efflux assay and the neuronal-glial co-culture model of epilepsy. These findings are significant because epilepsy is a widespread and debilitating neurological disorder with significant unmet medical need. Our findings contribute to a wealth of evidence supporting KCC2 potentiation as a viable therapeutic approach in epilepsy, including some of the first evidence supporting pharmacological KCC2 potentiation as antiepileptic. In doing so, our work could help

lay the foundation for the development of new antiepileptic treatments, which would benefit millions of people afflicted with epilepsy across the globe.

Future Directions

The most salient future directions stemming from this work relate to the chemical tools we have discovered and characterized. Natural extensions of the work in **Chapter 2** should be directed towards the discovery and development of KCC-directed insecticides. From **Chapter 3**, it is important to improve the pharmacological properties of our lead class, discover the lead class's mechanism-of-action on KCC2, and use the methodology developed herein to further develop KCC2 potentiator pharmacology.

Discovery and development of KCC-directed insecticides

While VU0463271 was sufficient to establish proof-of-concept for the insecticidal potential of KCC, it is not a suitable insecticide because of its pharmacokinetics and its toxicological potential in humans. The utility of VU0463271 is limited because it is not topically bioavailable when administered to insects (135). Topical bioavailability is essential for KCC-directed insecticides, since that is how nervous system-directed insecticides would be used in practice. Furthermore, VU0463271 is potentially toxic in humans because this compound is designed to inhibit human KCC2 (162), and given the seizure-liability associated with KCC2 inhibition (7), this compound could also present a seizure-liability in humans; however, VU0463271's poor pharmacokinetics in mammals may actually be beneficial from a safety perspective (162), since it is not stable in human plasma. There are two main approaches that can be used to aid the discovery and development of KCC-directed insecticides: use of medicinal chemistry to improve the insecticidal properties of VU0463271, and the discovery of new KCC-directed insecticides independent of VU0463271 using HTS.

For the medicinal chemistry-directed approach, efforts should initially be focused at discovering the structural determinants of VU0463271 that prevent this compound from having appreciable topical bioavailability, while maintaining activity at KCC2. VU0463271 itself is hydrophobic (XLOGP3-AA = 3.8) on par with other topically bioavailable insecticides (e.g. dieldrin XLOGP3-AA = 3.7), so the lack of topical bioavailability of VU0463271 is not likely due to VU0463271's interaction with the hydrophobic character of the cuticle barrier. VU0463271 may very well be able to enter the insect nervous system pharmacokinetically, but may be the substrate of a drug metabolizing enzyme that is preventing the compound from having appreciable exposure in the insect nervous system. Indeed, VU0463271 is rapidly metabolized in human serum, with a $t_{1/2}$ on the order of minutes (162), potentially by cleavage by an amidase. VU0463271 may very well be the substrate of a similar drug metabolizing enzyme in insects, which is therefore preventing its topical bioavailability. Regardless, initial studies should focus on derivatization of the molecule in ways that maintain inhibitory activity at KCC, but promote the topical bioavailability of the compound. As a secondary goal, future studies should also be focused on diverging compound activity from human KCC2, while maintaining on-target activity on KCC to limit potential adverse effects in humans stemming from KCC2 inhibition. Again, VU0463271's poor pharmacokinetic profile in humans may actually be an advantage in this scenario, since its poor pharmacokinetics will limit human toxicology associated with KCC2 inhibition. The development of VU0463271 analogs with topical bioavailability in insects, potent inhibitory activity at KCC, and, ideally, limited toxicological potential in humans, are an instrumental step translating these proof-of-concept findings into an insecticidal setting.

Alternatively, future efforts can be focused on discovering KCC inhibitors that are independent of VU0463271 using HTS. In our molecular characterization of KCC, we developed a high-throughput compatible, Tl$^+$ influx-based assay of both *Aedes aegypti* (135) and *Drosophila melanogaster* (197) in HEK293 cells. These assays are excellent tools that can be repurposed for HTS directed at finding KCC inhibitors. The tractability of this approach is bolstered by our

lab's previous success in using Tl$^+$ flux-based HTS to discover KCC2 inhibitors (75). By running an entirely new HTS, new chemical starting points can be discovered that ideally have the proper pharmacokinetics, KCC activity, and species selectivity useful for the development of a new class of KCC-directed insecticides.

Improvement of the pharmacological properties of the VU469 class of KCC2 potentiator

While VU0500469 analogs represent a promising new class of KCC2 potentiator, the scope of their practical use would benefit from improvement of their pharmacological properties. The two main properties that should be the primary focus of future work are the class's: potency and temperature-dependence.

Despite the efficacy of these compounds likely being suitable, as seen by the maximal activity of these compounds in the neuronal-glial co-culture model of epilepsy, the potency of these compounds is not ideal. Even the most potent analog of the VU0500469-class has a potency of 14.2 ± 0.7 µM in the Cl$^-$ flux assay. This potency is so low that it may preclude use of these compounds in *in vivo* experiments, owing to projected doses required for them being impractically large, and the inherent risk of off-target effects when compounds are used at higher concentrations. Therefore, increasing the potency of this class should be a priority for future medicinal chemistry work.

An unexpected finding from our work was the temperature-dependence of some members of the VU0500469 class, where they possessed inhibitory activity at room temperature and potentiator activity at 37°C. While this is not necessarily a problem from a therapeutic perspective, it hampers the use of these compounds as chemical probes because a number of assays of KCC2 activity in models of neurological disease are completed at room temperature, which would cause these compounds to act as KCC2 inhibitors in lieu of KCC2 potentiators. We do not believe the inhibitory activity of these compounds at room temperature is a requisite for the potentiator activity of these compounds at 37°C. We have come to this conclusion because there is no correlation

119

between potentiator activity of these compounds at 37°C and inhibitory activity at room temperature, and because the most chemically distinct member of the VU0500469 class, VU0496374, has no inhibitory activity at room temperature – although this compound has significantly diminished potentiator activity at room temperature. Therefore, it may be possible to remove the temperature-dependence of this scaffold through a dedicated medicinal chemistry effort going forward.

Another area of focus should be the pharmacokinetics of the VU0500469 class. The pharmacokinetic properties of the VU0500469-series are currently unknown; the assessment of VU0500469's pharmacokinetics should be the subject of future studies to determine their suitability for *in vivo* use and their therapeutic potential. Given the unknown status of these properties, the pharmacokinetics of the VU0500469 series will likely need to be addressed with future medicinal chemistry efforts as well.

Despite the need for additional medicinal chemistry work on this class, we have shown that this class is well-suited for further optimization. Through our screening of over 200 close analogs of VU0500469, we have helped develop a SAR for this scaffold, and have shown that this class can tolerate chemical change while maintaining activity at KCC2. Moreover, our work describes a suite of assays custom-tailored to measure KCC2 potentiation that can be used to quantify KCC2 activity throughout a medicinal chemistry program. Future medicinal chemistry efforts should be focused on maintaining efficacy at KCC2 and decreasing this scaffold's temperature dependence, while improving the potency of this series, and potentially its pharmacokinetic properties as well. These efforts would lead to the production of drug-like probes suitable for evaluating KCC2's therapeutic potential in a host of neurological disorders, and could lay the foundation for the discovery and development of KCC2-directed therapeutics.

Discovery of the mechanism of action of the VU469 class

We are confident that the VU0500469 class of KCC2 represents a new class of KCC2 potentiator. While we showed that this class acts distinctly from any other KCC2 potentiator described in the literature, its molecular target and the mechanism this compound uses to potentiate KCC2 activity remains unknown. It is therefore worthwhile to investigate its mechanism, as it could deepen our understanding of druggable mechanisms capable of potentiating KCC2 activity. The discovery of molecular targets and mechanisms of action of small molecules is difficult, and many approaches have been developed to facilitate this challenging process (198). One particular method that the VU0500469 class may be suitable for is chemical proteomic detection (199). This method traditionally uses a modified chemical probe featuring chemical groups responsible for photo-crosslinking and affinity purification to help isolate the molecular target(s) of a compound class, then uses proteomic detection to discover the identity of these protein targets (199, 200). VU0500469 is likely well-suited for this approach because of our studies illustrating that this compound can maintain activity at KCC2 in the face of chemical modification. However, the lower potency of this class may interfere with target identification as well, owing to the fact that installation of these moieties responsible for photo-crosslinking and affinity purification typically reduces compound potency further; if the potency of these compounds is reduced too far, it may be hard to distinguish binding necessary for this class's potentiation mechanism from off-target binding. Hence, it may be useful to improve the pharmacological properties first, then use an optimized probe for chemical proteomic detection. Regardless, the discovery of the mechanism of action of these compounds would be worthwhile in furthering our understanding of mechanisms of KCC2 potentiation and should be the subject of future studies.

Continued discovery of KCC2 potentiators

The methodology developed herein should be used to discover and develop new chemical matter capable of potentiating KCC2 activity going forward. KCC2 potentiator pharmacology is

still in its infancy, and would benefit from further development. More classes/scaffolds capable of potentiating KCC2 activity would give investigators flexibility in designing studies targeting KCC2 biology, and, from a therapeutic perspective, provide drug discovery programs with more leads useful for translating preclinical findings to a clinical setting. Continued HTS is a straightforward way to further develop KCC2 potentiator pharmacology. The methodology described in this work can readily be expanded upon to screen and triage hits from a larger chemical library to find novel chemical matter capable of potentiating KCC2. Moreover, it should be emphasized that the number of compounds screened to discover the VU0500469 class of KCC2 potentiator, ~23,000, is small by HTS standards. The use of larger and more diverse chemical libraries will likely discover improved KCC2 potentiators and chemical probes useful for providing insights into different mechanistic aspects of KCC2 potentiation. The discovery of these compounds stands to facilitate research into the fundamental biology of KCC2 in health and disease, and the development of KCC2-directed therapeutics.

REFERENCES

1.   Schulte JT, Wierenga CJ, Bruining H (2018) Chloride transporters and GABA polarity in developmental, neurological and psychiatric conditions. *Neurosci Biobehav Rev* 90:260–271.

2.   Fukuda A, Watanabe M (2019) Pathogenic potential of human SLC12A5 variants causing KCC2 dysfunction. *Brain Res* 1710:1–7.

3.   Raimondo J V., Burman RJ, Katz AA, Akerman CJ (2015) Ion dynamics during seizures. *Front Cell Neurosci* 9:419.

4.   Treiman DM (2001) GABAergic Mechanisms in Epilepsy. *Epilepsia* 42(s3):8–12.

5.   Woo N-S, et al. (2002) Hyperexcitability and epilepsy associated with disruption of the mouse neuronal-specific K-Cl cotransporter gene. *Hippocampus* 12(2):258–268.

6.   Lulan Chen, Li Wan, Zheng Wu, Wanting Ren, Yian Huang BQ& YW (2017) KCC2 downregulation facilitates epileptic seizures. *Sci Rep* 7. doi:10.1038/s41598-017-00196-7.

7.   Sivakumaran S, et al. (2015) Selective Inhibition of KCC2 Leads to Hyperexcitability and Epileptiform Discharges in Hippocampal Slices and In Vivo. *J Neurosci* 35(21):8291–8296.

8.   Hübner CA, et al. (2001) Disruption of KCC2 Reveals an Essential Role of K-Cl Cotransport Already in Early Synaptic Inhibition. *Neuron* 30(2):515–524.

9.   Kelley MR, et al. (2018) Locally Reducing KCC2 Activity in the Hippocampus is Sufficient to Induce Temporal Lobe Epilepsy. *EBioMedicine* 32:62–71.

10. Gagnon M, et al. (2013) Chloride extrusion enhancers as novel therapeutics for neurological diseases. *Nat Med* 19(11):1524–8.

11. Ferrini F, Lorenzo L-E, Godin AG, Quang M Le, De Koninck Y (2017) Enhancing KCC2 function counteracts morphine-induced hyperalgesia. *Sci Rep* 7(1):3870.

12. Tyzio R, et al. (2014) Oxytocin-mediated GABA inhibition during delivery attenuates autism pathogenesis in rodent offspring. *Science (80-)* 343(6171):675–679.

13. Merner ND, et al. (2015) Regulatory domain or CpG site variation in SLC12A5, encoding the chloride transporter KCC2, in human autism and schizophrenia. *Front Cell Neurosci* 9:386.

14. Tang X, et al. (2019) Pharmacological enhancement of KCC2 gene expression exerts therapeutic effects on human Rett syndrome neurons and Mecp2 mutant mice. *Sci Transl Med* 11(503):eaau0164.

15. Chen B, et al. (2018) Reactivation of Dormant Relay Pathways in Injured Spinal Cord by KCC2 Manipulations. *Cell* 174(3):521-535.e13.

16. Bilchak JN, Yeakle K, Caron G, Malloy D, Côté MP (2021) Enhancing KCC2 activity decreases hyperreflexia and spasticity after chronic spinal cord injury. *Exp Neurol* 338:113605.

17. Kahle KT, et al. (2016) The KCC2 Cotransporter and Human Epilepsy: Getting Excited About Inhibition. *Neuroscientist*:1073858416645087.

18. Cristo G Di, Awad PN, Hamidi S, Avoli M (2017) KCC2, EPILEPTIFORM SYNCHRONIZATION, AND EPILEPTIC DISORDERS. *Prog Neurobiol*. doi:10.1016/j.pneurobio.2017.11.002.

19. Duy PQ, David WB, Kahle KT (2019) Identification of KCC2 Mutations in Human Epilepsy Suggests Strategies for Therapeutic Transporter Modulation. *Front Cell Neurosci* 13:515.

20. Liu R, Wang J, Liang S, Zhang G, Yang X (2020) Role of NKCC1 and KCC2 in Epilepsy: From Expression to Function. *Front Neurol* 10:1407.

21. England MJ, Liverman CT, Schultz AM, Strawbridge LM (2012) Epilepsy across the spectrum: Promoting health and understanding. A summary of the Institute of Medicine report. *Epilepsy Behav* 25(2):266–276.

22. Aldenkamp AP (2006) Cognitive impairment in epilepsy: State of affairs and clinical relevance. *Seizure* 15(4):219–220.

23. Zielihski JJ (1974) Epilepsy and Mortality Rate and Cause of Death. *Epilepsia* 15(2):191–

201.

24.   Hirtz D, et al. (2007) How common are the "common" neurologic disorders? *Neurology* 68(5):326–37.

25.   French J 2007 (2007) Refractory epilepsy: Clinical overview. *Epilepsia* 48(SUPPL. 1):3–7.

26.   Munakata M, et al. (2007) Altered distribution of KCC2 in cortical dysplasia in patients with intractable epilepsy. *Epilepsia* 48(4):837–844.

27.   Shimizu-Okabe C, et al. (2011) KCC2 was downregulated in small neurons localized in epileptogenic human focal cortical dysplasia. *Epilepsy Res* 93(2–3):177–184.

28.   Aronica E, et al. (2007) Differential expression patterns of chloride transporters, Na+-K+-2Cl−-cotransporter and K+-Cl−-cotransporter, in epilepsy-associated malformations of cortical development. *Neuroscience* 145(1):185–196.

29.   Han P, Welsh CT, Smith MT, Schmidt RE, Carroll SL (2019) Complex Patterns of GABAergic Neuronal Deficiency and Type 2 Potassium-Chloride Cotransporter Immaturity in Human Focal Cortical Dysplasia. *J Neuropathol Exp Neurol.* doi:10.1093/jnen/nlz009.

30.   Blauwblomme T, et al. (2018) GABAergic transmission underlies interictal epileptogenicity in pediatric FCD. *Ann Neurol.* doi:10.1002/ana.25403.

31.   Conti L, et al. (2011) Anomalous levels of Cl− transporters cause a decrease of GABAergic inhibition in human peritumoral epileptic cortex. *Epilepsia* 52(9):1635–1644.

32.   Pallud J, et al. (2014) Cortical GABAergic excitation contributes to epileptic activities around human glioma. *Sci Transl Med* 6(244):244ra89.

33.   Wu J, et al. (2008) GABAA receptor-mediated excitation in dissociated neurons from human hypothalamic hamartomas. *Exp Neurol* 213(2):397–404.

34.   Muñoz A, Méndez P, Defelipe J, Alvarez-Leefmans FJ (2007) Cation-chloride cotransporters and GABA-ergic innervation in the human epileptic hippocampus. *Epilepsia* 48(4):663–673.

35.   Huberfeld G, et al. (2007) Perturbed chloride homeostasis and GABAergic signaling in

human temporal lobe epilepsy. *J Neurosci* 27(37):9866–9873.

36.   Kuang Y, et al. (2017) Low-frequency stimulation of the primary focus retards positive transfer of secondary focus. *Sci Rep* 7(1):345.

37.   Puskarjov M, et al. (2014) A variant of KCC2 from patients with febrile seizures impairs neuronal Cl- extrusion and dendritic spine formation. *EMBO Rep* 15(6):723–9.

38.   Kahle KT, et al. (2014) Genetically encoded impairment of neuronal KCC2 cotransporter function in human idiopathic generalized epilepsy. *EMBO Rep* 15(7):766–74.

39.   Stödberg T, et al. (2015) Mutations in SLC12A5 in epilepsy of infancy with migrating focal seizures. *Nat Commun* 6(1):8038.

40.   Saitsu H, et al. (2016) Impaired neuronal KCC2 function by biallelic SLC12A5 mutations in migrating focal seizures and severe developmental delay. *Sci Rep* 6(1):30072.

41.   Saito T, Ishii A, Sugai K, Sasaki M, Hirose S (2017) A de novo missense mutation in *SLC12A5* found in a compound heterozygote patient with epilepsy of infancy with migrating focal seizures. *Clin Genet* 92(6):654–658.

42.   Khirug S, et al. (2010) A Single Seizure Episode Leads to Rapid Functional Activation of KCC2 in the Neonatal Rat Hippocampus. *J Neurosci* 30(36).

43.   Tornberg J, Voikar V, Savilahti H, Rauvala H, Airaksinen MS (2005) Behavioural phenotypes of hypomorphic KCC2-deficient mice. *Eur J Neurosci* 21(5):1327–1337.

44.   Watanabe M, et al. (2019) Developmentally regulated KCC2 phosphorylation is essential for dynamic GABA-mediated inhibition and survival. *Sci Signal* 12(603). doi:10.1126/scisignal.aaw9315.

45.   Silayeva L, et al. (2015) KCC2 activity is critical in limiting the onset and severity of status epilepticus. *Proc Natl Acad Sci U S A* 112(11):3523–8.

46.   Kelley MR, et al. (2016) Compromising KCC2 transporter activity enhances the development of continuous seizure activity. *Neuropharmacology* 108:103–110.

47.   Chen L-Y, Lévesque M, Avoli M (2020) KCC2 antagonism and gabaergic synchronization

in the entorhinal cortex in the absence of ionotropic glutamatergic receptor signalling. *Neuropharmacology* 167:107982.

48. Raol YH, et al. (2020) The role of KCC2 in hyperexcitability of the neonatal brain. *Neurosci Lett*:135324.

49. Magloire V, Cornford J, Lieb A, Kullmann DM, Pavlov I (2019) KCC2 overexpression prevents the paradoxical seizure-promoting action of somatic inhibition. *Nat Commun* 10(1):1225.

50. Moore YE, Deeb TZ, Chadchankar H, Brandon NJ, Moss SJ (2018) Potentiating KCC2 activity is sufficient to limit the onset and severity of seizures. *Proc Natl Acad Sci U S A*:201810134.

51. Carter BM, Sullivan BJ, Landers JR, Kadam SD (2018) Dose-dependent reversal of KCC2 hypofunction and phenobarbital-resistant neonatal seizures by ANA12. *Sci Rep* 8(1):11987.

52. Kang SK, Ammanuel S, Adler DA, Kadam SD (2020) Rescue of PB-resistant neonatal seizures with single-dose of small-molecule TrkB antagonist show long-term benefits. *Epilepsy Res* 159. doi:10.1016/j.eplepsyres.2019.106249.

53. Kipnis PA, Sullivan BJ, Carter BM, Kadam S (2020) TrkB-agonists prevent postischemic emergence of refractory neonatal seizures in mice. *JCI Insight*. doi:10.1172/jci.insight.136007.

54. Dzhala VI, Staley KJ (2020) KCC2 chloride transport contributes to the termination of ictal epileptiform activity. *eneuro*:ENEURO.0208-20.2020.

55. Cardarelli R, Jones K, Pisella LI, Wobst HJ (2017) The small molecule CLP257 does not modify activity of the K+/Cl– co–transporter KCC2 but it does potentiate GABAA receptor activity. *Nat Med* in press(12). doi:10.1038/nm.4442.

56. Payne JA (1997) Functional characterization of the neuronal-specific K-Cl cotransporter : implications for [K+]o regulation. *Am J Physiol - Cell Physiol* 273(5).

57. Li H, et al. (2007) KCC2 Interacts with the Dendritic Cytoskeleton to Promote Spine Development. *Neuron* 56(6):1019–1033.

58. Warmuth S, Zimmermann I, Dutzler R (2009) X-ray Structure of the C-Terminal Domain of a Prokaryotic Cation-Chloride Cotransporter. *Structure* 17(4):538–546.

59. Agez M, Schultz P, Medina I, Baker DJ, Burnham M (2017) Molecular architecture of potassium chloride co-transporter KCC2. *Sci Rep* accepted(October):1–14.

60. Xie Y, et al. (2020) Structures and an activation mechanism of human potassium-chloride cotransporters. *Sci Adv* 6(50):eabc5883.

61. Chi X, et al. (2020) Cryo-EM structures of the full-length human KCC2 and KCC3 cation-chloride cotransporters. *Cell Res* 617:2–4.

62. Zhang S, et al. (2021) The structural basis of function and regulation of neuronal cotransporters NKCC1 and KCC2. *Commun Biol* 4(1):226.

63. Uvarov P, et al. (2007) A novel N-terminal isoform of the neuron-specific K-Cl cotransporter KCC2. *J Biol Chem* 282(42):30570–6.

64. Delpire E, Guo J (2020) Cryo-EM structures of DrNKCC1 and hKCC1: A new milestone in the physiology of cation-chloride cotransporters. *Am J Physiol - Cell Physiol* 318(2):C225–C237.

65. Hartmann A-M, et al. (2010) Differences in the large extracellular loop between the K(+)-Cl(-) cotransporters KCC2 and KCC4. *J Biol Chem* 285(31):23994–4002.

66. Lee HHC, et al. (2007) Direct protein kinase C-dependent phosphorylation regulates the cell surface stability and activity of the potassium chloride cotransporter KCC2. *J Biol Chem* 282(41):29777–29784.

67. Friedel P, et al. (2015) WNK1-regulated inhibitory phosphorylation of the KCC2 cotransporter maintains the depolarizing action of GABA in immature neurons. *Sci Signal* 8(383):ra65.

68. Puskarjov M, Ahmad F, Kaila K, Blaesse P (2012) Activity-Dependent Cleavage of the K-

Cl Cotransporter KCC2 Mediated by Calcium-Activated Protease Calpain. *J Neurosci* 32(33).

69.   Markkanen M, et al. (2017) Implications of the N-terminal heterogeneity for the neuronal K-Cl cotransporter KCC2 function. *Brain Res* 1675:87–101.

70.   Cordshagen A, Busch W, Winklhofer M, Nothwang HG, Hartmann A-M (2018) Phospho-regulation of the intracellular termini of K-Cl cotransporter 2 (KCC2) enables flexible control of its activity. *J Biol Chem*:jbc.RA118.004349.

71.   Markkanen M, et al. (2014) Distribution of neuronal KCC2a and KCC2b isoforms in mouse CNS. *J Comp Neurol* 522(8):1897–1914.

72.   Markkanen M, et al. (2017) Implications of the N-terminal heterogeneity for the neuronal K-Cl cotransporter KCC2 function. *Brain Res* 1675:87–101.

73.   Gagnon KB, Delpire E (2013) Physiology of SLC12 transporters: lessons from inherited human genetic mutations and genetically engineered mouse knockouts. *Am J Physiol Cell Physiol* 304(8):C693-714.

74.   Rivera C, Voipio J, Payne JA (1999) The K + / Cl - co-transporter KCC2 renders GABA hyperpolarizing during neuronal maturation. 397(January):251–255.

75.   Delpire E, et al. (2009) Small-molecule screen identifies inhibitors of the neuronal K-Cl cotransporter KCC2. *Proc Natl Acad Sci U S A* 106(13):5383–8.

76.   Payne JA, Stevenson TJ, Donaldson LF (1996) Molecular characterization of a putative K-Cl cotransporter in rat brain: A neuronal-specific isoform. *J Biol Chem* 271(27):16245–16252.

77.   Williams JR, Sharp JW, Kumari VG, Wilson M, Payne JA (1999) The neuron-specific K-Cl cotransporter, KCC2: Antibody development and initial characterization of the protein. *J Biol Chem*. doi:10.1074/jbc.274.18.12656.

78.   Llano O, et al. (2015) KCC2 regulates actin dynamics in dendritic spines via interaction with β-PIX. *J Cell Biol* 209(5).

79. Gauvain G, et al. (2011) The neuronal K-Cl cotransporter KCC2 influences postsynaptic AMPA receptor content and lateral diffusion in dendritic spines. *Proc Natl Acad Sci U S A* 108(37):15474–15479.

80. Uvarov P, Ludwig A, Markkanen M, Rivera C, Airaksinen MS (2006) Upregulation of the neuron-specific K+/Cl- cotransporter expression by transcription factor early growth response 4. *J Neurosci* 26(52):13463–13473.

81. Rivera C, et al. (2002) BDNF-induced TrkB activation down-regulates the K+-Cl-cotransporter KCC2 and impairs neuronal Cl- extrusion. *J Cell Biol* 159(5):747–52.

82. Markkanen M, Uvarov P, Airaksinen MS (2008) Role of upstream stimulating factors in the transcriptional regulation of the neuron-specific K-Cl cotransporter KCC2. *Brain Res* 1236:8–15.

83. Karadsheh MF, Delpire E (2001) Neuronal Restrictive Silencing Element Is Found in the KCC2 Gene: Molecular Basis for KCC2-Specific Expression in Neurons. *J Neurophysiol* 85(2):995–997.

84. Barbato C, et al. (2010) MicroRNA-92 modulates K(+) Cl(−) co-transporter KCC2 expression in cerebellar granule neurons. *J Neurochem* 113(3):591–600.

85. Ludwig A, et al. (2011) Early growth response 4 mediates BDNF induction of potassium chloride cotransporter 2 transcription. *J Neurosci* 31(2):644–649.

86. Rivera C, et al. (2004) Mechanism of activity-dependent downregulation of the neuron-specific K-Cl cotransporter KCC2. *J Neurosci*. doi:10.1523/JNEUROSCI.5265-03.2004.

87. Silayeva L, et al. (2015) KCC2 activity is critical in limiting the onset and severity of status epilepticus. *Proc Natl Acad Sci U S A* 112(11):3523–8.

88. Watanabe M, Wake H, Moorhouse AJ, Nabekura J (2009) Clustering of neuronal K+-Cl-cotransporters in lipid rafts by tyrosine phosphorylation. *J Biol Chem* 284(41):27980–27988.

89. Lee HHC, Jurd R, Moss SJ (2010) Tyrosine phosphorylation regulates the membrane

trafficking of the potassium chloride co-transporter KCC2. *Mol Cell Neurosci* 45(2):173–179.

90. Conway LC, et al. (2017) N-ethylmaleimide increases KCC2 activity by modulating transporter phosphorylation. *J Biol Chem*:jbc.M117.817841.

91. Roussa E, et al. (2016) The membrane trafficking and functionality of the K+-Cl− co-transporter KCC2 is regulated by TGF-β2. *J Cell Sci* 129(18).

92. Mahadevan V, et al. (2014) *Kainate Receptors Coexist in a Functional Complex with KCC2 and Regulate Chloride Homeostasis in Hippocampal Neurons* doi:10.1016/j.celrep.2014.05.022.

93. Pressey JC, et al. (2017) A kainate receptor subunit promotes the recycling of the neuron-specific K-Cl-co-Transporter KCC2 in hippocampal neurons. *J Biol Chem* 292(15):6190–6201.

94. Blaesse P, et al. (2006) Oligomerization of KCC2 correlates with development of inhibitory neurotransmission. *J Neurosci* 26(41):10407–10419.

95. Ivakine E a, et al. (2013) Neto2 is a KCC2 interacting protein required for neuronal Cl^{-} regulation in hippocampal neurons. *Proc Natl Acad Sci U S A* 110(9):3561–3566.

96. Mahadevan V, et al. (2017) Native KCC2 interactome reveals PACSIN1 as a critical regulator of synaptic inhibition. *Elife* 6. doi:10.7554/eLife.28270.

97. Dunham PB, Stewart GW, Ellory JC (1980) Chloride-activated passive potassium transport in human erythrocytes. *Proc Natl Acad Sci U S A* 77(3 I):1711–1715.

98. Hannaert P, Alvarez-Guerra M, Pirot D, Nazaret C, Garay R (2002) Rat NKCC2/NKCC1 cotransporter selectivity for loop diuretic drugs. *Naunyn Schmiedebergs Arch Pharmacol* 365(3):193–199.

99. Savardi A, et al. (2020) Discovery of a Small Molecule Drug Candidate for Selective NKCC1 Inhibition in Brain Disorders. *Chem* 6(8):2073–2096.

100. Delpire E, Lauf PKK (1992) Kinetics of DIDS inhibition of swelling-activated K-Cl cotransport in low K sheep erythrocytes. *J Membr Biol* 126(1):89–96.

101. Kaji D, Amblard J (1986) Volume-sensitive K transport in human erythrocytes. *J Gen Physiol* 88(6):719–738.

102. Wulff H (2008) New light on the "old" chloride channel blocker DIDS. *ACS Chem Biol* 3(7):399–401.

103. Garay RP, Nazaret C, Hannaert PA, Cragoe EJ (1988) Demonstration of a [K+,Cl-]-cotransport system in human red cells by its sensitivity to [(dihydroindenyl)oxy]alkanoic acids: regulation of cell swelling and distinction from the bumetanide-sensitive [Na+,K+,Cl-]-cotransport system. *Mol Pharmacol* 33(6).

104. Cragoe EJ, et al. (1982) Agents for the Treatment of Brain Injury. 1. (Aryloxy)alkanoic Acids. *J Med Chem* 25(5):567–579.

105. Boulenguez P, et al. (2010) Down-regulation of the potassium-chloride cotransporter KCC2 contributes to spasticity after spinal cord injury. *Nat Med* 16(3):302–307.

106. Pégurier C, et al. (2010) Benzyl prolinate derivatives as novel selective KCC2 blockers. *Bioorganic Med Chem Lett* 20(8):2542–2545.

107. Lebon F, et al. (2012) Towards a KCC2 blocker pharmacophore model. *Bioorganic Med Chem Lett* 22(12):3978–3982.

108. Delpire E, et al. (2012) Further optimization of the K-Cl cotransporter KCC2 antagonist ML077: Development of a highly selective and more potent in vitro probe. *Bioorganic Med Chem Lett* 22(14):4532–4535.

109. Sivakumaran S, et al. (2015) Selective Inhibition of KCC2 Leads to Hyperexcitability and Epileptiform Discharges in Hippocampal Slices and In Vivo. *J Neurosci* 35(21).

110. Mapplebeck JCS, et al. (2019) Chloride Dysregulation through Downregulation of KCC2 Mediates Neuropathic Pain in Both Sexes. *Cell Rep* 28(3):590-596.e4.

111. Zhao Y, Shen J, Wang Q, Zhou M, Cao E Inhibitory and Transport Mechanisms of the

Human Cation-Chloride Cotransport KCC1. doi:10.1101/2020.07.26.221770.

112. Lauf PK, Theg BE (1980) A chloride dependent K+ flux induced by N-ethylmaleimide in genetically low K+ sheep and goat erythrocytes. *Biochem Biophys Res Commun* 92(4):1422–1428.

113. Zhang J, et al. (2020) Staurosporine and NEM mainly impair WNK-SPAK/OSR1 mediated phosphorylation of KCC2 and NKCC1. *PLoS One* 15(5):e0232967.

114. Chen B, et al. (2018) Reactivation of Dormant Relay Pathways in Injured Spinal Cord by KCC2 Manipulations. *Cell* 174(3):521-535.e13.

115. Gagnon M, et al. (2017) Gagnon et al. reply: The small molecule CLP257 does not modify activity of the K+/Cl– co–transporter KCC2 but it does potentiate GABAA receptor activity. *Nat Med* in press(12):12–15.

116. Yamada K, et al. (2016) Small-molecule WNK inhibition regulates cardiovascular and renal function. *Nat Chem Biol* 12(11):896–898.

117. Gary Gilliland D, Griffin JD (2002) The roles of FLT3 in hematopoiesis and leukemia. *Blood* 100(5):1532–1542.

118. Kaytor MD, Orr HT (2002) The GSK3β signaling cascade and neurodegenerative disease. *Curr Opin Neurobiol* 12(3):275–278.

119. Mody I, De Koninck Y, Otis TS, Soltesz I (1994) Bridging the cleft at GABA synapses in the brain. *Trends Neurosci*. doi:10.1016/0166-2236(94)90155-4.

120. Rowley NM, Madsen KK, Schousboe A, Steve White H (2012) Glutamate and GABA synthesis, release, transport and metabolism as targets for seizure control. *Neurochem Int*. doi:10.1016/j.neuint.2012.02.013.

121. Khazipov R, et al. (2004) Developmental changes in GABAergic actions and seizure susceptibility in the rat hippocampus. *Eur J Neurosci*. doi:10.1111/j.0953-816X.2003.03152.x.

122. Olsen RW, Wamsley JK, Lee RJ, Lomax P (1986) Benzodiazepine/barbiturate/GABA

receptor-chloride ionophore complex in a genetic model for generalized epilepsy. *Adv Neurol.*

123. Sigel E, Buhr A (1997) The benzodiazepine binding site of GABAA receptors. *Trends Pharmacol Sci.* doi:10.1016/s0165-6147(97)90675-1.

124. Olsen RW (2006) Picrotoxin-like channel blockers of GABAA receptors. *Proc Natl Acad Sci U S A.* doi:10.1073/pnas.0601121103.

125. Bloomquist JR (2003) Chloride channels as tools for developing selective insecticides. *Archives of Insect Biochemistry and Physiology* doi:10.1002/arch.10112.

126. Casida JE, Durkin KA (2015) Novel GABA receptor pesticide targets. *Pestic Biochem Physiol.* doi:10.1016/j.pestbp.2014.11.006.

127. Nakao T, Banba S, Nomura M, Hirase K (2013) Meta-diamide insecticides acting on distinct sites of RDL GABA receptor from those for conventional noncompetitive antagonists. *Insect Biochem Mol Biol.* doi:10.1016/j.ibmb.2013.02.002.

128. Ozoe Y, Asahi M, Ozoe F, Nakahira K, Mita T (2010) The antiparasitic isoxazoline A1443 is a potent blocker of insect ligand-gated chloride channels. *Biochem Biophys Res Commun.* doi:10.1016/j.bbrc.2009.11.131.

129. Asahi M, Kobayashi M, Matsui H, Nakahira K (2015) Differential mechanisms of action of the novel γ-aminobutyric acid receptor antagonist ectoparasiticides fluralaner (A1443) and fipronil. *Pest Manag Sci.* doi:10.1002/ps.3768.

130. Arroyo JP, Kahle KT, Gamba G (2013) The SLC12 family of electroneutral cation-coupled chloride cotransporters. *Mol Aspects Med* 34(2–3):288–298.

131. Gamba G (2005) Molecular physiology and pathophysiology of electroneutral cation-chloride cotransporters. *Physiol Rev* 85(2):423–93.

132. Rivera C, Voipio J, Kaila K (2005) Two developmental switches in GABAergic signalling: The K+-Cl- cotransporter KCC2 and carbonic anhydrase CAVII. *J Physiol.* doi:10.1113/jphysiol.2004.077495.

133. Chamma I, Chevy Q, Poncer JC, Lévi S (2012) Role of the neuronal K-Cl co-transporter KCC2 in inhibitory and excitatory neurotransmission. *Front Cell Neurosci*. doi:10.3389/fncel.2012.00005.

134. Hekmat-Scafe DS, Lundy MY, Ranga R, Tanouye MA (2006) Mutations in the K+/Cl- cotransporter gene kazachoc (kcc) increase seizure susceptibility in Drosophila. *J Neurosci*. doi:10.1523/JNEUROSCI.4998-05.2006.

135. Prael FJ, et al. (2018) Use of chemical probes to explore the toxicological potential of the K^+/Cl^- cotransporter (KCC) as a novel insecticide target to control the primary vector of dengue and Zika virus, Aedes aegypti. *Pestic Biochem Physiol* 151. doi:10.1016/j.pestbp.2018.03.019.

136. Gámez AD, Gutiérrez AM, García R, Whittembury G (2012) Recent experiments towards a model for fluid secretion in Rhodnius Upper Malpighian Tubules (UMT). *J Insect Physiol*. doi:10.1016/j.jinsphys.2011.12.008.

137. Gutiérrez AM, Hernández CS, Whittembury G (2004) A model for fluid secretion in Rhodnius upper Malpighian tubules (UMT). *J Membr Biol*. doi:10.1007/s00232-004-0723-6.

138. Linton SM, O'Donnell MJ (1999) Contributions of K+:Cl- cotransport and Na+/K+-ATPase to basolateral ion transport in malpighian tubules of Drosophila melanogaster. *J Exp Biol*.

139. Piermarini PM, Hine RM, Schepel M, Miyauchi J, Beyenbach KW (2011) Role of an apical K,Cl cotransporter in urine formation by renal tubules of the yellow fever mosquito (Aedes aegypti). *Am J Physiol - Regul Integr Comp Physiol* 301(5). Available at: http://ajpregu.physiology.org/content/301/5/R1318.short [Accessed November 5, 2017].

140. Hekmat-scafe DS, Lundy MY, Ranga R, Tanouye MA (2006) Mutations in the K+ / Cl- Cotransporter Gene kazachoc (kcc) Increase Seizure Susceptibility in Drosophila. *J Neurosci* 26(35):8943–8954.

141. Kahle KT, et al. (2014) Genetically encoded impairment of neuronal KCC2 cotransporter

function in human idiopathic generalized epilepsy. *EMBO Rep* 15(7):766–74.

142. Woo N-S, et al. (2002) Hyperexcitability and epilepsy associated with disruption of the mouse neuronal-specific K-Cl cotransporter gene. *Hippocampus* 12(2):258–268.

143. Raymond V, Sattelle DB (2002) Novel animal-health drug targets from ligand-gated chloride channels. *Nat Rev Drug Discov*. doi:10.1038/nrd821.

144. Nakao T (2017) Mechanisms of resistance to insecticides targeting RDL GABA receptors in planthoppers. *Neurotoxicology*. doi:10.1016/j.neuro.2016.03.009.

145. Hekmat-Scafe DS, et al. (2010) Seizure sensitivity is ameliorated by targeted expression of K +-Cl- cotransporter function in the mushroom body of the Drosophila brain. *Genetics* 184(1):171–183.

146. Chen R, et al. (2019) Functional Coupling of K+-Cl- Cotransporter (KCC) to GABA-Gated Cl- Channels in the Central Nervous System of Drosophila melanogaster Leads to Altered Drug Sensitivities. *ACS Chem Neurosci* 10(6):2765–2776.

147. Piermarini PM, Hine RM, Schepel M, Miyauchi J, Beyenbach KW (2011) Role of an apical K,Cl cotransporter in urine formation by renal tubules of the yellow fever mosquito (Aedes aegypti). *Am J Physiol - Regul Integr Comp Physiol*. doi:10.1152/ajpregu.00223.2011.

148. Gibson DG, et al. (2009) Enzymatic assembly of DNA molecules up to several hundred kilobases. *Nat Methods*. doi:10.1038/nmeth.1318.

149. Chen R, Swale DR (2018) Inwardly Rectifying Potassium (Kir) Channels Represent a Critical Ion Conductance Pathway in the Nervous Systems of Insects. *Sci Rep*. doi:10.1038/s41598-018-20005-z.

150. Bloomquist JR (2003) Mode of action of atracotoxin at central and peripheral synapses of insects. *Invertebr Neurosci*. doi:10.1007/s10158-003-0027-z.

151. Swale DR, Sun B, Tong F, Bloomquist JR (2014) Neurotoxicity and mode of action of N, N-diethyl-Meta-toluamide (DEET). *PLoS One*. doi:10.1371/journal.pone.0103713.

152. Duffy JB (2002) GAL4 system in Drosophila: A fly geneticist's Swiss army knife. *Genesis*.

doi:10.1002/gene.10150.

153. Busson D, Pret A-M (2007) GAL4/UAS Targeted Gene Expression for Studying Drosophila Hedgehog Signaling (Humana Press), pp 161–201.

154. Fischer JA, Giniger E, Maniatis T, Ptashne M (1988) GAL4 activates transcription in Drosophila. *Nature*. doi:10.1038/332853a0.

155. St Johnston D (2002) The art and design of genetic screens: Drosophila melanogaster. *Nat Rev Genet*. doi:10.1038/nrg751.

156. Livak KJ, Schmittgen TD (2001) Analysis of relative gene expression data using real-time quantitative PCR and the 2-ΔΔCT method. *Methods*. doi:10.1006/meth.2001.1262.

157. Pridgeon JW, et al. (2008) Susceptibility of Aedes aegypti, Culex quinquefasciatus say, and Anopheles quadrimaculatus say to 19 pesticides with different modes of action. *J Med Entomol*. doi:10.1603/0022-2585(2008)45[82:SOAACQ]2.0.CO;2.

158. Larson NR, et al. (2017) Toxicology of potassium channel-directed compounds in mosquitoes. *Neurotoxicology*. doi:10.1016/j.neuro.2016.05.021.

159. Islam RM, Bloomquist JR (2015) A method for assessing chemically-induced paralysis in headless mosquito larvae. *MethodsX*. doi:10.1016/j.mex.2014.12.002.

160. Swale DR, et al. (2016) An insecticide resistance-breaking mosquitocide targeting inward rectifier potassium channels in vectors of Zika virus and malaria. *Sci Rep*. doi:10.1038/srep36954.

161. Raphemot R, et al. (2013) Eliciting Renal Failure in Mosquitoes with a Small-Molecule Inhibitor of Inward-Rectifying Potassium Channels. *PLoS One*. doi:10.1371/journal.pone.0064905.

162. Delpire E, et al. (2012) Further optimization of the K-Cl cotransporter KCC2 antagonist ML077: Development of a highly selective and more potent in vitro probe. *Bioorganic Med Chem Lett*. doi:10.1016/j.bmcl.2012.05.126.

163. Zhao X, Salgado VL, Yeh JZ, Narahashi T (2003) Differential actions of fipronil and dieldrin

insecticides on GABA-gated chloride channels in cockroach neurons. *J Pharmacol Exp Ther.* doi:10.1124/jpet.103.051839.

164. Löscher W, Puskarjov M, Kaila K (2013) Cation-chloride cotransporters NKCC1 and KCC2 as potential targets for novel antiepileptic and antiepileptogenic treatments. *Neuropharmacology* 69:62–74.

165. Dargaei Z, et al. (2018) Restoring GABAergic inhibition rescues memory deficits in a Huntington's disease mouse model. *Proc Natl Acad Sci U S A.* doi:10.1073/pnas.1716871115.

166. Riekki R, et al. (2008) Altered synaptic dynamics and hippocampal excitability but normal long-term plasticity in mice lacking hyperpolarizing GABAA receptor-mediated inhibition in CA1 pyramidal neurons. *J Neurophysiol.* doi:10.1152/jn.00606.2007.

167. Ganguly K, Schinder AF, Wong ST, Poo M ming (2001) GABA itself promotes the developmental switch of neuronal GABAergic responses from excitation to inhibition. *Cell.* doi:10.1016/S0092-8674(01)00341-5.

168. Reid WR, et al. (2014) Transcriptional analysis of four family 4 P450s in a Puerto Rico strain of Aedes aegypti (Diptera: Culicidae) compared with an orlando strain and their possible functional roles in permethrin resistance. *J Med Entomol.* doi:10.1603/ME13228.

169. Zhang D, Gopalakrishnan SM, Freiberg G, Surowy CS (2010) A Thallium Transport FLIPR-Based Assay for the Identification of KCC2-Positive Modulators. *J Biomol Screen* 15(2):177–184.

170. Deans RM, et al. (2016) Parallel shRNA and CRISPR-Cas9 screens enable antiviral drug target identification. doi:10.1038/nCHeMBIO.2050.

171. Hekmat-Scafe DS, et al. (2010) Seizure sensitivity is ameliorated by targeted expression of K+-Cl- cotransporter function in the mushroom body of the Drosophila brain. *Genetics* 184(1):171–83.

172. Kahle KT, Khanna A, Clapham DE, Woolf CJ (2014) Therapeutic restoration of spinal

inhibition via druggable enhancement of potassium-chloride cotransporter kcc2-mediated chloride extrusion in peripheral neuropathic pain. *JAMA Neurol* 71(5):640–645.

173. Akita T, Fukuda A (2020) Intracellular Cl $^-$ dysregulation causing and caused by pathogenic neuronal activity.

174. Raimondo J V, Richards BA, Woodin MA (2017) Neuronal chloride and excitability — the big impact of small changes. *Curr Opin Neurobiol* 43:35–42.

175. Williams JR, Sharp JW, Kumari VG, Wilson M, Payne JA (1999) The neuron-specific K-Cl cotransporter, KCC2: Antibody development and initial characterization of the protein. *J Biol Chem* 274(18):12656–12664.

176. Saito T, Ishii A, Sugai K, Sasaki M, Hirose S (2017) A *de novo* missense mutation in *SLC12A5* found in a compound heterozygote patient with epilepsy of infancy with migrating focal seizures. *Clin Genet*. doi:10.1111/cge.13049.

177. Magloire V, Cornford J, Lieb A, Kullmann DM, Pavlov I (2019) KCC2 overexpression prevents the paradoxical seizure-promoting action of somatic inhibition. *Nat Commun* 10(1):1225.

178. Grimley JS, et al. (2013) Visualization of Synaptic Inhibition with an Optogenetic Sensor Developed by Cell-Free Protein Engineering Automation. *J Neurosci* 33(41):16297–16309.

179. Campeau E, et al. (2009) A versatile viral system for expression and depletion of proteins in mammalian cells. *PLoS One* 4(8). doi:10.1371/journal.pone.0006529.

180. Zhang J-H, Chung TDY, Oldenburg KR (1999) A Simple Statistical Parameter for Use in Evaluation and Validation of High Throughput Screening Assays. *J Biomol Screen* 4(2):67–73.

181. RDKit Available at: https://www.rdkit.org/ [Accessed January 4, 2021].

182. Friedel P, et al. (2017) A novel view on the role of intracellular tails in surface delivery of the potassium-chloride cotransporter KCC2. *eNeuro* 4(4). doi:10.1523/ENEURO.0055-17.2017.

183. Pacico N, Mingorance-Le Meur A, Coco S, Pravettoni E, Fumagalli G (2014) New In Vitro Phenotypic Assay for Epilepsy: Fluorescent Measurement of Synchronized Neuronal Calcium Oscillations. *PLoS One* 9(1):e84755.

184. Weaver CD, Harden D, Dworetzky SI, Robertson B, Knox RJ (2004) A Thallium-Sensitive, Fluorescence-Based Assay for Detecting and Characterizing Potassium Channel Modulators in Mammalian Cells. 671–677.

185. Medina I, et al. (2014) Current view on the functional regulation of the neuronal K(+)-Cl(-) cotransporter KCC2. *Front Cell Neurosci* 8(February):27.

186. Peltason L, Bajorath J (2008) Molecular Similarity Analysis in Virtual Screening. *Silico Med Chem Comput Methods to Support Drug Des*:120–149.

187. Friedel P, et al. (2017) A Novel View on the Role of Intracellular Tails in Surface Delivery of the Potassium-Chloride Cotransporter KCC2. *eNeuro* 4(4). Available at: http://www.eneuro.org/content/4/4/ENEURO.0055-17.2017 [Accessed August 14, 2017].

188. Mahadevan V, Woodin MA (2016) Regulation of neuronal chloride homeostasis by neuromodulators. *J Physiol* 594(10):2593–2605.

189. AlAmri MA, Kadri H, Alderwick LJ, Simpkins NS, Mehellou Y (2017) Rafoxanide and Closantel Inhibit SPAK and OSR1 Kinases by Binding to a Highly Conserved Allosteric Site on Their C-terminal Domains. *ChemMedChem* 12(9):639–645.

190. Zhang J, et al. (2020) Modulation of brain cation-Cl− cotransport via the SPAK kinase inhibitor ZT-1a. *Nat Commun* 11(1):78.

191. Zhao Y, Shen J, Wang Q, Zhou M, Cao E (2020) Inhibitory and Transport Mechanisms of the Human Cation-Chloride Cotransport KCC1. *bioRxiv*. doi:10.1101/2020.07.26.221770.

192. Hasenhuetl PS, Freissmuth M, Sandtner W (2016) Electrogenic binding of intracellular cations defines a kinetic decision point in the transport cycle of the human serotonin transporter. *J Biol Chem* 291(50):25864–25876.

193. Fontana ACK, et al. (2007) Enhancing Glutamate Transport: Mechanism of Action of

Parawixin1, a Neuroprotective Compound from Parawixia bistriata Spider Venom. *Mol Pharmacol* 72(5). Available at: http://molpharm.aspetjournals.org.proxy.library.vanderbilt.edu/content/72/5/1228 [Accessed June 14, 2017].

194. Delpire E, Lauf PK (1991) Kinetics of Cl-dependent K fluxes in hyposmotically swollen low K sheep erythrocytes. *J Gen Physiol* 97(2):173–193.

195. Kenakin T, Jenkinson S, Watson C (2006) Determining the potency and molecular mechanism of action of insurmountable antagonists. *J Pharmacol Exp Ther* 319(2):710–723.

196. Gentry PR, Sexton PM, Christopoulos A (2015) Novel allosteric modulators of G protein-coupled receptors. *J Biol Chem* 290(32):19478–19488.

197. Chen R, et al. (2019) Functional Coupling of K^+-Cl^- Cotransporter (KCC) to GABA-Gated Cl^- Channels in the Central Nervous System of Drosophila melanogaster Leads to Altered Drug Sensitivities. *ACS Chem Neurosci* 10(6). doi:10.1021/acschemneuro.8b00697.

198. Bunnage ME, Gilbert AM, Jones LH, Hett EC (2015) Know your target, know your molecule. *Nat Chem Biol* 11(6):368–372.

199. Kubota K, Funabashi M, Ogura Y (2019) Target deconvolution from phenotype-based drug discovery by using chemical proteomics approaches. *Biochim Biophys Acta - Proteins Proteomics* 1867(1):22–27.

200. Li Z, et al. (2013) Design and Synthesis of Minimalist Terminal Alkyne-Containing Diazirine Photo-Crosslinkers and Their Incorporation into Kinase Inhibitors for Cell- and Tissue-Based Proteome Profiling. *Angew Chemie* 125(33):8713–8718.